

SOIL STRUCTURE INTERACTION UNDER THE  
INFLUENCE OF WAVE LOADING

CENTRE FOR NEWFOUNDLAND STUDIES

**TOTAL OF 10 PAGES ONLY  
MAY BE XEROXED**

(Without Author's Permission)

RICHARD DOUGLAS NANCARROW







SOIL STRUCTURE INTERACTION

UNDER THE INFLUENCE OF WAVE LOADING

BY

© Richard Douglas Nancarrow, B.Ap.Sc.

A thesis submitted to the School of Graduate  
Studies in partial fulfilment of the  
requirements for the degree of  
Master of Engineering

Department of Ocean Engineering  
Memorial University of Newfoundland

May 1988

St. John's

Newfoundland

Permission has been granted to the National Library of Canada to microfilm this thesis and to lend or sell copies of the film.

The author (copyright owner) has reserved other publication rights, and neither the thesis nor extensive extracts from it may be printed or otherwise reproduced without his/her written permission.

L'autorisation a été accordée à la Bibliothèque nationale du Canada de microfilmer cette thèse et de prêter ou de vendre des exemplaires du film.

L'auteur (titulaire du droit d'auteur) se réserve les autres droits de publication; ni la thèse ni de longs extraits de celle-ci ne doivent être imprimés ou autrement reproduits sans son autorisation écrite.

ISBN 0-315-50451-X

### ABSTRACT

An experimental program was carried out to examine the influence of the presence of an offshore structure on the pore pressures in a soil bed under the influence of wave loading. A bed of silt 0.4 m deep was placed in a wave tank and subjected to waves ranging in frequency from 0.6 to 1.2 Hz. generated by a flap type wavemaker. Pore pressures in the soil bed and wave heights were measured and recorded. Then a model of a gravity based offshore oil exploration platform was placed on a sand berm over the soil bed and subjected to waves at the same frequencies as without the model. The bottom pressure wave data was compared to those predicted by linear wave theory and pore pressures in the soil bed for the case without the model in place were compared with those predicted by the Putnam-Liu solution. Also, pore pressures with and without the model in place were compared. It was found linear wave theory accurately predicts the magnitude of the bottom pressure wave, while measured pore pressures varied considerably from those predicted by the Putnam-Liu solution, depending on frequency. It was found that the pore pressures were lower in both sand and silt when the model was in the tank for similar wave heights and frequencies and that pore pressures built up rapidly in the sand berm with wave loading.

#### ACKNOWLEDGEMENTS

I would like to thank NSERC for providing funding assistance for this research project and the Department of Ocean Engineering for providing teaching fellowships. Without the assistance of the gang in the wave tank at MUN, I would never have conquered the mysteries of instrumentation. I would also like to thank Dr. Jack Clark, my supervisor, for his guidance in the preparation of this thesis. Finally, I would like thank the ladies of my house, Donna, Karen and Tanya for tolerating a sometimes crotchety husband and dad during the preparation of this thesis.

TABLE OF CONTENTS

	<u>Page</u>
1.0 INTRODUCTION	1
1.1 Background	1
1.2 Objectives	2
1.3 Experimental Program	2
2.0 LITERATURE REVIEW	4
2.1 Pore Pressures in Permeable Beds	4
2.1.1 Basic Theories	6
2.1.2 Field Observations	8
2.2 Wave Generation in the Laboratory	10
2.3 Similitude and Scale Factors	12
3.0 EQUIPMENT	19
3.1 Soil-Wave Tank	19
3.1.1 Model Soil	19
3.1.2 Soil Installation	21
3.1.3 Wavemaker	22
3.2 Instrumentation	23
3.2.1 Pore Pressure Measurement	23
3.2.2 Wave Probe	24
3.3 Data Acquisition	24
3.4 Similitude Considerations-Wave Tank Experiment	24
4.0 PROCEDURES	26
4.1 Calibration	26
4.1.1 Wavemaker	26
4.1.2 Wave Tank	26
4.1.3 Pore Pressure Measuring Equipment	26

4.2 Soil Consolidation	27
4.3 Model Installation	28
4.4 Wave Tank Tests	29
5.0 RESULTS AND ANALYSES	30
5.1 Data Conditioning	30
5.2 Experimental Results	31
5.2.1 Introduction	31
5.2.2 Bottom Pressure Wave	31
5.2.3 Pore Water Pressures	32
5.2.3.1 Measured and Theoretical Values - No Model	33
5.2.3.2 Pore Pressure Build Up	34
5.2.3.3 Phase Analyses - No Model	35
5.2.3.4 Phase Analyses - Model in Place	37
5.2.3.5 Comparison of Results - Soil Bed Alone and Model in Place	43
5.3 Discussion	50
5.3.1 Pore Water Pressures - No Model	50
5.3.2 Pore Water Pressures - Model	52
5.3.3 Pore Pressure Build Up	53
5.3.4 Similitude Considerations	55
5.3.5 Comparison with Other Work	55
6.0 CONCLUSIONS AND RECOMMENDATIONS	57
6.1 Conclusions	57
6.2 Recommendations	58
Tables	59
Figures	67
References	193
Appendices	201

LIST OF TABLES

<u>Number</u>		<u>Page</u>
1	Scale Factor Comparison for Froude and Reynolds Numbers	59
2	Scale Factors Used Based on the Froude Number	59
3	Comparison of Actual and Theoretical Wave Heights	60
4	Burial Depth of Transducers	61
5	Actual and Theoretical Bottom Pressures	61
6	Comparison of Theoretical and Actual Pore Pressures/Wave Height for four Frequencies-Model in Place and Out	62
7	Phase Lag Between Wave Probe and Transducers	63
8	Transducer and Wave Probe Peak Response Times	64
9	Comparison of Pressure Coefficient with Liu(1985)	64
10	Comparison of Pore Pressures with Cheng and Liu (1986)	65

LIST OF FIGURES

<u>Number</u>		<u>Page</u>
1	Wave Tank Layout	67
2	Wave Pressures on Ocean Floor	68
3	Grain Size Distribution Curve - Silt	69
4	Grain Size Distribution Curve - Sand	70
5	Cross and Piezometric Stone	71
6	Transducer Locations - No Model	72
7	Model and Model Used in Experiment	73
8	Transducer Locations - With Model	74
9	Transducer Output - Bottom Pressure Wave	75
10	Tr. 1, 3 - 0.63 Hz. Act. and Theo. Pore Pressures	76
11	Tr. 2, 4 - 0.63 Hz. Act. and Theo. Pore Pressures	77
12	Tr. 1, 3 - 0.81 Hz. Act. and Theo. Pore Pressures	78
13	Tr. 2, 4 - 0.81 Hz. Act. and Theo. Pore Pressures	79
14	Tr. 1, 3 - 1.00 Hz. Act. and Theo. Pore Pressures	80
15	Tr. 2, 4 - 1.00 Hz. Act. and Theo. Pore Pressures	81
16	Tr. 1, 3 - 1.15 Hz. Act. and Theo. Pore Pressures	82
17	Tr. 2, 4 - 1.15 Hz. Act. and Theo. Pore Pressures	83
18	Tr. 1, 4 - 0.63 Hz. $Z/Z_0$ and $P/P_0$	84
19	Tr. 3 - 0.63 Hz. $Z/Z_0$ and $P/P_0$	85
20	Tr. 1, 4 - 0.81 Hz. $Z/Z_0$ and $P/P_0$	86
21	Tr. 3 - 0.81 Hz. $Z/Z_0$ and $P/P_0$	87
22	Tr. 1, 4 - 1.00 Hz. $Z/Z_0$ and $P/P_0$	88
23	Tr. 3 - 1.00 Hz. $Z/Z_0$ and $P/P_0$	89
24	Tr. 1, 4 - 1.15 Hz. $Z/Z_0$ and $P/P_0$	90

25	Tr. 3 - 1.15 Hz. Z/Zo and P/Po	91
26	Tr. 1 - Pore Pressure and Frequency	92
27	Tr. 2 - Pore Pressure and Frequency	93
28	Tr. 3 - Pore Pressure and Frequency	94
29	Tr. 4 - Pore Pressure and Frequency	95
30	Tr. 1 - Pore Pressure Build Up - Model in Place	96
31	Tr. 2 - Pore Pressure Build Up - Model in Place	97
32	Tr. 3 - Pore Pressure Build Up - Model in Place	98
33	Tr. 4 - Pore Pressure Build Up - Model in Place	99
34 - 81	Wave Probe and Pore Pressure Transducer Outputs - Soil Bed Alone	100 - 147
82 - 126	Wave Probe and Pore Pressure Transducer Outputs - Model in Place	148 - 192

## 1.0 INTRODUCTION

### 1.1 Background

Bottom founded offshore structures for hydrocarbon exploration in ice-infested waters, such as the Canadian Beaufort Sea, are designed to operate in extreme environmental conditions, including low temperatures, severe sea states and high ice loadings. Caisson structures, such as the Mobile Arctic Caisson (MAC), operated by Gulf Canada Resources Inc., the Caisson Retained Island, operated by Esso Resources Canada Ltd., Tarsuit and the Single Steel Drilling Caisson (SSDC) operated by Dome Petroleum Ltd. have been successfully used in the Canadian Beaufort Sea. (Jefferies et al, 1985). In the American Beaufort Sea, the Concrete Island Drilling System (CIDS) and Super CIDS have been developed for use. The geotechnical investigation for the installation of such caissons consists usually of an extensive field program to characterize the foundation soils and mathematical and physical modelling to represent the soil-structure interaction. Included in this is the estimation of the pore water pressure under the caisson during installation, when large excess pore pressures can develop, and operation, when pore pressures can build up in certain soil types under wave or ice loading to the point that soil strength is reduced and failure occurs. Most theoretical and experimental investigations into liquefaction from cyclic loading have been

carried out without consideration of soil structure interaction, although some investigations have been made of the pore pressure field under pipelines during wave loading (Liu et al, 1979), (Cheng and Liu, 1986) and a gravity platform (Spidsoe et al, 1986). Mynett and Mei (1982) developed a model to predict stresses and pore water pressures beneath a rectangular caisson under the influence of wave loading and Liu (1985) developed an integral solution to wave induced seepage flow in a porous bed under a gravity structure using two dimensional potential flow theory.

---

### 1.2 Objectives

The objectives of this project were:

- to measure soil pore water pressures under the influence of wave loading in a model soil bed and sand berm under two conditions, with a model of a gravity based structure in place and in the soil bed and sand berm without the model;
- compare these measurements with theoretical predictions.

### 1.3 Experimental Program

A 100:1 model of an offshore caisson structure was constructed and placed on a sand berm on a soil bed in a large concrete tank filled with water. Waves were generated by a flap type wave maker and wave energy absorbed by a pebble beach; (Figure 1). Pore water pressures in the soil bed and berm were measured, as well as wave height and horizontal and vertical

deflection of the model under various combinations of wave height and frequency.

For each experimental run, pore pressure and wave height data were digitized and stored on floppy disc and backed up on eight track FM tape. Model deflection data were recorded by a strip chart recorder. Pore pressures and wave height frequency data were analyzed with a digital signal analyzer. Theoretical values for pore pressure distribution in the unloaded and loaded soil are compared with experimental results. An assessment of the experimental technique is made and recommendations for modifications in the experimental design and equipment are presented.

## 2.0 LITERATURE REVIEW

### 2.1 Pore Pressures in Permeable Beds

Water waves that move over a permeable seabed exert a boundary pressure at the bed-water interface and will cause cyclic variations in the fluid pressures, and stresses in the bed. Effective stress will vary in response to wave loading. As soil strength is related to effective stress, waves can affect stability and bed strength. There have been a number of investigations of the problem of fluid flow induced in a porous bed by water waves. Some investigations have dealt only with the flow and pressure field in the pore fluid, while others have dealt with the state of stress in the soil skeleton as well.

Liu(1973), Massel(1976), Moshagen and Torum(1975), Putnam(1949), Reid and Kaljura(1957), Dawe and Chari, (1986) examined the hydraulics of waves interacting with saturated beds of isotropic permeability. All assumed that the porous beds were rigid and non-deformable. All except Moshagen and Torum (1975) assumed that the pore fluid was incompressible as well. The fluid flow in the bed is assumed to be governed by Darcy's Law and this, along with the assumption of a rigid bed with isotropic permeability and incompressible water leads to the Laplace equation for the pore water pressure. One of the key results of this theory is that pore water pressure

response is independent of the bed permeability.

Some refinements to the basic approach have been made to include anisotropic permeability, Sleath(1970), stratified permeability, Liu(1973) and compressible unsaturated pore fluid, Nakamura(1973).

A different approach has been taken by Doyle(1973), Prevost and Hughes(1978) and Mallard and Dalrymple(1977). They considered the bed to be an elastic continuum with no fluid flow taking place. This leads to a solid mechanics problem and assuming that the change in pore pressure is equal to the change in octahedral stress in the elastic continuum, similar expressions for pore water pressure as derived by the Laplace equation result.

Yamamoto(1978) and Madsen(1978) developed comprehensive theories based on the Biot(1941) three dimensional consolidation theory. Both authors developed exact, closed form solutions for bed stresses, displacements and pore water pressures for water waves propagating over a porous bed. Their theories are comprehensive and account for soil properties, such as permeability, shear modulus and density and assume that the soil skeleton obeys Hooke's Law and that fluid flow obeys Darcy's Law. The theoretical results of their analyses indicate that bed response is strongly dependent on the permeability  $k$  and the stiffness ratio  $G/K$ ,

where  $G$  is the shear modulus of the porous medium and  $K$  is the apparent bulk modulus of the pore fluid, where the apparent bulk modulus is a function of the degree of saturation of the soil.

Seed et al(1976) have proposed a method for estimating the liquefaction potential of seafloor sands under wave loading and the magnitudes of the residual pore pressures.

They represent the complex pattern of storm waves by packets of uniform harmonic waves with the height, period and length of the wave being specified for each packet. The residual pore water pressure is determined using the number of cycles of stress which cause liquefaction. The method was further generalized by Siddhartan and Finn(1979) who wrote a computer program to predict residual pore water pressures and liquefaction potential.

### 2.1.1 Basic Theories

Analysis of pore water pressures is usually based on the description of a pressure wave on the sea floor. (Figure 2). The pressure wave is characterized by most investigators by linear wave theory assuming the sea floor to be rigid and impermeable. The wave pressure,  $P_b$ , on the sea floor is given by

$$P_b = P_o * \sin(\lambda * x - \omega * T) \quad (1)$$

$$P_o = \delta_o * H / 2 * \cosh(\lambda * d) \quad (2)$$

where:

$P_0$  = Amplitude of the pressure wave

$\gamma_w$  = unit weight of water

$\lambda$  = wave number  $2\pi/L$

$L$  = wave length

$d$  = depth of water

$\omega$  = circular frequency

$T$  = wave period

$H$  = wave height.

Putnam (1949) assumed incompressible flow, Darcy's Law and hydraulic isotropy and showed that Laplace equation was applicable. Liu et al (1979) gave a simple expression for the pore pressure  $p$ , at depth  $z$  in a soil bed of thickness  $d_s$ , based on the Putnam solution.

$$P = P_0 \cdot \cosh(\lambda(d_s - z)) / \cosh(\lambda d_s) \quad (3)$$

This has become known as the Putnam-Liu solution.

Sleath (1970) considered hydraulic anisotropy with permeability  $k_h$ ,  $k_v$  in the horizontal and vertical directions.

Moshagen and Torum(1975) assumed the water to be compressible and the soil skeleton to be rigid. This approach leads to the heat conduction equation. A number of investigators, including Yamamoto(1978) and Finn et al(1983) have stated that

the assumptions used by the authors are unrealistic and lead to rapid attenuation of pore water pressure with depth.

### 2.1.2 Field Observations

Performance monitoring of the Molikpaq while deployed on a drill site (Tarsiut P-45) was discussed by Rogers et al (1986). The caisson, berm and foundation soils were extensively instrumented to monitor performance and to provide data for future structures. Instrumentation monitored by the data-acquisition and signal conditioning system included total pressure cells distributed uniformly over the base of the caisson to measure soil stress and hydrostatic pressure and five strings of electric piezometers installed in the sand core and berm to monitor pore water pressure response to ice loads.

Results of pore pressure monitoring indicate that excess pore water pressures developed in the clay and silty clay foundation soils immediately after caisson set down. The excess pore water pressure ranged from 260 to 280 kPa, approximately equal to the initial load on the foundation. After 275 days, the excess pore pressure was in the order of 150 kPa.

Becker et al(1985) discussed performance of foundation clay materials under two caisson structures at Tarsiut and Kadluk in the Canadian Beaufort Sea.

Tarsiut was located in 21 meters of water and consisted of four concrete caisson structures set on a sand berm and a sand core over silty clay and stiff silt. Foundation monitoring included total pressure panels, strain gauges, extensometers, inclinometers and piezometers. The excess pore water pressure after two months was 170 kPa and continued to rise to 190 kPa for an additional three months before beginning to dissipate.

Esso Resources Canada Ltd. used the octagonal Caisson Retained Island at Kadiuk in 14 meters of water. The CRI was placed on a sand berm overlying stiff silty clay and the core filled with sand. Foundation instrumentation included pore pressure cells and deflectometers installed into the clay. Initial measured pore water pressure was 100 kPa and rose to 224 kPa six months after the end of construction. Dissipation occurred but the rate was not known because of transducer failure. These effects could not be explained by additional construction or alteration in surface facilities or wave or ice action. The authors offer a number of hypotheses to explain the effect related to the nature of the loading and initial state of stress. The clay is locally initially critically stressed and through time dependent strain development and stress distribution, adjacent soil elements become critically stressed, which in turn could lead to high pore water pressures.

## 2.2 Wave Generation in the Laboratory

Models of marine structures are often tested in the laboratory under simulated random or periodic wave conditions using a wave tank facility with a device capable of mechanical oscillation called a wavemaker. There are three basic common wavemaker configurations, the wedge, flap and piston. Each type is used for a particular application depending on the type of wave (deep, intermediate or shallow water) needed.

Wavemaker theory is based on potential flow theory. The theory was first proposed by Havelock (1929). Biesel (1951) used the assumptions of potential flow theory and solved the first-order linearised hydrodynamic equations of motion caused by the sinusoidal oscillation of a wavemaker in a rectangular wave tank. Both piston and flap types were considered and formulae developed relating the stroke,  $s$ , wave amplitude,  $a$ , wavelength  $L$  and water depth  $d$ . These are:

for the piston type:

$$a/s = 2 * \sinh^2(\lambda * d) / (\lambda * d + \sinh(\lambda * d) * \cosh(\lambda * d)) \quad (4)$$

for the flap type:

$$a/s = \frac{2 * \sinh(\lambda * d) * (1 - \cosh(\lambda * d) + \lambda * d * \sinh(\lambda * d))}{\lambda * d * (\lambda * d + \sinh(\lambda * d) * \cosh(\lambda * d))} \quad (5)$$

The ratio  $a/s$  is referred to as the wavemaker gain factor. For shallow water conditions, the above equations become

$$a/s = \lambda*d = 2\pi d/L$$

(6)

Biesel's theory has been verified by many researchers. Gilbert et al (1970) produced a series of graphs which included  $a/s-d/gT^2$  for flap, piston and wedge type wave generators as well as non-dimensional hydrodynamic forces and moments on the wave maker and hinge.

Others have extended Biesel's theory to account for different wave tank configurations other than the standard rectangular shape. Hyun (1981) presented a solution for a flap type wave maker hinged at intermediate depth in a constant depth. Hudspeth and Chen (1981) further extended the theory for a hinged type wave maker of variable draft by considering a wave tank of two constant depth regimes, separated by a gradually sloped region.

Wave generation in a tank is complicated by the presence of parasitic and reflected waves. The harmonic oscillation of the wavemaker produces secondary waves of higher frequency besides the basic wave desired, called parasitic waves. Most of the parasitic waves are damped out within one water depth of the wavemaker, but some persist. The most important of these is one that is twice the frequency of the generated wave. Various techniques exist to minimize the effect of parasitic waves, including the generation of a wave of the same wavelength but out of phase to cancel them and the selection of the proper wavemaker type for the frequency range

desired.

Beaches are used to minimize reflected waves, but complete absorption of wave energy is not usually achieved. Part of the incident wave gets reflected by the beach and travels back to the wavemaker and in this manner, gets reflected up and down the tank. As well, the test body in the tank reflect waves in a similar fashion. As reflection cannot be completely eliminated, estimates should be made of the beach reflection coefficient to ensure that it is below ten percent (Keating and Webber, 1977). Various techniques exist to determine beach reflection coefficients including measuring simultaneously the wave heights at two or more points and determining the reflected and incident wave energy analytically or graphically.

### 2.3 Similitude and Scale Factors

Physical models are used to investigate the behaviour of the prototype under controlled conditions. Often, physical phenomena that occur in nature are too complex to be investigated by analytical techniques. A model is used to represent the prototype and subject it to forces or other changes under controlled conditions. The use of hydraulic and hydrodynamic models is well established. However, the inherent problems with soil modelling make it more difficult and challenging. As a result, physical soil modelling is not used

as extensively as other types.

Models are characterized by a scale factor, which is the proportional amount by which each dimension of the prototype is reduced. For example, a 100 meter length in the prototype becomes two meters in the model at a scale of 1:50. Other quantities, such as force and time, are reduced by appropriate scale factors, using the principles of similarity theory to arrive at the required dimensionless ratios or scale factors (Sharp 1981).

Soil modelling can be classified broadly into two types, depending on how it is carried out. Modelling done in the laboratory without a centrifuge is referred to as conventional or 1g modelling, while centrifuge modelling is referred to as  $Ng$  modelling, with  $N$  being the gravity and the geometric scale factor.

The fundamental problem with soil modelling is the inability to simultaneously scale all relevant physical phenomena, such as particle size, stress levels and water-related effects. This is primarily due to the granular nature of soil and the dependence of most of the properties of soil on the size of the individual grains. The particle size is not normally scaled because in doing so, the basic characteristics of the soil will change. For example, a prototype sand with a mean diameter of one millimetre becomes a silt sized particle in a model at a scale of 1:100. Sand and silt are quite different

in their mechanical and physical properties, sand being a non-cohesive, permeable material while silt may be cohesive, and relatively impermeable.

In 1g modelling, prototype stress levels are more difficult to achieve. The contact stress is the weight of the structure divided by the contact area of the foundation. As the model size decreases, its volume and hence its weight, decrease at the ratio of the scale factor cubed, while the area only decreases as the ratio of the scale factor squared. To compensate, the density should increase by the scale factor or the gravitational field should increase so that the contact stress remains the same.

Water related phenomena, such as flow in soil normally occur in the laminar flow range. To properly scale this flow regime, the Reynolds number is used to establish scale factors. The use of this dimensionless number assumes that viscous forces in the permeant are dominant over gravity forces. On the other hand, external forces which cause flow often are dominated by gravity forces, such as ocean waves. In this case, the Froude number is the correct dimensionless number to establish scale factors. This basic conflict between the concurrent requirements for Froude and Reynolds number scale factors, gives rise to scaling problems in soil modelling. Table 1 shows scale factors used for the Froude and Reynolds

numbers.

To overcome some of the problems in soil modelling, a centrifuge can be used, where the model and soil mass are subjected to a simulated gravitational field by means of high speed rotation. Rowe (1975) states that the purpose of the centrifuge is to increase the self weight of the soil particles by the same proportion as the ratio of the dimensions of the prototype to the model. This results in an identical distribution of initial gravitational stress in the model and the prototype which in turn permits the application of structural boundary stresses equal in magnitude to those in the prototype. If the same soil and stress paths are used, both total and water pressures are properly scaled. Irrespective of the raised  $g$  field, a model undergoes much faster pore pressure changes by drainage than does the prototype. Similarity of consolidation time factors can be achieved using a pore fluid such as oil which has a high viscosity and by raising the frequency of cyclic forces, if required.

A discussion of water effects in geotechnical physical modelling was carried out by Goodings (1984). Scaling laws for various flow regimes were developed and compared. The basis for the discussion of laminar steady state seepage is Darcy's Law,

$$v=ki$$

(7)

where

v=discharge velocity

k=coefficient of permeability

i=hydraulic gradient

From this, scale factors for simple drainage for both lg and centrifuge models are developed. Goodings states that if prototype soil and permeants are used, permeability will be the same in model and prototype. As well, hydraulic gradient will be the same as long as all lengths are properly scaled. In a lg model, the above discussion implies that the time for drainage will be reduced by the scale factor, N, because:

$$\begin{aligned}t_m &= L_m/v \\ &= L_p/N * 1/v_p \\ &= t_p/N\end{aligned}\tag{8}$$

where:

subscript m applies to model

subscript p applies to prototype

t = time

L = length

v = velocity

If the model is subjected to an increase in self weight of N times, the boundary geometric conditions should remain the same; however, the boundary water pressures which cause the flow to occur and the resulting water pressure at all points will increase N times as a result of the increase in the self

weight of the permeant. These two effects combine to give the time scale for the centrifuge as

$$t_m = t_p/N^2 \quad (9)$$

Goodings (1984) also discusses seepage such as primary consolidation, liquefaction and groundwater surges. Terzaghi's theory of one dimensional consolidation is used to develop scaling relationships. The author states that for similarity in seepage rates, the dimensionless time factor,  $T_v$ , should be the same for both model and prototype,

$$(T_v)_p = (T_v)_m \quad (10)$$

where

$$T_v = C_v t/h^2$$

$C_v$  = coefficient of consolidation

$h$  = longest drainage path

$t$  = time

For the same soil in model and prototype subjected to the same stress history,  $(c_v)_m = (c_v)_p$ . Thus

$$(T_v)_m = (T_v)_p \quad (11)$$

which gives

$$t_m/t_p = 1/N^2 \quad (12)$$

Goodings concludes by stating that total similarity can't be

achieved simultaneously because of conflicts in the scale factors for various phenomena. Significant phenomena should be modelled in similarity and influences assumed to be secondary should be proven so.

### 3.0. EQUIPMENT

#### 3.1 Soil-Wave Tank

The wave tank for this experiment was adapted from an existing tank in which iceberg scour testing had previously been carried out. The concrete tank had a movable carriage on tracks for movement up and down its length. The tank measured 13.5 m by 2.8 m by 0.8 m, with 0.2 m thick walls. In this work the towing carriage was used during the beach reflection tests and as an instrumentation support.

The wavemaker was installed in the end of the tank as shown in Figure 1. A sloping beach up to the soil bed extended from the wavemaker. The soil bed was approximately five metres long with a beach of angular pebbles at the end to absorb wave energy and minimize reflection.

##### 3.1.1 Model Soil

The silt used in the model was obtained from a settling pond in a rock crushing plant in St. John's. The following tests were carried out in the laboratory (Morin and Cameron 1987): Atterberg limits, grain size, unidimensional consolidation, permeability, direct shear box and CIU triaxial tests. Soil grain size curves are given in Figure 3, the silt and Figure 4, the sand used in the berm construction. The silt was found to have a low Plasticity Index, with a Liquid Limit of 26%,

Plastic Limit 23 % and the Plasticity Index of 3 %.

The consolidation test was carried out on the silt at an initial water content of 38%. At this water content, the material was a viscous mud and was easy to place in the oedometer ring. Falling head permeability tests were carried out at the end of each load increment. Permeability was obtained from the slope of the head versus logarithm time curve and found to range from  $1.3 \times 10^{-9}$  m/s to  $3.1 \times 10^{-9}$  m/s. The results of the consolidation test are:

Compression Index:  $C_c = 0.12$

Coefficient of Consolidation:  $C_v = 8.4 \times 10^{-7}$  m<sup>2</sup>/s

Tangent Modulus:  $M = 34 * \sigma'_v$

$C_k = \Delta e / \Delta \log k = 0.52$

where  $e$  is the void ratio.

Morin and Cameron (1987) report that there is good agreement between the coefficient of consolidation calculated by Taylor's method and that determined from the modulus and permeability.

The silt material was frozen in 38 mm diameter cylinders prior to mounting in the triaxial testing equipment and allowed to thaw over night. Three samples were tested at consolidation pressures of 40, 70 and 120 kPa. The results of the test are summarized below.

Angle of internal friction:  $\phi' = 29.5^\circ$  (no cohesion intercept)

Pore Pressure Parameter at failure:  $A_r = 0.60$

Direct shear box tests were carried out on the material by Morin and Cameron (1987) and also as part of this experiment. The results obtained from shear box tests differed considerably from the triaxial tests, owing partially to the different stress paths and the difficulties encountered in mounting of the sample and maintaining the gap between the halves of the shear box during testing. The results are summarized below.

cohesion intercept :  $c' = 2 \text{ kPa}$

angle of internal friction:  $\phi' = 36^\circ$

### 3.1.2 Soil Installation

The soil was installed in the tank so that water could be drawn out from under the soil bed to aid in consolidation during the course of the experiment. To do this, a layer of 1 mm plastic was placed over the concrete bottom of the tank. On top of the plastic membrane was placed a series of plastic pipes at 300 mm intervals to provide an underdrain system. The pipes were covered with a geotextile and then the soil placed. The soil was mixed in a cement mixer by hand with water to form a thick slurry. During mixing, the lumps of soil were broken down as completely as possible. After mixing,

the slurry was screened to remove coarse particles.

The soil was transported to the wave tank in cement buggies and poured slowly down a chute through water to minimize air. The soil was allowed to consolidate under its own weight for approximately four months prior to instrumentation. At this time, shear strength of the silt, measured by a Pilcon Vane, ranged from 2 kPa to 10 kPa. The shear strength of the silt varied with depth, with top 10 mm layer ranging from 6 to 10 kPa, while at 100 mm it ranged from 2 to 6 kPa and from 4 to 12 kPa at 300 mm.

### 3.1.3 Wavemaker

The wavemaker, a flap type, was custom made for the project. The motor was capable of various speeds through a sliding pulley arrangement which allowed board frequency of from approximately 0.6 Hz. to 1.5 Hz. Wavemaker stroke could be varied from approximately 27 to 55 millimetres. This variation in both frequency and stroke allowed the generation of waves of different heights and frequencies as required for the testing program.

Considerable time was spent determining the characteristics of the board and the relationship between wavemaker stroke, frequency and wave height. Details of the wavemaker calibration are given in section 4.1.1.

### 3.2 Instrumentation

#### 3.2.1 Pore Pressure Measurement

Pore pressures were measured using buried piezometric stones connected to strain gauge pressure transducers by tubing, stainless steel in the soil and tank and plastic from there on to the transducer. Stones, tubing and transducers wells were saturated prior to use. The transducer-tubing connection was designed so that:

- (1) water could be drained from the buried piezometric stones;
- (2) water could be forced through the stones;
- (3) air could be drained from the entire system;
- (4) the transducers could be calibrated by a known head. The transducer/tubing connection, designated a cross is shown in Figure 5.

Pore pressures were measured at four locations as shown in Figure 6. A Druck miniature transducer was used for part of the data collection but failed during testing.

The pore pressure measuring equipment was calibrated initially by using the cross and a known head of water. During the experiments, it was calibrated by filling and emptying the tank. Details of system calibration are given in section 4.1.3.

The transducers were connected to a 10 channel instrumentation amplifier, which supplied power to the transducers, as well as amplifying the output signal.

### 3.2.2 Wave Probe

The wave probe was a custom made capacitance type and exhibited good linearity at all wave heights.

### 3.3 Data Acquisition

Output from the instrumentation amplifier was logged by a 3497 Hewlett Packard Data Logger and recorded on a Hewlett Packard FM instrumentation tape recorder. The data logger was controlled by a Hewlett Packard 86 computer. Computer programs were written to start the data logger, read approximately four seconds data, unpack it and store it on disc. The wave probe was operated from its own power supply and its signal was sent to the data logger and tape recorder as well.

The data acquisition system was capable of measuring at approximately 110 Hertz, giving a frequency of 22 Hertz per measuring device. Eighty points per channel were taken in during each run, giving a total run time of approximately four seconds. A program was written to examine the data using the HP graphics capability.

### 3.4 Similitude Considerations for Wave Tank Experiment

The Mobile Arctic Caisson (MAC) or Molikpaq, built by Gulf Resources Canada Inc. (GRCI) provided the basic dimensions and concept for the model in this project. (Rogers et al 1986). The Molikpaq consists of an octagonal steel annulus which supports a deck housing modular drilling and support equipment. The model was constructed in a cylindrical shape, rather than an octagon for ease of construction and to allow a closed form solution of the wave forces on the structure, if required (Figure 7).

The geometric scale chosen was 1:100 which allowed the generation of model waves with periods ranging from 0.8 to 1.7 seconds, corresponding to prototype periods of 8 to 17 seconds. Scale factors were derived from the Froude number, because of the dominance of gravity forces. The scale factors used are shown in Table 2.

Soil grain size was not scaled and fresh water at 20 degrees Celsius was used as the permeant resulting in a conventional 1g model without modification.

## 4.0 PROCEDURES

### 4.1 Calibration

#### 4.1.1 Wavemaker

Wavemaker response was investigated by operating it at 20 frequency-stroke combinations and measuring wave heights with a capacitance wave probe and a metal meter stick. The predicted and measured wave heights are shown in Table 3. Further discussion of the wavemaker is in Appendix 1.

#### 4.1.2 Wave Tank

The reflection coefficient of the beach was found to range from 8 to 10 percent. A detailed analysis of wave tank characteristics was not carried out in this project, as wave heights were measured directly.

#### 4.1.3 Pore Pressure Measuring Equipment

The transducers were calibrated using the apparatus shown in Figure 5. The response was found to be linear and consistent. The transducers were calibrated by noting the voltage at particular values of head and determining the slope of the curve of head against voltage to arrive at calibration factors to convert voltage to head. It was found that initial head on the transducer changed the response slightly. For example, if the tank was filled with water and then the calibration was done while emptying the tank, a higher value for the

calibration factor was obtained than for calibrating the tank during filling. This difference varied but ranged up 10% higher. The tank was to be filled during the tests, so the values with the tank initially full were used for calibration. As well, slightly higher calibration factors were found with the piezometric stones buried than on the soil bed surface.

These differences in calibration factors were likely due to variations in transducer response at the different initial heads.

#### 4.2 Soil Consolidation

The soil was placed in the tank as a slurry and allowed to consolidate under its own weight for approximately four months prior to testing. The soil bed had been underlain with a system of plastic tubing laid over the polyethylene layer. The plastic tubing was connected to a header and to a single line which was attached to an aluminum box which could be evacuated of air. By this method, it was thought that the consolidation process could be speeded up. Water would be drawn through the soil mass and cause consolidation and remove air in the soil as well.

For approximately one week, this was tried. A vacuum was placed on the consolidation box and water drawn through for six to eight hours per day. Settlement was monitored by a

settlement plate and after consolidation, the shear strength checked again. Approximately 1000 litres of water were removed from the soil but no change in the settlement plate or the shear strength was observed. Little or no additional consolidation of the soil took place, probably because soil had acquired structure during the initial placement which was stronger than the forces in the consolidation process.

Transducer burial depth for both cases is shown in Table 4 and Figures 6 and 8. The difference in burial depth noted is due to the sand core in the model, which was approximately 340 mm in depth. Transducer 3 was not buried under the model, so its depth of burial does not change.

#### 4.3 Model Installation

To simulate the prototype installation of the MAC, which is installed on a dredged sand berm, the model was placed on a sand berm on top of the model soil bed. The soil bed was covered with a geotextile so that the sand would not penetrate the soft silt. The berm was installed over a two day period to allow for some consolidation of the silt and profiles taken of the top of the model soil and top of the berm during installation by measuring down with a meter stick from a fixed point on the carriage of the wave tank. After the berm had been placed, the model was floated into place over the berm and ballasted with water. The centre core was then filled with

sand and again profiles taken of the top of the model soil. A total of 25 mm settlement took place beneath the centre of the model caisson during the time the model was in the tank.

#### 4.4 Wave Tank Tests

Tests series were run as follows:

- prior to placement of the sand berm, with the transducers on the surface of the soil bed
- prior to placement of the model, with the berm in place
- with model and berm in place
- with model and berm in place for an extended (one hour) test to monitor pore pressure build up at one wave height

For each test series, four frequencies and four wavemaker strokes were used to provide a series of wave heights and wave lengths. In total, 36 tests were carried out and the following parameters monitored and recorded:

- wave height
- pore pressure from the four pressure transducers

## 5.0 RESULTS AND ANALYSES

### 5.1 Data Conditioning

Data from the pore pressure transducers were noisy and had to be smoothed by a Fourier smoothing technique (Aubanel and Oldham 1985) before being analyzed. Noise sources were the building power supply, stray voltages from operating equipment and response characteristics of the transducers, which were operating at the low end of their response range and required high amplification. The frequencies of these noise sources were higher than those of the phenomena under investigation which were in the range of 0.6 to 1.2 Hertz. A Fourier transformation produces the frequency spectrum and these high frequencies can be eliminated. The inverse Fourier transform of the spectrum with the high frequency noise removed results in a smoothed data set. The degree of smoothing could be varied in the program and the minimum smoothing required to produce an acceptable output was used, so that relevant data were not lost. The best degree of smoothing was a trial and error procedure because a frequency range to eliminate could not be specified. The smoothing technique worked well although it would occasionally produce a straight line because of large spikes in the data. In this case, the degree of smoothing was reduced or the data examined to remove obvious outliers.

The data presented show the pressure wave in the soil bed, not the absolute value of pressure. To arrive at the pressure wave, the pressure at each transducer without waves was measured and subtracted from the pressures during wave loading. With the wavemaker turned off, data were collected for four seconds and the resulting voltages averaged to arrive at a voltage for the stillwater case. This voltage was then subtracted from the voltages collected during the wave loading and the pressure wave in the soil determined.

## 5.2 Experimental Results

### 5.2.1 Introduction

The experimental results are presented in this section. The Putnam-Liu solution was used to generate theoretical values for pore pressure in the soil bed. The limitations of this approach are discussed.

### 5.2.2 Bottom Pressure Wave

The bottom pressure wave was measured at four frequencies by placing the four transducers in a line perpendicular to the direction of wave travel directly beneath the wave probe. Linear wave theory was used to predict the magnitude of the bottom pressure wave. A typical unsmoothed example of transducer output is shown in Figure 9. The measured values were normalized by wave height and compared with those predicted by theory.

The results indicate that the linear wave theory accurately predicts the bottom pressure wave as shown in Table 5. At 0.63 Hz. and 0.81 Hz., the measured value is within 1% of the predicted value. At 1.0 Hz. and 1.15 Hz., the measured values vary from the predicted values up to 8%. This is likely because the lower frequency waves are closer in form to that predicted by linear wave theory. As the wave steepness increases with increased frequency and stroke, the wave form becomes less like a linear wave.

### 5.2.3 Pore Water Pressures

Pore pressure data from four pressure transducers were collected for four frequencies 0.63, 0.81, 1.0, 1.15 Hz. and four wavemaker strokes 27, 34, 41, and 48 mm for both cases, Model and No Model. To collect these data, the wavemaker was started and the waves allowed to stabilize for approximately five minutes. The data acquisition system was then started and approximately four seconds of data collected.

It should be noted that the data for transducer 4 may not be representative. When the piezometric stone and tubing were removed from the tank at the end of the experiment, the piezometric stone had separated from the end of the tubing.

#### 5.2.3.1 Measured and Theoretical Values - No Model

The smoothed pore pressure data were compared with theoretical

values generated by a computer program for the same wave height, frequency and soil depth based on the Putnam-Liu solution. Figures 10 to 17 show the measured and theoretical pore pressures plotted against wave height for the four frequencies used.

The graphs show that the measured and theoretical values are comparable for Transducers 1, 2 and 3, but the measured values are consistently low for Transducer 4.

In Figures 18 to 25 normalized depth in the soil bed is plotted against normalized pressure. Normalized pressure was determined by dividing the pressure at a particular transducer by the magnitude of the bottom pressure wave as measured by transducer 2, which was not buried. Normalized depth was determined by dividing the transducer burial depth by the total depth of the soil bed. The data for transducers 1 and 4 are presented separately from the data for transducer 3 because the theoretical pore pressure changes for transducer 3 as the water depth is different than for the other two transducers because transducer 3 was not buried in the sand berm. The results are summarized in Table 6.

In Figures 26 to 29, the actual and theoretical normalized pore pressure is plotted against frequency for each transducer.

Transducer 1 is shown in Figure 26. The lower frequency waves

(longer period and wave length) show the greatest pore pressure response to wave loading. The percentage of theoretical pore pressure response is as follows: 0.63 Hz - 86 %, 0.81 Hz - 72 %, 1.00 Hz - 88 % and 1.15 Hz - 139 %.

Transducer 2 is shown in Figure 27. The percentage of theoretical pore pressure response is as follows: 0.63 Hz - 95 %, 0.81 Hz - 89 %, 1.00 Hz - 64 % and 1.15 Hz - 71 %.

Transducer 3 is shown in Figure 28. The percentage of theoretical pore pressure response is as follows: 0.63 Hz - 98 %, 0.81 Hz - 135 %, 1.00 Hz - 141 % and 1.15 Hz - 161 %.

Transducer 4 is shown in Figure 29. The percentage of theoretical pore pressure response is as follows: 0.63 Hz - 37 %, 0.81 Hz - 33 %, 1.00 Hz - 27 % and 1.15 Hz - 43 %.

#### 5.2.3.2 Pore Pressure Build Up

To investigate pore pressure build up in the model soil and the berm with the model in place, the model was subjected to waves of 1.0 Hz. at a stroke of 27 mm for approximately 1 hour. Pore pressure and wave height data were collected every 3.5 minutes for four seconds. The total pore pressure, not just the amplitude of the pressure wave, was found for each transducer and the difference between the total pressures at each time interval found to determine pore pressure build

up. The results are shown in Figures 30 to 33.

It can be seen that there is no build up of pore pressure for transducers 1 and 3 located in the silt but there is a clear indication of pore pressure build up in transducer 2 located in the sand. Transducer 4, located in the sand, shows no evidence of pore water pressure build up.

#### 5.2.3.3 Phase Analyses-No Model

The wave probe output and transducer outputs for 16 cases, four strokes with four frequencies for each stroke are shown in Figures 34 to 81. Transducers 1, 2 and 4 were virtually in the same vertical plane perpendicular to the direction of wave travel while transducer 3 was located 1170 mm from 1, 2 and 4 in the direction of the beach. The wave probe was located 400 mm from transducers 1, 2 and 4 in the direction of the wavemaker.

To examine the relationship between the water waves and the pressure waves in the soil, phase lags between transducers 1, 2 and 4, transducer 3 and the wave probe were calculated using the theoretical wavelength for the given water depth and frequency. For example, for transducer 3, using the theoretical wave length of 2807 mm for a wave of 0.63 Hz. (period = 1.59 seconds) in a water depth of 0.43 m (at the wavemaker), the horizontal distance between the transducers

of 1170 mm represents a phase lag of  $1170/2807 * 1.59$  or 0.66 seconds. Similarly, the phase lag from the wave probe to transducers 1, 2 and 4 is  $400/2807 * 1.59$  or 0.23 seconds. Similar results can be found for the other frequencies and are summarized in Table 7.

The results for the sixteen frequency/stroke combinations are shown in Table 8.

General observations can be made about the phase analyses. Transducers 1, 2 and 4 respond in a specific order, depending on the frequency with a time lag between the response. Transducer 1 usually responds first, although it is the deepest and is in the silt, except at a frequency of 1.15 Hz., in which case transducer 4 responds first. In only one case does transducer 2 respond before the others, and that is at the lowest frequency and stroke combination of 0.63 Hz. and 27 mm.

The time lag between the wave probe response and the response of transducers 1, 2 and 4 is a function of the distance between the two measuring devices. The theoretical values agree reasonably well with the observed values for 0.63 Hz. and 1.00 Hz. with an average variation of 9% for 0.63 Hz. and 20% for 1.00 Hz. However, the observed values do not agree with the theoretical values for 0.81 Hz. and 1.15 Hz., although the results are consistent for each frequency for the four strokes used. The observed value for 0.81 Hz. is

about 3 times theory and about 2 times for 1.15 Hz.

#### 5.2.3.4 Phase Analyses-Model in Place

The wave probe output and transducer outputs for 16 cases, four strokes with four frequencies for each transducer is shown in Figures 82 to 126. The wave probe was located approximately 2300 mm ahead of the transducers 1, 2 and 4. The model caused a great deal of wave reflection, especially at higher frequencies, which can be clearly seen in the wave probe output plots. Also, transducer 3 was effectively blocked from the incident waves of the wavemaker and would receive a combination of waves diffracted around the model and reflected from the beach.

#### A: Wavemaker Stroke 27 mm

Figures 83 and 84 (0.63 Hz.) show a main peak at 0.84 seconds and secondary peak at 0.28 seconds (difference 0.56 seconds) for transducer 1, a main peak at 0.38 seconds and secondary peak at 0.94 seconds (difference 0.56 seconds) for transducer 2, 1.06 seconds for transducer 3 and main peak at 1.00 seconds and secondary peak at 1.66 seconds (difference 0.60 seconds) for transducer 4.

In Figure 82, the reflected wave from the model can clearly be seen, especially at 2.41 seconds with another minor peak at 2.94 seconds. The peak of the wave occurs at 2.75 seconds,

giving a time difference between the peak and the leading reflected wave of 0.31 seconds and between this secondary peak and previous main peak of 1.16 seconds and between the two minor peaks (2.94 and 2.41 seconds) of 0.53 seconds.

As the location of the wave probe is approximately 2300 mm (1.30 seconds) ahead of the transducers, a major transducer response should occur at approximately 1.22 seconds, the location of the first peak, plus 1.30 seconds, or 2.52 seconds. Transducer 1 shows a peak at 2.50 seconds, which is likely from this phenomena. The secondary peak in transducer 1 at 1.81 seconds is likely from the reflected wave, which can be seen in the wave probe plot at 0.7 seconds. Transducer 2 shows a secondary peak at 2.50 seconds, corresponding to the wave registering on the wave probe 1.30 seconds earlier.

It was observed that waves were reflected from the model and re-reflected to the wave board. Depending on the frequency and the distance between the wave maker and the model, a standing wave could have been created, resulting in waves up to twice the incident wave height. This phenomena is likely the cause of the peak at approximately 1.88 seconds in the output for transducer 2. It can be seen that transducer 3 is not subjected to this effect and shows no secondary peaks. The output for transducer 4 shows two peaks, a secondary one at 3.22 seconds and a major one at 2.53 seconds. This is

similar to the output of transducer 2, with a time difference between peaks of 0.69, identical to transducer 2, but shifted ahead in time by 0.72 seconds.

Transducer 3 is located 3470 mm, or 1.96 seconds, after the wave probe and a peak in the output should occur at approximately 3.21 seconds, as a wave peak occurs at 1.25 seconds. Examination of the plot for transducer 3 shows a peak at 2.63 seconds. This difference is likely due to the energy loss around the model and wave diffraction.

Figures 86 and 87 (0.81 Hz.) show a main peak at 0.84 seconds and secondary peak at 1.25 seconds (difference 0.41 seconds) for transducer 1, a main peak at 0.88 seconds and secondary peak at 1.31 seconds (difference 0.43 seconds) for transducer 2, 1.31 seconds for transducer 3 and main peak at 1.41 seconds and secondary peak at 1.94 seconds (difference 0.53 seconds) for transducer 4. Indications of the reflected wave can be seen in Figure 85, although they are not particularly large.

Figures 89 and 90 (1.00 Hz.) show a main peak at 1.41 seconds and secondary peak at 1.03 seconds (difference 0.38 seconds) for transducer 1, a main peak at 1.14 seconds and secondary peak at 1.49 seconds (difference 0.35 seconds) for transducer 2, 1.78 seconds for transducer 3 and main peak at 1.47 seconds and secondary peak at 1.96 seconds (difference 0.49 seconds)

for transducer 4.

In Figure 88, the reflected wave from the model can clearly be seen, especially at 0.94 seconds, 2.94 seconds and 3.01 seconds. The peak of the wave occurs at 1.31 seconds and 2.31 seconds, giving a time difference between the peak and the reflected wave of 0.37 seconds. This compares well with the time difference shown between the peaks and secondary peaks of transducers 1 and 2. Again, the response of transducers 1 and 2 are comparable to that at 0.63 Hz., with transducer 2 showing response out of phase to the wave.

Figures 92 and 93 (1.15 Hz.) show only main peaks in the data. This could be due to over smoothing or transducer response lag. All transducers show single peaks approximately 1.12 seconds apart, equal to the wave period.

B: Wavemaker Stroke 34 mm

Figures 95 and 96 (0.63 Hz.) show evidence of two peaks in the data, although it is not particularly clear because the transducer response is so small. In this case, transducers 1 and 2 appear to show similar response characteristics, with a peak followed by a secondary peak, unlike data at stroke 27 mm, where in transducer 1, the secondary peak preceded the peak. It is not evident where the reflected wave occurs in the wave probe plot, although it probably is just after the main peak, with another possible reflection approximately 0.31 seconds later.

Figures 98 and 99 (0.81 Hz.) clearly show two peaks in the

transducer data. Wave peaks appear at 0.28, 1.50 and 2.72 seconds, with probable reflections at 0.1 seconds, 1.31 seconds and 2.56 seconds. The differences between the peaks is 1.23 seconds the same as between the secondary peaks. The time lag between the wave probe and the transducers for this wavelength is 1.41 seconds, giving possible peaks responses at 1.69 and 2.92 seconds, with secondary response at 1.50 and 2.73 seconds. Transducer 1 shows two approximately equal peaks 0.47 seconds apart, with peaks at 1.94 and 2.41 seconds. Transducer 2 shows a peak at 2.04 seconds, with a secondary peak at 2.42 seconds. Transducer 4 shows a peaks at 1.25 and 2.50 seconds and secondary peaks at 1.91 and 3.16 seconds. It appears that there is a lag of approximately 0.45 seconds in all transducer response between theoretical and observed.

Figures 101 and 102 (1.00 Hz.) show only one peak in the transducer data, while the wave probe output plot clearly shows the reflected wave. It is possible that the frequency was such that the reflected wave was cancelled out when it reached the model. The response of transducer 4 is very low.

C: Wavemaker Stroke 41 mm

Figures 104 and 105 (0.63 Hz.) show equal peaks at 0.78 seconds and 1.38 seconds for transducer 1, peaks at 0.81 seconds and 2.25 seconds and secondary peaks at 0.46 and 3.00 seconds for transducer 2, a single peak at 1.38 and 3.00 seconds for transducer 3 and equal peaks at 0.84, 1.56, 2.28 and 3.19 seconds for transducer 4. The wave probe shows peaks

at 0.81 and 2.41 seconds, with the reflected wave appearing in the trough of the main wave at 0.22, 1.81 and 3.38 seconds. The time lag for this frequency is 1.30 seconds, giving a possible peak response at 0.52 and 2.11 seconds and secondary peaks at 1.52 and 3.11 seconds. It can be seen that the double peaks correspond approximately to the theoretical peak and secondary responses at 0.52 and 1.52 seconds for transducer 1, and the peak response of transducer 2 corresponds to the theoretical peak response of the wave at 2.11 seconds. Transducer 4 seems to lag behind the theoretical response.

Figures 107 and 108 (0.63 Hz.) show peaks at 0.78 seconds and 2.06 seconds for transducer 1 with secondary peaks at 0.31, 1.56 and 2.81 seconds, peaks at 0.34, 1.59 and 2.28 seconds and secondary peaks at 0.78, 2.03 and 3.28 seconds for transducer 2, a single peak at 0.91 and 2.16 seconds for transducer 3 and peaks at 0.91, 2.19 and 3.41 and secondary peaks at 1.44 and 2.69 seconds for transducer 4. The wave probe shows peaks at 1.06 and 2.28 seconds, with the reflected wave at 0.80, 2.03 and 3.25 seconds. The time lag for this frequency is 1.41 seconds, giving a possible peak response at 1.24 and 2.47 seconds and secondary peaks at 0.98 and 2.21 seconds. Transducer 1 shows peaks at 0.78 and 2.06, corresponding approximately to the reflected wave, while transducers 2 and 4 lag behind the peak response by 0.34 seconds.

Figures 110 and 111 (1.00 Hz.) show only one peak in the transducer data, while the wave probe output plot clearly shows the reflected wave. It is possible that the frequency was such that the reflected wave was cancelled out when it reached the model.

Figures 113 and 114 (1.15 Hz.) are presented to show that at this frequency and stroke, the waves are non uniform with varying amplitude and mixing of the reflected wave from the model and the incident wave. The transducer responses show similar trends as the wave.

D: Wavemaker Stroke 48 mm (Figures 115-126)

These data show similar results as for previous data sets, but the non uniformity of the waves make the analyses difficult. They are presented for information only.

5.2.3.5 Comparison of Results - Soil Bed Alone and Model in Place

The assumptions used and the boundary conditions imposed do not allow the use of the Putnam-Liu solution with a structure in or on the soil bed. To get some indication of the effect of the model on the pore pressure the two cases, model in and model out were compared.

The magnitudes of the pore pressure readings differ between the two cases. In most cases, the pore pressure is less under the model than in the soil bed alone. Also, measurements made

in the soil bed alone show that the pore pressure wave oscillates around zero, as would be expected if no pore pressure had built up. With the model in the tank, variations in this trend are seen as discussed below.

For example, comparing transducer response with and without the model at the 0.63 Hz. and 27 mm stroke, the following can be seen. The wave probe traces are similar, although the wave is approximately 10 % smaller for the case Model Installed. (Figures 34 and 82.) Both waves are slightly elevated; that is, the crests are higher the stillwater level than the troughs are below. Transducer 1 shows an amplitude of approximately 60 Pa with no offset, while with the model installed, the amplitude is approximately 18 Pa with an offset of +34 Pa. Similarly transducer 2 has an amplitude of 130 Pa with no offset, while with the model installed the amplitude is 36 Pa with an offset of +10 Pa. Transducer 3 has an amplitude of 100 Pa with no offset while with the model installed, the amplitude becomes 150 Pa with an offset of +24 Pa. For transducer 4, the amplitude is 26 Pa with no offset while with the model installed, the amplitude is 8 Pa with an offset of +13 Pa.

A comparison of the wave probe outputs for the two cases at 0.81 Hz and a stroke of 27 mm shows that the waves are different in magnitude. In Figure 37 the wave is 44 mm while in Figure 85, the wave is 60 mm in height. Comparing the

transducer outputs, transducer 1 has an amplitude of 35 Pa with an offset of +5 Pa while with the model in, the amplitude is 10 Pa with an offset of +35 Pa. Transducer 2 shows an amplitude of 135 Pa with an offset of +5 Pa while with the model, the amplitude is 25 Pa with an offset of +9 Pa. Transducer 3 shows an amplitude of 90 Pa with no offset while with the model the amplitude is 63 Pa with an offset of +21 Pa. Transducer 4 shows an amplitude of 30 Pa with no offset, while with the model, the amplitude is 3 Pa with an offset of +13 Pa.

The next set of data to compare is that at a frequency of 1 Hz and a stroke of 27 mm. Figures 40 and 88 show the wave forms which in this case are much different. Figure 40 shows a wave of 60 mm with equal portions above and below the stillwater level and a smooth form, while Figure 88 shows clearly the reflected wave from the model and a magnitude of 38 mm. Transducer 1 shows an amplitude of 25 with no offset while with the model in, the amplitude of the wave is 40 Pa with an offset of +45 Pa. Transducer 2 shows an amplitude of 125 Pa with no offset, while with the model in the amplitude is 25 Pa with an offset of +12 Pa. Transducer 3 shows an amplitude of 75 Pa with no offset, while with the model in, the amplitude is 90 Pa with an offset of +25 Pa. Transducer 4 shows an amplitude of 20 Pa with no offset, while with the model in, the amplitude is 9 Pa with an offset of +14 Pa. Comparing 1.15 Hz. and 27 mm stroke, the wave probe outputs

are again different. Figure 43 shows the wave at 66 mm, with 36 mm above the stillwater and 30 below, while Figure 91 shows a wave with two distinct peaks, and with a magnitude of 46 mm, 10 mm above the stillwater level and 36 below the stillwater level. Transducer 1 shows an amplitude of 22 Pa with no offset, while with the model in the amplitude is 18 Pa with an offset of +74 Pa. Transducer 2 shows an amplitude of 80 Pa with no offset, while with the model in, the amplitude is 24 Pa, with an offset of +11 Pa. Transducer 3 shows an amplitude of 37 Pa with no offset, while with the model in the amplitude is 25 Pa with an offset of +43 Pa. Transducer 4 shows an amplitude of 18 Pa with no offset, while with the model in, the amplitude is 6 Pa with an offset of +13 Pa.

The next series of data with stroke of 34 mm and frequency of 0.63 Hz. are compared in Figures 46 and 94. The wave forms are similar with the model in case showing some indications of the reflected wave. The wave height in Figure 46 is 48 mm with an equal crest and trough, while with the model is 32 with an 18 mm crest and 14 mm trough. Comparing the output for transducer 1, in the soil bed alone the amplitude is 90 Pa with an offset of +10 Pa, while with the model in, the amplitude is 15 Pa with an offset of +15 Pa. Transducer 2 shows an amplitude of 190 Pa with an offset of +30 Pa, while with the model in the amplitude is 32 Pa with no offset. Transducer 3 shows an amplitude of 130 Pa with no offset,

while with the model in the amplitude is 160 Pa with an offset of +10 Pa. Transducer 4 has an amplitude of 45 Pa with no offset, while with the model in, the amplitude is 8 Pa with an offset of +4 Pa.

At 0.81 Hz, the wave height is 50 mm with equal crest and trough, while with the model in the wave height becomes 80 mm, again with equal crests and troughs. Transducer 1 shows an amplitude of 50 Pa with no offset, while with the model in, the amplitude is 13 Pa with an offset of +19 Pa. Transducer 2 shows an amplitude of 160 Pa with no offset, while with the model in the amplitude is 36 Pa with an offset of +4 Pa. Transducer 3 shows an amplitude of 120 Pa with no offset, while with the model in, the amplitude is 85 Pa with an offset of +15 Pa. Transducer 4 has an amplitude of 37 Pa with no offset, while with the model in, the amplitude is 9 Pa with an offset of +9 Pa.

Comparing Figures 52 and 100 for frequency of 1.00 Hz and stroke of 34 mm, it can be seen that the wave forms and heights are quite different. In Figure 52, the wave height is 84 mm, with a crest of 48 mm and a trough of 36 mm with a smooth wave form, while in Figure 100, the reflected wave can clearly be seen, and the wave height is 42 mm with a 22 mm crest and 20 mm trough. Transducer 1 has an amplitude of 35 Pa with no offset, while with the model in, the amplitude is

12 Pa with an offset of +84 Pa. Transducer 2 shows an amplitude of 165 Pa with no offset, while with the model in, the amplitude is 8 Pa, with an offset of +8 Pa. Transducer 3 has an amplitude of 100 Pa with no offset, while with the model in the amplitude is 75 Pa, with an offset of +35 Pa. Transducer 4 shows an amplitude of 32 Pa with no offset, while with the model in, the amplitude is 3 Pa with an offset of +12 Pa.

The data set for 1.15 Hz and stroke of 34 mm could not be smoothed, so the next comparison will be made of Figures 58 and 103 at 0.63 Hz and 41 mm. In Figure 58 the wave form is smooth and has a height of 60 mm with equal crest and trough. Figure 103 shows a spiky wave form in which a number of different reflected waves can be seen and with a height of 40 mm, with a crest of 27 mm and a trough of 12 mm. Transducer 1 has an amplitude of 110 Pa with an offset of +7 Pa, while with the model in the amplitude is 20 Pa with an offset of +25 Pa. Transducer 2 shows an amplitude of 245 Pa with an offset of +25 Pa, while with the model in, the amplitude is 40 Pa with an offset of +5 Pa. Transducer 3 shows an amplitude of 132 Pa with an offset of +17 Pa, while with the model in the amplitude is 215 Pa, with an offset of +35 Pa. Transducer 4 shows an amplitude of 55 Pa with no offset, while with the model in, the amplitude is 4 Pa with an offset of +20 Pa. Comparing the data at 0.81 Hz. and stroke 41 mm, the wave

height is 66 mm with a 36 mm crest and 30 mm trough compared to a height of 88 mm with equal crest and trough with the model installed. Transducer 1 shows an amplitude of 50 Pa with no offset while with the model installed the amplitude is 22 Pa with an offset of +20 Pa. Transducer 2 shows an amplitude of 190 Pa with no offset, while with the model in, the amplitude is 45 Pa with an offset of +15 Pa. Transducer 3 shows an amplitude of 180 Pa with no offset, while with the model installed the amplitude is 85 Pa with an offset of +35 Pa. Transducer 4 shows an amplitude of 46 Pa with no offset, while with the model installed the amplitude is 10 Pa, with an offset of +10 Pa.

Comparing Figures 64 and 109 at 1 Hz, it can be seen that the wave forms are different, with the reflected wave showing up clearly in Figure 109. The wave height in Figure 64 is 100 mm, with a crest of 60 mm and a trough of 40 mm. Transducer 1 shows an amplitude of 40 pascal with no offset, while with the model installed, the amplitude is 16 Pa with an offset of +75 Pa. Transducer 2 shows and amplitude of 190 Pa with no offset, while with the model installed, the amplitude is 25 Pa with an offset of +25 Pa. Transducer 3 shows an amplitude of 120 Pa with no offset while with the model in, the amplitude is 85 Pa, with an offset of +55 Pa. Transducer 4 shows an amplitude of 38 Pa with no offset, while with the model installed the amplitude is 7 Pa with an offset of +50 Pa.

At 1.15 Hz and stroke 41 mm, Figures 67 and 112 are compared. The wave form in Figure 112 is very irregular, as the heights of the crests and the troughs are unequal during the sampling. These data are presented for information only and will not be analyzed. Similarly, the data for all frequencies at stroke 48 mm are presented for information. The irregularity of the wave forms with the model installed make comparison difficult with the case soil bed alone.

### 5.3 Discussion

#### 5.3.1 Pore Water Pressures - No Model

In order to understand some of the phenomena occurring, it is useful to refer to the general theories for pore pressure response by Yamamoto(1978) and Madsen(1978). As discussed in the literature review, the Putnam-Liu solution and Moshagen and Torum model are limiting cases of these more general theories. When the stiffness of the porous medium is much smaller than that of the pore fluid, such as is the case for saturated soft soils, Yamamoto predicts that the bed response becomes independent of permeability and has no phase lag. The pressure response approaches the Putnam-Liu solution for a rigid bed and incompressible pore fluid and the solution by Prevost et al(1975) for an elastic continuum without pore fluid. On the other hand, if the stiffness of the porous medium is much larger than that of the pore fluid, such as for partially saturated dense sands, the pressure response

approaches the solution of Moshagen and Torum for a rigid porous bed and compressible pore fluid. The pressure then attenuates rapidly and the phase lag increases linearly as the distance from the bed surface.

The use of the Putnam-Liu solution to predict pore water pressures in this experiment is limited by a number of factors. The Putnam-Liu solution assumes a homogeneous saturated soil bed, while the physical model was composed of a two layer soil system, separated by a geotextile. As well, the sand may not have been saturated. The silt had been in the tank for 4 months and had been subjected to a vacuum for a week in an attempt to consolidate it, so it is reasonable to assume that the degree of saturation was close to 100%. On the other hand, the sand had been in the tank for less than one month and could have been less than totally saturated.

This may help to explain some of the observations. Transducer 1 usually responded prior to transducers 2 and 4. These results are not consistent with the more general theories or the simple Putnam-Liu solution. If there was phase lag in the response with depth, then the order of response should be 2, 4 and then 1, which was never observed. If there was no phase lag with depth, then the transducers would likely respond together. It is likely that the sand was unsaturated causing a phase lag in transducers 2 and 4. In the saturated silt,

however, there was no phase lag. Also transducers 2 and 4 show larger pressure attenuation than transducers 1 and 3 which would be the case if the sand was not fully saturated.

### 5.3.2 Pore Water Pressures - Model

Comparison of the data for the soil bed alone and the model installed reveals some unusual features. With the model installed, there is an elevation of pore pressure for all the transducers. This axis shift, which is always positive, varies from a few Pa to up to 84 Pa, but appears to be consistent for each transducer with transducer 1 the largest with an average shift of 43 Pa, transducer 3 - 30 Pa transducer 4 - 16 Pa and transducer 2 - 13 Pa. The reasons for this shift are not clear, but it is noted that the largest shifts occur in the transducers in the silt, 1 and 3 and the smallest shifts are in the sand, transducers 2 and 4. Also, the shift occurs only with the model in the tank, so it is reasonable to infer that the model influences the shift in some manner, although a shift in transducer 3 would not be expected because the model was not placed over it. However, a change in the water level due to a standing wave between the model and the wavemaker could have raised the water surface and caused an increase in the pore pressure due to the increase in hydrostatic head. The overall increase in head for transducer 3 would be in the order of 3 mm (30 Pa). There is some indication in the wave probe data that this was taking

place. Overall, the crests are larger than the troughs, although it is not possible to quantify a relationship between a large positive shift in pore pressure and increase in water elevation. Also if this was taking place it would be expected that all transducers would show similar shifts. A possible explanation for this discrepancy, however, could be the effect of the model in damping out pore pressure response directly beneath it from the wave loading. It could effectively isolate transducers 2 and 4 from the wave environment to a greater degree than transducers 1 and 3. The loss of wave energy around the model could explain why transducer 1 shows a larger shift than transducer 3.

During wave loading, the model did move and oscillate in response to the wave loading. It is possible that the rocking of the relatively stiff model and sand core/berm unit over the softer silt caused a change in the stress state in the silt leading to the shift in measured pore pressure.

### 5.3.3 Pore Pressure Build Up

Liquefaction occurs when excess pore water pressure exceeds the overburden weight, causing the soil to lose all shear resistance and act like a liquid. Excess pore water pressures will dissipate by drainage but can build up under cyclic loading because drainage is not complete before the next cycle. Residual pore water pressures caused by cyclic wave action are generally determined by the Seed (1977) method to

take into account the degradation in shear and bulk moduli with increasing pore water pressure. The degradation of the moduli has a significant effect on both the levels of pore water pressure and the possible depth of liquefaction. In this experiment, no attempt was made to predict pore pressure build up because of the complexity of the method and lack of required geotechnical data.

However, it is well established that sands are particularly susceptible to pore pressure build up, both from earthquake loading and wave loading. The susceptibility is based on a number of factors including density, void ratio, number of applied cycles and permeability. If the sand is highly permeable, then pore pressures will dissipate as rapidly as they are formed. Below a critical permeability, pore pressures will not build up under wave loading because of the limited seepage. There does not appear to be a good definition of this permeability range because of the complexity of the phenomena, although Demars(1980) suggests the range above which excess pore water pressures will dissipate as rapidly as they are formed is a medium coarse silt.

In this experiment, the increase in pore water pressure at transducer 2 was approximately 65 Pa in 65 minutes or an average of 1 Pa per minute. The hydrostatic pore water pressure due to position in the sand core at transducer 2,

340 mm below the stillwater level is 3300 Pa. The increase in pore water pressure is about 2 % of the hydrostatic, so the soil was still quite stable and not near liquefaction. It is possible that additional wave loading would have resulted in more build up.

#### 5.3.4 Similitude Considerations

As the model testing was carried out at 1g, it is not possible to accurately predict all aspects of prototype behaviour. The wave heights, periods, wavelengths, water depth, model size and berm dimensions were all scaled properly at a scale of 1:100. For example, the frequency range, 0.63 Hz. to 1.15 Hz., (period ranging from 1.6 seconds to 0.87 seconds) corresponds to waves with 16 to 8.7 second periods, which are found in the Beaufort Sea at a Froude time scale of 1:10. As well, the water depth of 0.43 m (43 m prototype) is within the range of depths in which such caisson structures are deployed. On the other hand, water related phenomena, which were a key part of this experiment, were not scaled properly, and it would not be possible to make any quantitative predictions on prototype behaviour based on the results of this experiment.

#### 5.3.5 Comparison with Other Experimental Work

Liu(1985) considered wave induced pore pressures under a caisson with a continuous bottom. The results of his work are compared with these experimental results, noting that

there are some differences between the two cases. The physical model used in this work consisted of two concentric cylinders connected on the bottom, with a sand core, while Liu(1985) considered a continuous bottom. As a result, the boundary conditions change and the solution of the velocity potential would result in different expressions for the pore pressure field at the caisson bottom in each case. Also, no upward seepage is allowed in Liu(1985) while seepage would take place in the sand core in this experiment.

Liu(1985) defines a pressure coefficient,  $C_p = p/P_o$ , where  $P_o$  is the wave induced dynamic pressure on the sea bottom and  $p$  is the pore water pressure. He presents graphs of  $C_p$  as a function of the distance,  $x/B$ , measured from the front toe of the structure, where  $B$  is the caisson width. He shows a number of plots, using  $kB$ , the wave number times the caisson width and  $d/B$ , soil depth divided by caisson width as parameters.  $C_p$  was calculated and the results shown in Table 9.

The trend in these results are similar to Liu(1985) in that with increasing frequency, the parameter  $C_p$  increases. Cheng and Liu(1986) compared experimental results of pore pressure measurements with those predicted by the Putnam-Liu solution and a poroelastic solution and found that the Putnam-Liu solution over predicted pore water pressure response, the

7

poroelastic solution gave results that agreed more with lab data and as frequency increased, the agreement with lab data gets poorer.

The results of this experiment show that the Putnam-Liu solution tends to over predict the pore pressures, as shown in Table 10. The ratios shown in the Table are the pore pressure predicted by the Putnam-Liu solution divided by the measured pore pressures without the model in place.

For the transducers located in the silt, the Putnam-Liu solution over predicts at the lower frequencies and under predicts at the higher frequencies, which is opposite to what Cheng and Liu(1986) found. As the frequency decreases, the agreement with the Putnam-Liu solution becomes better.

## 6.0 CONCLUSIONS AND RECOMMENDATIONS

### 6.1 Conclusions

1. Linear wave theory accurately predicted the magnitude of the bottom pressure wave.
2. The Putnam-Liu solution to Darcy's law, which was used to estimate pore pressures in this experiment, does not account for soil properties, and is a limited form of a more general solution to this type of problem.
3. In the sand, the measured pressures were lower than predicted and showed a phase lag. This was likely due to a small amount of air in the sand.
4. In the silt, the measured pressures were generally higher than predicted and did not show a phase lag.
5. The soil wave tank performed well in the experiment, except for some minor instrumentation problems. The pressure transducers were not the best choice for measuring the very small pressure changes observed and the piezometric stones used were not robust enough to stand up to the long testing period.
6. The model was too large for the wave tank. It caused a

great deal of reflected wave energy and obscured the data .

7. The transducer located in the sand core indicated build up of pore pressure over time. There was no build up of pore pressure noted in the silt.

#### 6.2 Recommendations

1. If further work is to be carried out in the soil-wave tank, it would be useful to carry out a study to define the operating characteristics of the system, particularly the reflection coefficient of the beach as a function of frequency and stroke and the wavemaker characteristics.

2. It is difficult and potentially dangerous to change the stroke of the wavemaker because of the potential for the wavemaker to collapse. A better method to do so should be designed.

3. As part of recommended wave tank operating study, the maximum model size should be investigated.

4. More robust instrumentation should be used to measure pore pressures. The piezometric stones were not strong enough to stand up to the rigors of being buried and subjected to long term wave loading. The Druck miniature pore pressure transducer may be the best choice for this type of work.

TABLE 1

Scale Factor Comparison for Froude and Reynolds Numbers

	<u>Reynolds</u>	<u>Froude</u>
Time	$1/N^2$	$1/N$
Velocity	$N$	$1/N$

where  $N$  is the geometric scale factor

TABLE 2

Scale Factors Used Based on the Froude Number

Length	1:100
Velocity	1:10
Time	1:10
Stress/Pressure	1:100

TABLE 3

## Comparison of Actual and Theoretical Wave Heights

<u>F(hz)</u>	<u>S</u>	<u>Hr</u>	<u>Hp</u>	<u>Ht</u>	<u>Ht/Hp</u>
0.63	27	28	27	41	1.48
0.63	34	39	37	52	1.41
0.63	41	47	45	63	1.40
0.63	48	55	56	74	1.32
0.63	55	85	65	84	1.29
0.81	27	42	40	60	1.50
0.81	34	55	55	75	1.36
0.81	41	67	67	91	1.36
0.81	48	77	86	106	1.23
0.81	55	90	100	122	1.22
1.00	27	45	40	75	1.88
1.00	34	75	66	95	1.44
1.00	41	83	78	114	1.46
1.00	48	90	89	134	1.51
1.00	55	110	106	153	1.44
1.15	27	68	68	83	1.22
1.15	34	90	86	105	1.22
1.15	41	110	103	126	1.22
1.15	48	115	106	148	1.40
1.15	55	140	124	169	1.36

Hr = height measured by ruler. Ht = theoretical height.

Hp = height measured by wave probe. S = stroke.

All dimensions in millimetres.

TABLE 4Burial Depth of Transducers (m)

<u>Transducer</u>	<u>With Model</u>	<u>No Model</u>
1	0.611	0.377
2	0.340	0.000
3	0.162	0.162
4	0.425	0.192

TABLE 5Actual and Theoretical Bottom Pressures

<u>Freq. (Hz)</u>	<u>Po/Hp(Ac)</u>	<u>Po/Hp(Th)</u>	<u>Diff(%)</u>
0.63	6.90	6.84	+0.9
0.81	5.16	5.20	-0.8
1.00	3.18	3.40	-6.5
1.15	2.36	2.18	+8.3

TABLE 6

## Comparison of Actual and Theoretical Pore Pressures

F(hz)	S(mm)	No Model				Model			
		Tr1	Tr2	Tr3	Tr4	Tr1	Tr2	Tr3	Tr4
0.63	27	3.10	6.59	4.87	1.44	1.81	2.08	8.89	0.69
0.63	34	2.58	6.96	5.44	2.31	0.76	1.88	9.91	0.27
0.63	41	3.48	8.42	4.63	2.03	1.67	2.05	11.0	0.87
<u>0.63</u>	48	3.74	7.69	6.23	1.83	0.78	1.21	2.44	0.79
Avg.		3.23	7.42	5.29	1.90	1.01	1.81	8.07	0.66
Theo.		3.74	7.79	5.38	5.08				
0.81	27	1.80	6.09	4.23	1.14	1.08	0.88	2.00	0.40
0.81	34	1.25	6.11	4.84	1.00	0.45	0.75	2.06	0.23
0.81	41	1.68	5.59	4.47	1.28	0.54	1.13	2.44	0.65
<u>0.81</u>	48	1.46	5.92	4.81	1.20	1.20	2.34	1.96	0.88
Avg.		1.55	5.93	4.59	1.16	0.82	1.28	2.12	0.54
Theo.		2.14	6.64	3.41	3.50				
1.00	27	0.97	2.31	2.26	0.48	2.31	1.21	4.51	0.77
1.00	34	1.00	3.90	2.68	0.50	3.91	0.75	3.20	0.61
1.00	41	0.74	3.76	2.23	0.68	2.38	0.87	1.83	1.59
<u>1.00</u>	48	0.81	3.32	2.46	0.60	0.85	1.23	1.95	1.69
Avg.		0.88	3.32	2.41	0.57	2.36	1.02	2.87	1.17
Theo.		1.00	5.16	1.71	2.13				
1.15	27	1.00	2.62	1.46	0.62	3.26	0.93	1.96	0.59
1.15	34	0.53	2.64	1.03	0.57	3.68	0.61	1.42	0.95
1.15	41	0.63	3.05	1.44	0.55	0.92	0.34	0.96	0.26
<u>1.15</u>	48	0.55	3.13	1.42	0.55	1.99	1.88	3.04	2.42
Avg.		0.68	2.86	1.34	0.57	2.46	0.94	1.85	1.06
Theo.		0.49	4.03	0.83	1.32				

where F = frequency(Hertz), S = wavemaker stroke(mm)

Note that all pore pressures have been divided by wave height.

TABLE 7

Phase Lag between Wave Probe and Transducers (sec)

	0.63 Hz.	0.81 Hz.	1.00 Hz.	1.15 Hz.
Wave Probe to Tr. 1, 2 and 4	0.23	0.24	0.27	0.30
Wave Probe to Tr. 3.	0.89	0.94	1.06	1.18
Tr. 1, 2 and 4 to Tr. 3	0.66	0.72	0.80	0.88

TABLE 8

Transducer and Wave Probe Peak Response Times (sec)

<u>Figures</u>	<u>Tr#1</u>	<u>Tr#2</u>	<u>Tr#3</u>	<u>Tr#4</u>	<u>WP</u>
34, 35, 36	1.57	1.56	2.20	1.59	1.36
37, 38, 39	1.31	1.37	2.00	1.44	0.60
40, 41, 42	0.53	0.59	1.28	0.52	0.34
43, 44, 45	0.81	0.91	1.70	0.91	0.16
46, 47, 48	0.81	0.81	1.50	1.00	0.62
49, 50, 51	1.19	1.22	1.88	1.25	0.50
52, 53, 54	0.84	0.88	1.63	0.88	0.65
55, 56, 57	1.06	1.09	1.86	1.03	0.41
58, 59, 60	0.72	0.72	1.25	0.72	0.46
61, 62, 63	0.91	0.91	1.56	0.92	0.19
64, 65, 66	0.91	0.94	1.67	0.94	0.89
67, 68, 69	0.34	0.38	1.19	0.31	0.62
70, 71, 72	0.41	0.44	1.03	0.53	0.23
73, 74, 75	0.56	0.59	1.22	0.63	1.14
76, 77, 78	0.31	0.36	1.13	0.41	0.09
79, 80, 81	1.16	1.17	1.95	1.13	0.58

Tr = Transducer

WP = Wave Probe

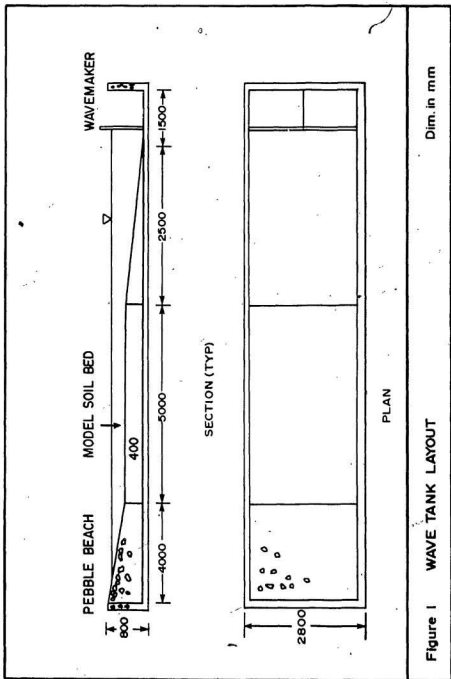
TABLE 9

Comparison of Pressure Coefficient with Liu(1985)

<u>Freq(Hz)</u>	<u>kB</u>	<u>C<sub>p</sub>(Liu)</u>	<u>C<sub>p</sub>(my work)</u>
0.63	1.96	0.36	0.28
0.81	1.85	0.37	0.18
1.00	1.33	0.43	0.28
1.15	1.04	0.47	0.34

TABLE 10  
Comparison of Results with Cheng and Liu(1986)

	<u>0.63 Hz</u>	<u>0.81 Hz</u>	<u>1.00 Hz</u>	<u>1.15 Hz</u>
Trans 1 (Silt)	1.2	1.4	1.0	0.9
Trans 3 (Silt)	1.1	0.8	0.8	0.7



Dim. in mm

Figure 1 WAVE TANK LAYOUT

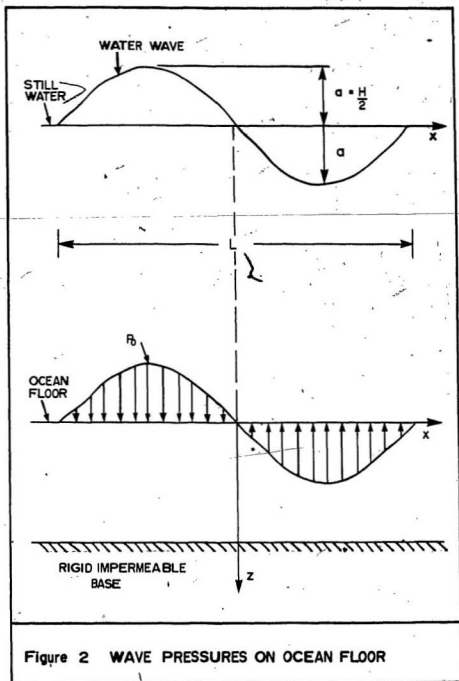
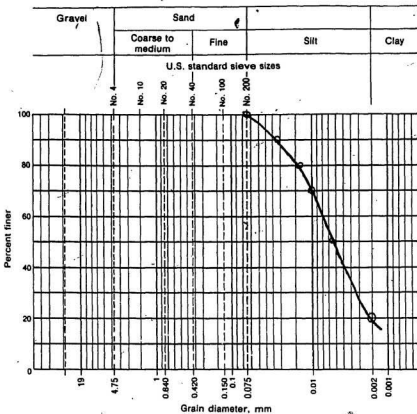


Figure 2 WAVE PRESSURES ON OCEAN FLOOR

**GRAIN SIZE DISTRIBUTION**

Data Sheet 6

Project Soil-Wave Tank Job No. \_\_\_\_\_  
 Location of Project MUN Boring No. WT1-86 Sample No. 0-3  
 Description of Soil Lundrigan Silt Depth of Sample \_\_\_\_\_  
 Tested By Cameron Date of Testing 86-09-23



Visual soil description \_\_\_\_\_

Soil classification: \_\_\_\_\_  
 System \_\_\_\_\_

FIGURE 3



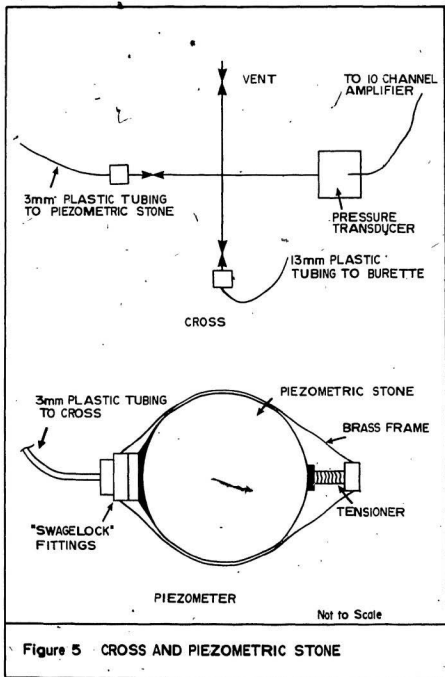
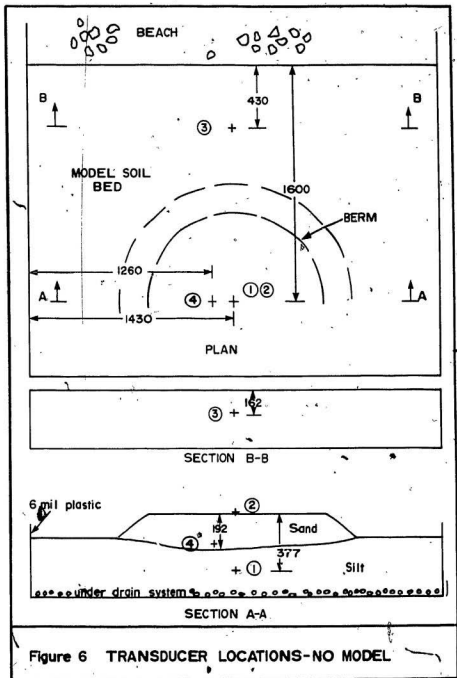


Figure 5 CROSS AND PIEZOMETRIC STONE



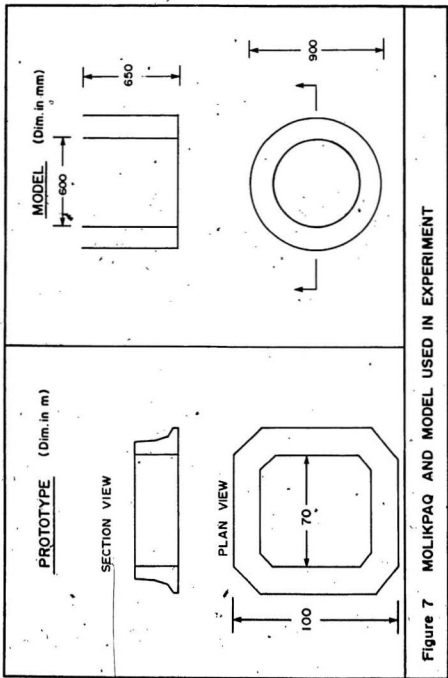
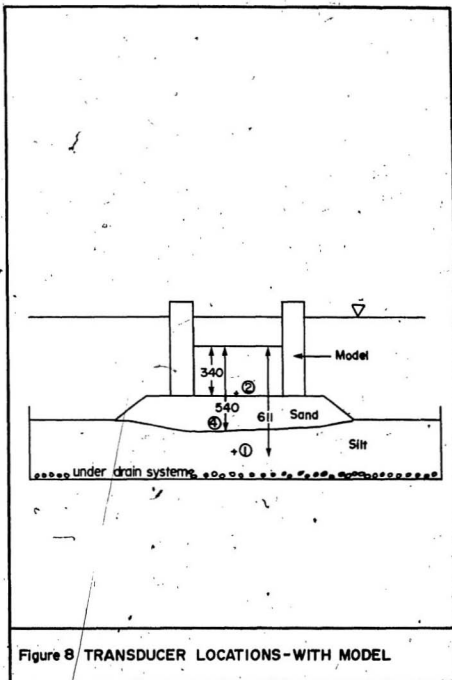
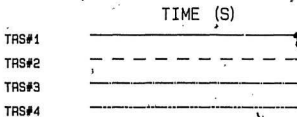
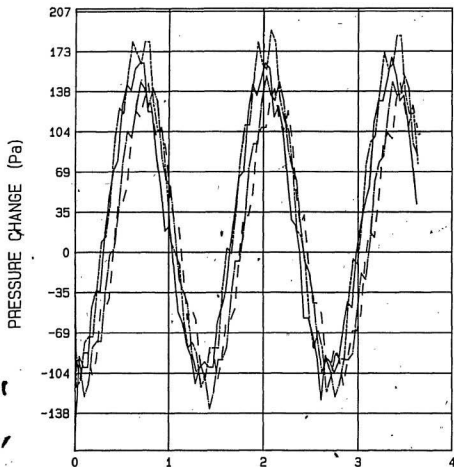


Figure 7 MOLIKAQ AND MODEL USED IN EXPERIMENT





F=0.63 Hz. S=27 mm.

Figure 9.

Figure 10 - Trans. 1 and 3. - 0.63 Hz.

Actual and Theoretical Pore Pressures

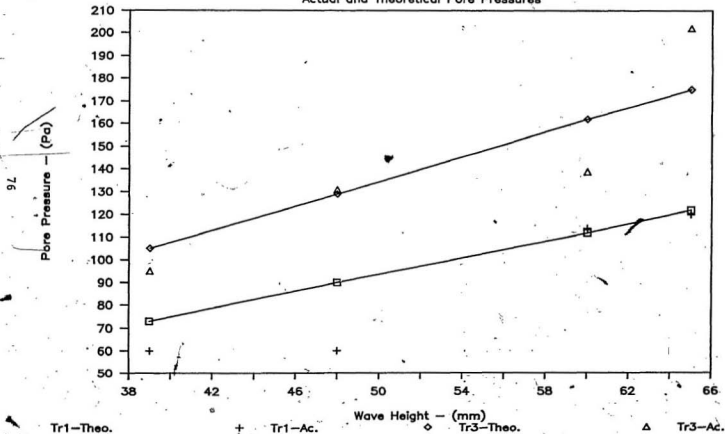


Figure. 11 - Trans. 2 and 4. - 0.63 Hz.

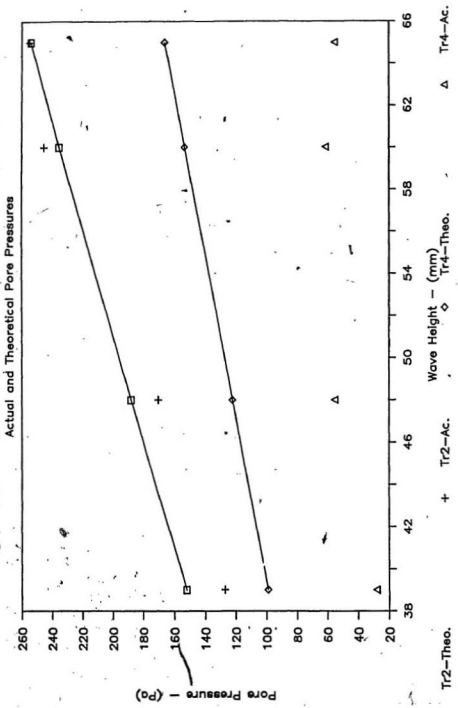


Figure 12 - Trans. 1 and 3. - 0.81 Hz.

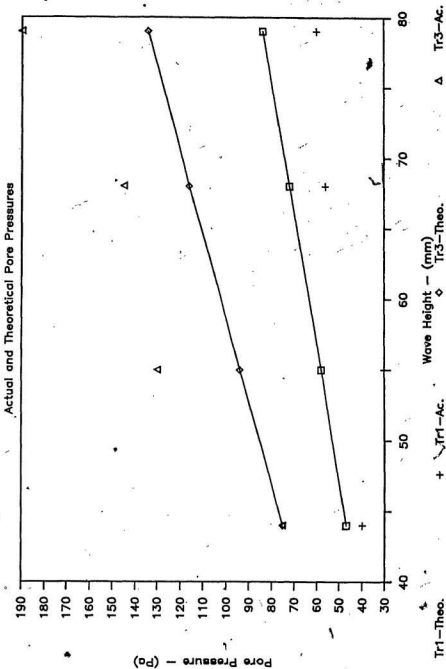


Figure 13 - Trans. 2 and 4. - 0.81 Hz.

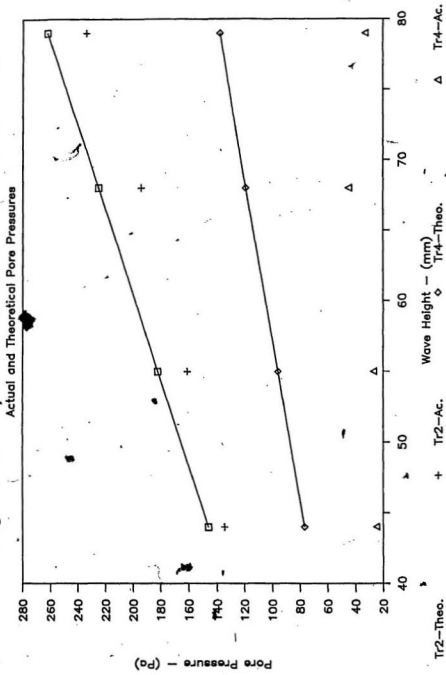


Figure 14 - Trans. 1 and 3. - 1.00 Hz.

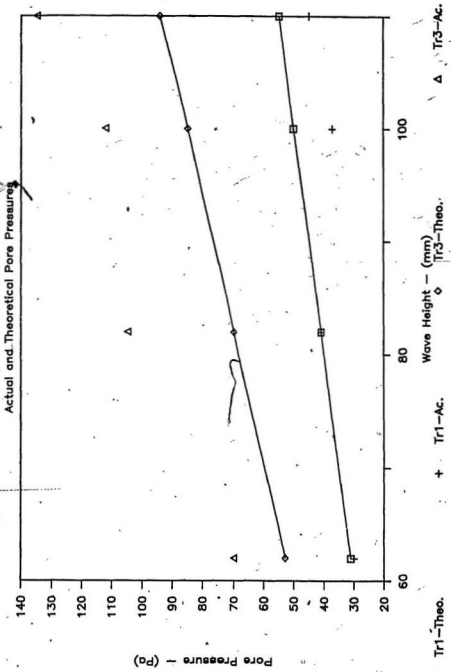


Figure 15 - Trans. 2 and 4. - 1.00 Hz.

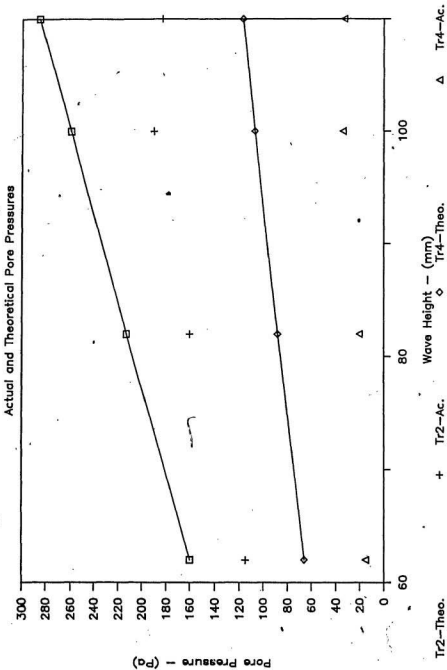


Figure 16 — Trans. 1 and 3. — 1.15 Hz.

Actual and Theoretical Pore Pressures

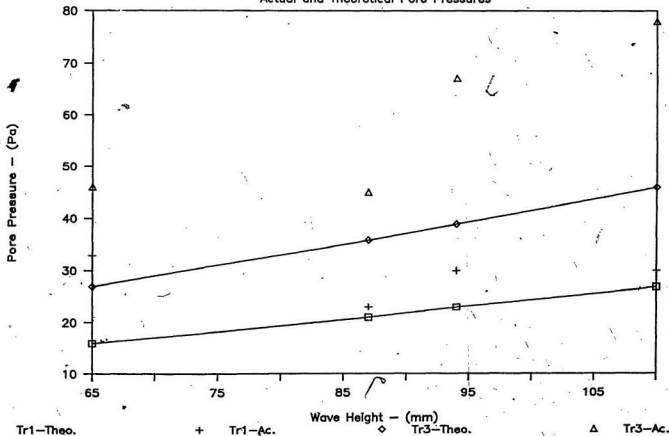


Figure 17 - Trans. 2 and 4. - 1.15 Hz.

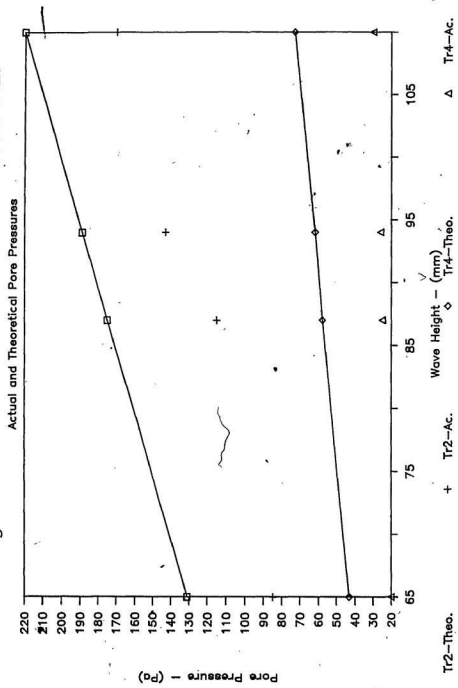


Figure 18 — Trans. 1 and 4, — 0.63 Hz.  
 $Z/Z_0$  and  $P/P_0$

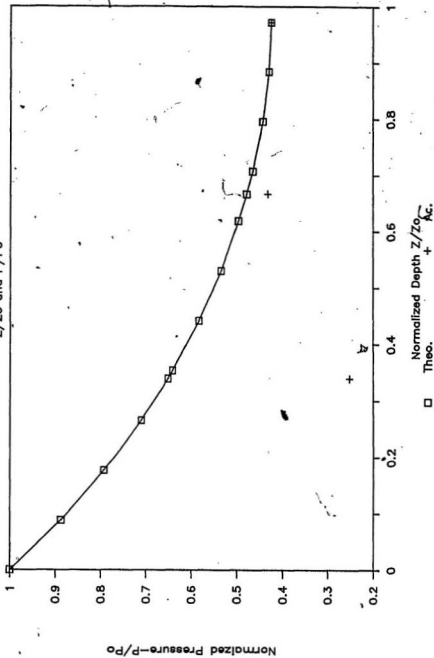


Figure 19 - Trans. 3. - 0.63 Hz.  
 $Z/Z_0$  and  $P/P_0$

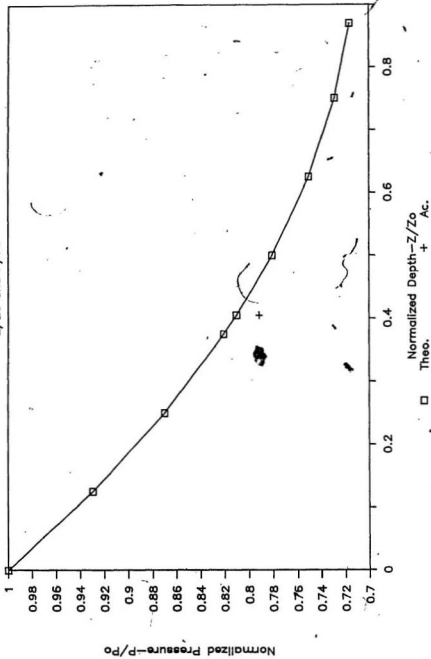


Figure 20 - Trans. 1 and 4. - 0.81 Hz.  
 $z/Z_0$  and  $P/P_0$

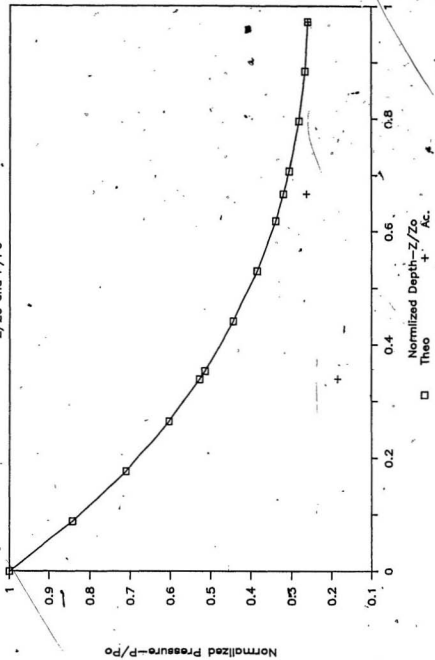


Figure 21 — Trans. 3, — 0.81 Hz.  
 $Z/Z_0$  and  $P/P_0$

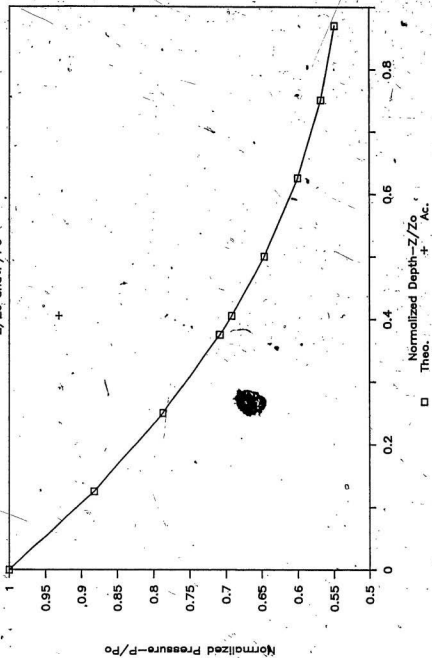


Figure 22  $\pm$  Trans. 1 and 4. - 1.00 Hz.

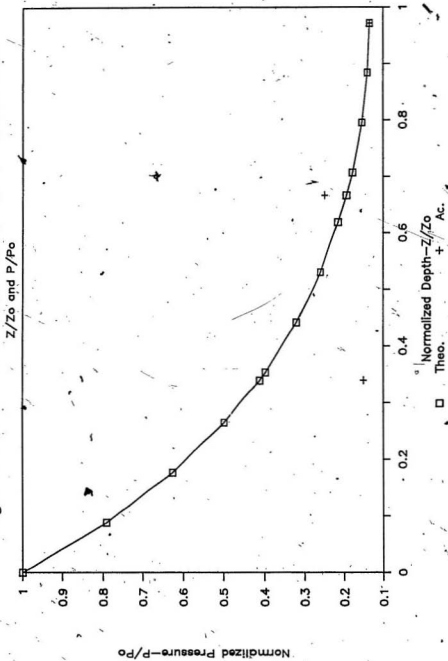


Figure 23 - Trans. 3 - 1.00 Hz.

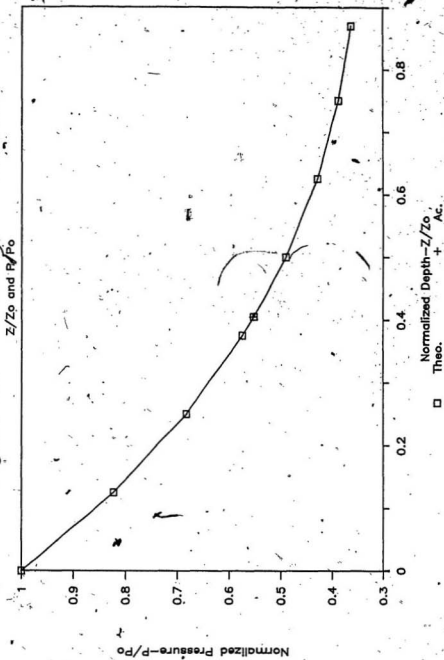


Figure 24 - Trans. 1 and 4. - 1.15 Hz.  
 $Z/Z_0$  and  $P/P_0$

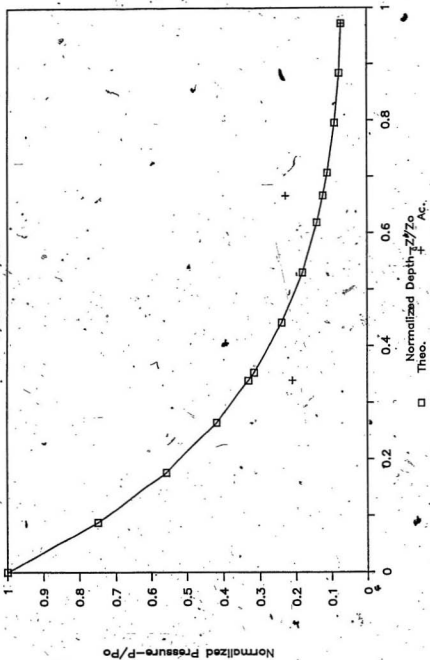


Figure 25 - Trans 3. - 1.15 Hz.  
 $z/z_0$  and  $P/P_0$

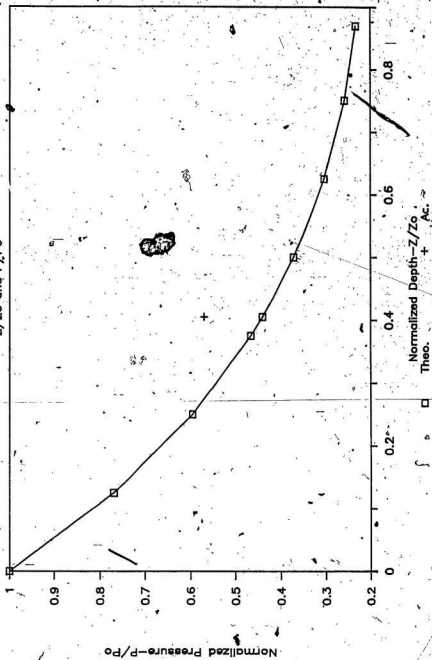


FIGURE 26

Transducer 1

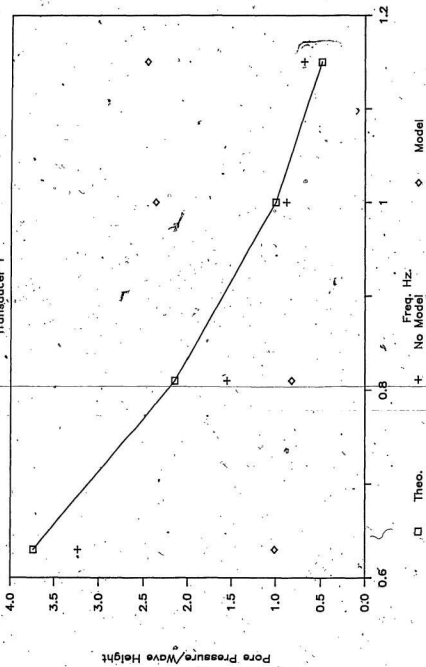


FIGURE 27

Transducer 2

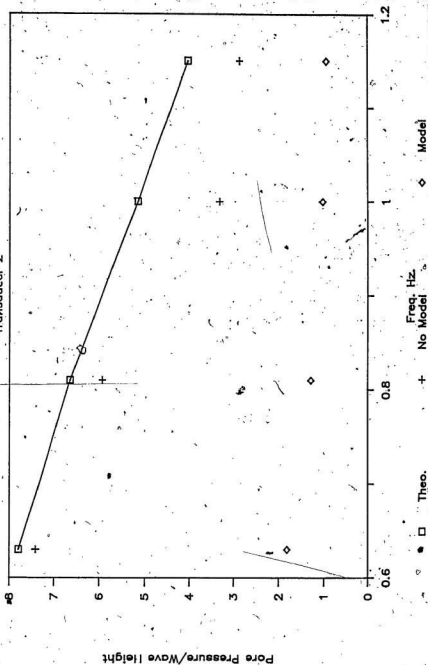


FIGURE 28

Transducer 3

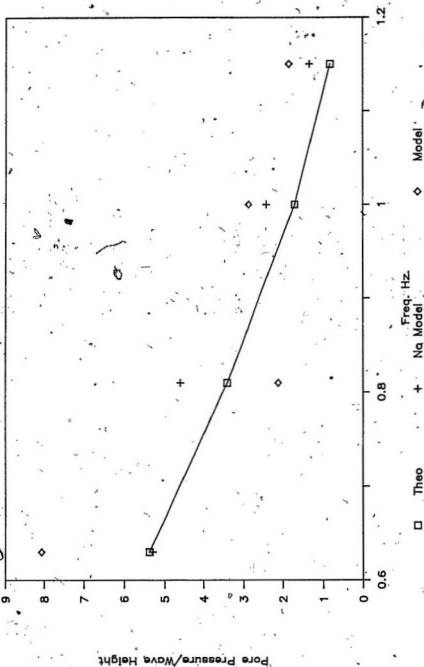


FIGURE 29

Transducer 4

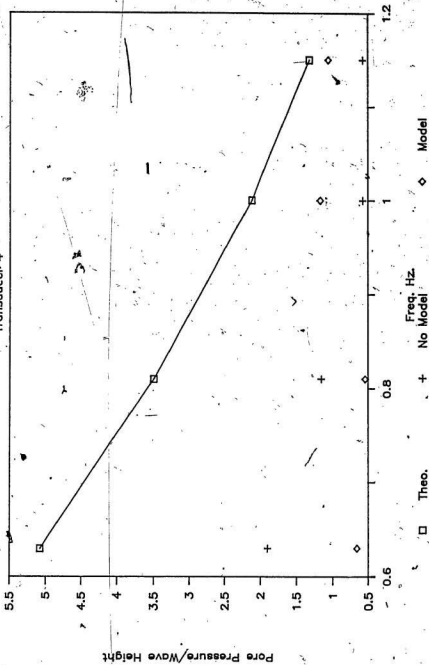


Figure 30

Pore Pressure Build-Up—Model in Place

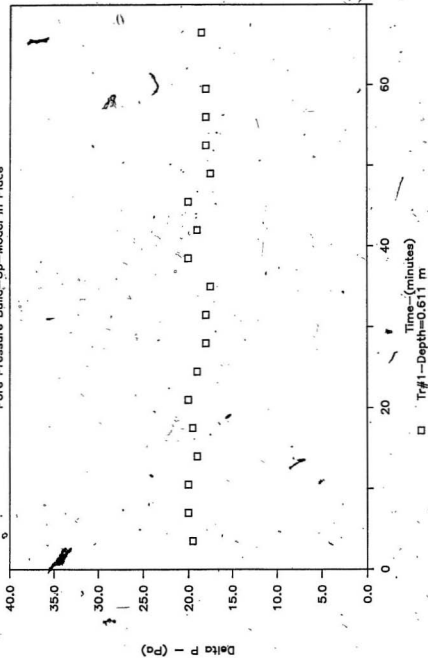


Figure 31.

Pore Pressure Build-Up—Model In Place

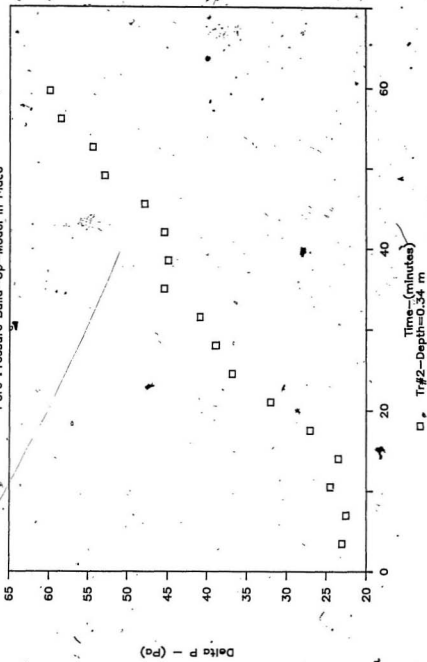


Figure 32  
Pore Pressure Build-Up—Model in Place

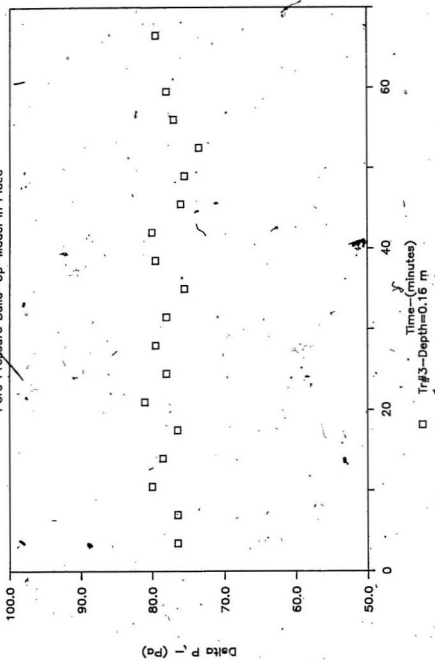
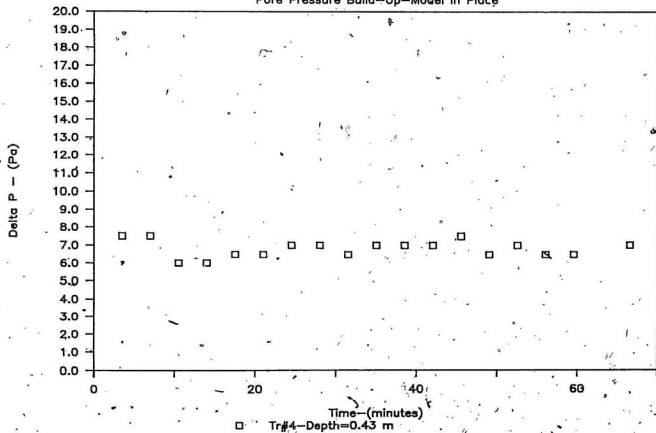
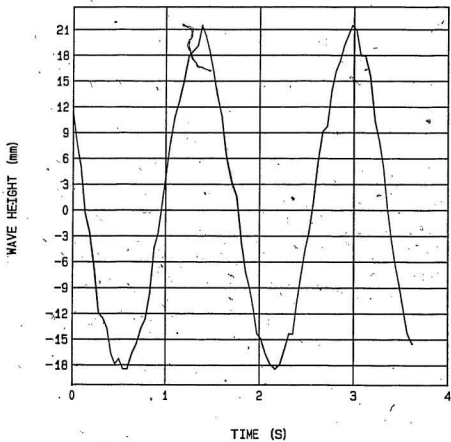


Figure 33

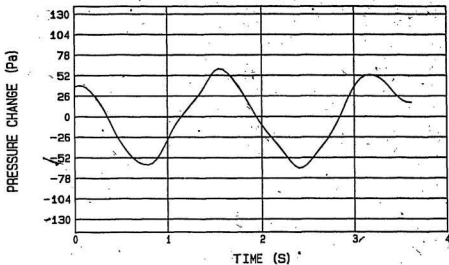
Pore Pressure Build-Up-Model in Place



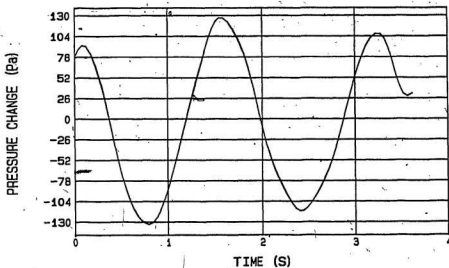


*f*  
 $F=0.63 \text{ Hz}$ ,  $S=27 \text{ mm}$ .

FIGURE 34

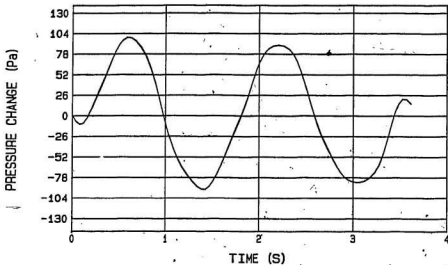


TR# 1 DEPTH= 377 mm.  
 FREQ= .63 Hz. STROKE= 27 mm

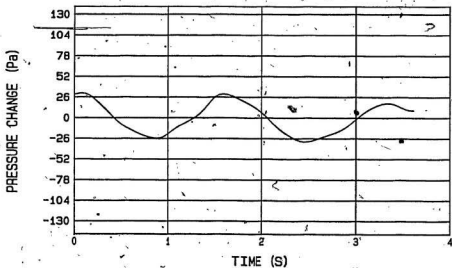


TR# 2 DEPTH= 0 mm.  
 FREQ= .63 Hz. STROKE= 27 mm

FIGURE 35

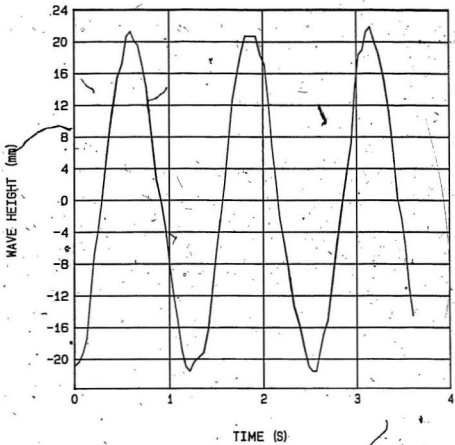


TR# 3 DEPTH= 162 mm.  
 FREQ= .63 Hz. STROKE= 27 mm



TR# 4 DEPTH= 192 mm.  
 FREQ= .63 Hz. STROKE= 27 mm

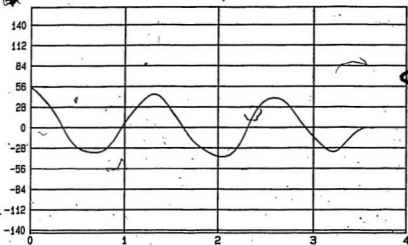
FIGURE 36



F=0.81 Hz . S=27 mm.

FIGURE 37

PRESSURE CHANGE (Pa)

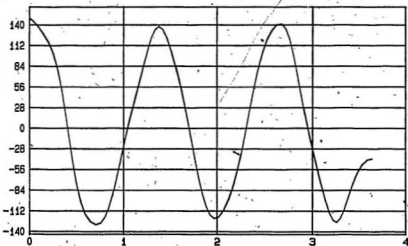


TIME (S)

TR# 1 DEPTH= 377 mm.

FREQ= .81 Hz. STROKE= 27 mm

PRESSURE CHANGE (Pa)

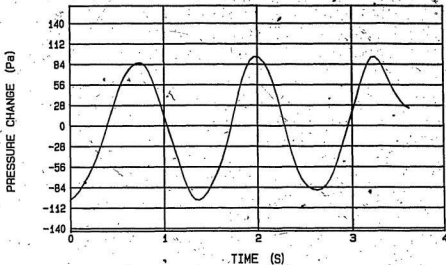


TIME (S)

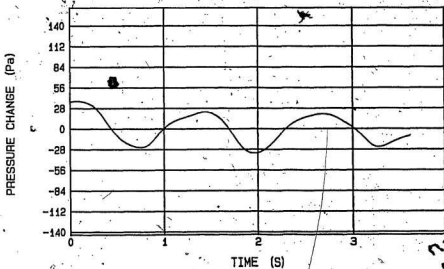
TR# 2 DEPTH= 0 mm.

FREQ= .81 Hz. STROKE= 27 mm

FIGURE 38

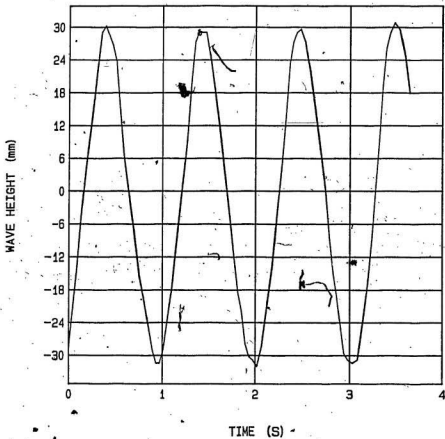


TR# 3 DEPTH= 162 mm.  
 FREQ= .81 Hz. STROKE= 27 mm



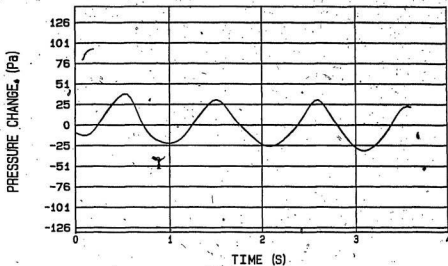
TR# 4 DEPTH= 192 mm.  
 FREQ= .81 Hz. STROKE= 27 mm

FIGURE 39

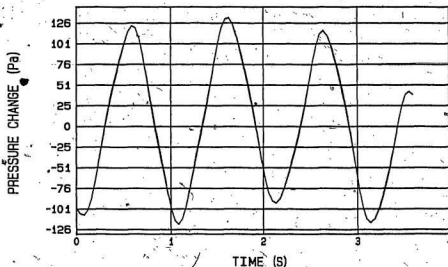


$F=1.00$  Hz.  $S=27$  mm.

FIGURE 40

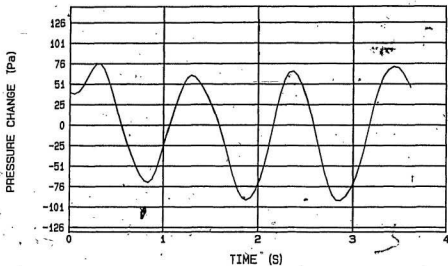


TR# 1 DEPTH= 37 mm.  
 FREQ= 1 Hz. STROKE= 27 mm

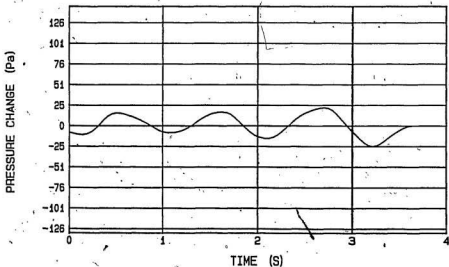


TR# 2 DEPTH= 0 mm.  
 FREQ= 1 Hz. STROKE= 27 mm

FIGURE 41

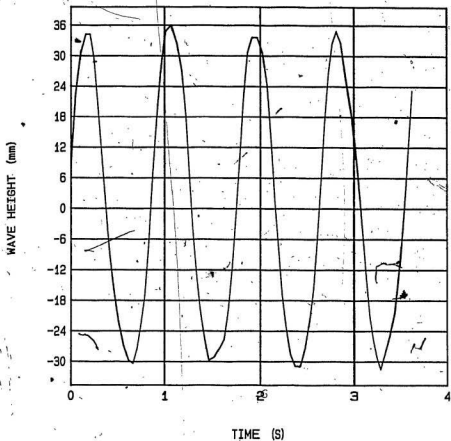


TR# 3 DEPTH= 162 mm.  
 FREQ= 1 Hz. STROKE= 27 mm



TR# 4 DEPTH= 192 mm.  
 FREQ= 1 Hz. STROKE= 27 mm

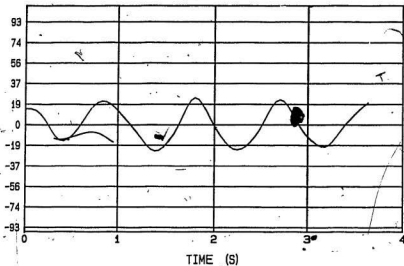
FIGURE 42



$F=1.15$  Hz.  $S=27$  mm.

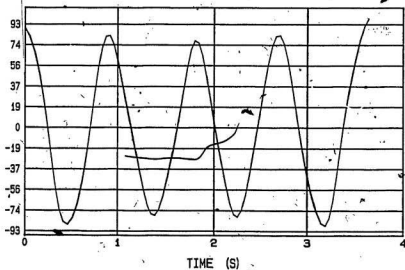
FIGURE 43

PRESSURE CHANGE (Pa)



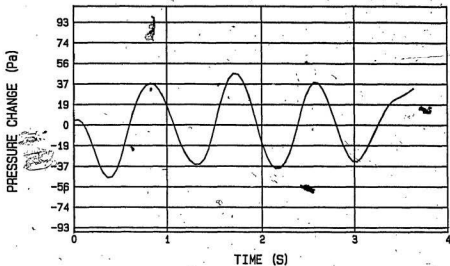
TR# 1 DEPTH= 377 mm.  
FREQ= 1.15 Hz. STROKE= 27 mm

PRESSURE CHANGE (Pa)

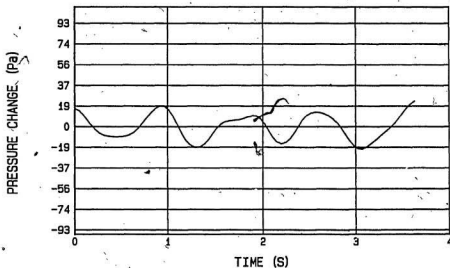


TR# 2 DEPTH= .0 mm.  
FREQ= 1.15 Hz. STROKE= 27 mm

FIGURE 44

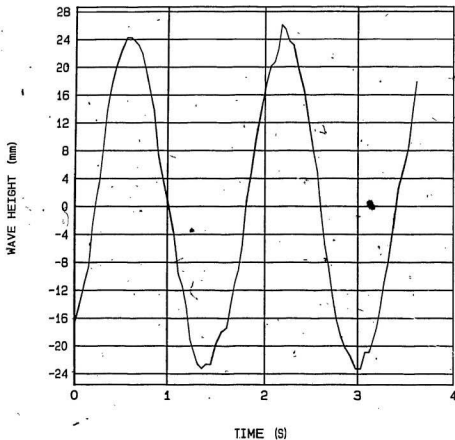


TR# 3 DEPTH= 162 mm.  
 FREQ= 1.15 Hz. STROKE= 27 mm



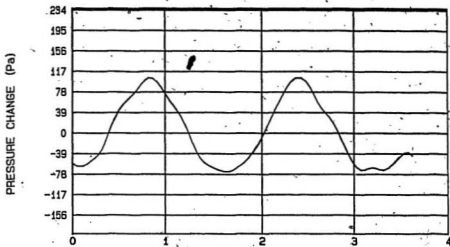
TR# 4 DEPTH= 192 mm.  
 FREQ= 1.15 Hz. STROKE= 27 mm

FIGURE 45



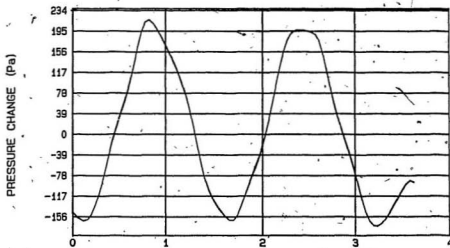
$F=0.63$  Hz.  $S=34$  mm.

FIGURE 46



TIME (S)

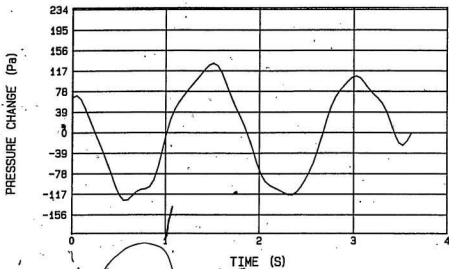
TR# 1 DEPTH= 377 mm.  
 FREQ= .63 Hz. STROKE= 34 mm



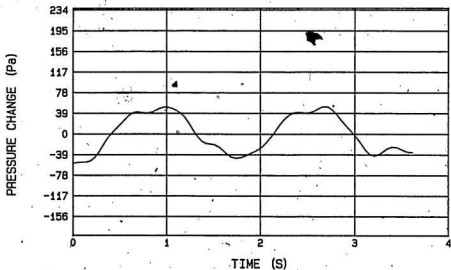
TIME (S)

TR# 2 DEPTH= 0 mm.  
 FREQ= .63 Hz. STROKE= 34 mm

FIGURE 47

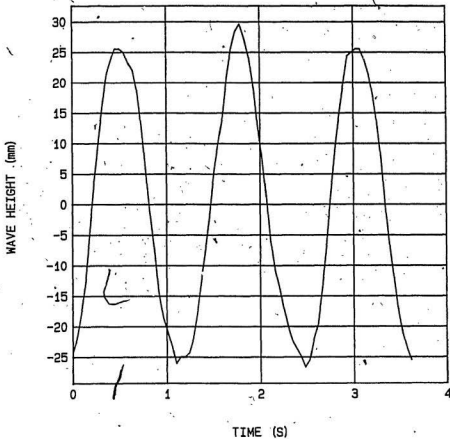


TR# 3 DEPTH= 162 mm.  
 FREQ= .63 Hz. STROKE= 34 mm



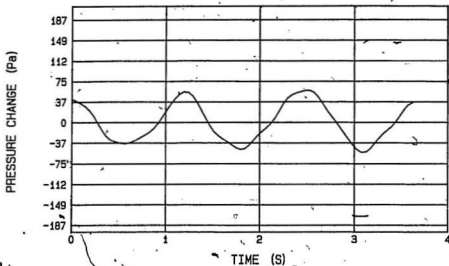
TR# 4 DEPTH= 192 mm.  
 FREQ= .63 Hz. STROKE= 34 mm

FIGURE 48

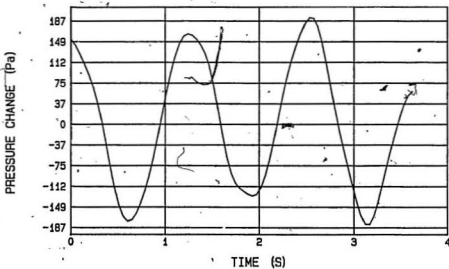


$F=0.81$  Hz.  $S=34$  mm.

FIGURE 49

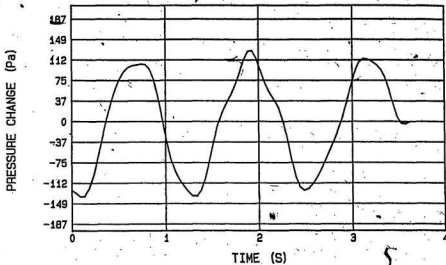


TR# 1 DEPTH= 377 mm.  
 FREQ= .81 Hz. STROKE= 34 mm

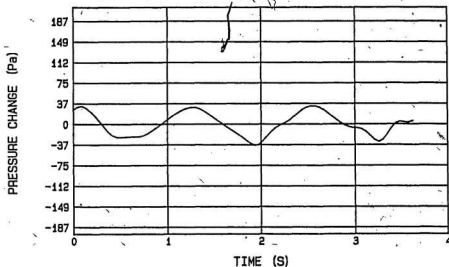


TR# 2 DEPTH= 0 mm.  
 FREQ= .81 Hz. STROKE= 34 mm

FIGURE 50

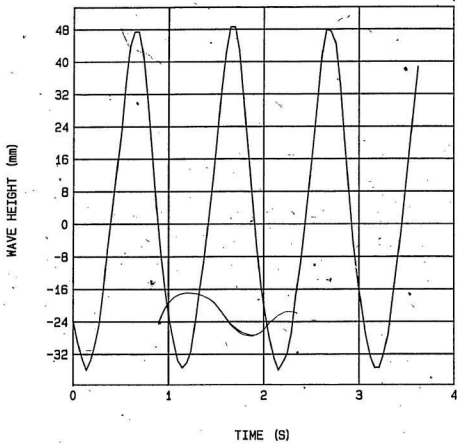


TR# 3 DEPTH= 162 mm.  
 FREQ= .81 Hz. STROKE= 34 mm



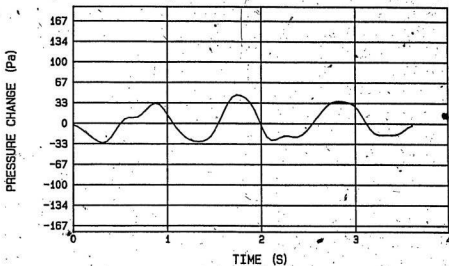
TR# 4 DEPTH= 192 mm.  
 FREQ= .81 Hz. STROKE= 34 mm

FIGURE 51

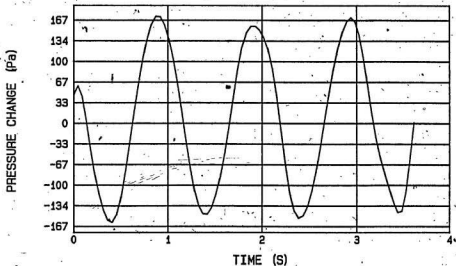


$F=1.00$  Hz:  $S=34$  mm.

FIGURE 52

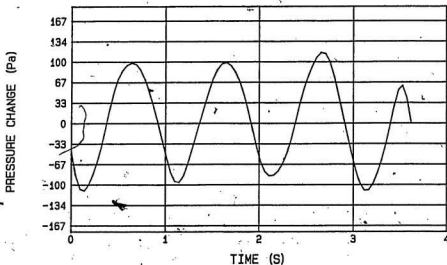


TR# 1 DEPTH= 377 mm.  
 FREQ= 1 Hz. STROKE= 34 mm

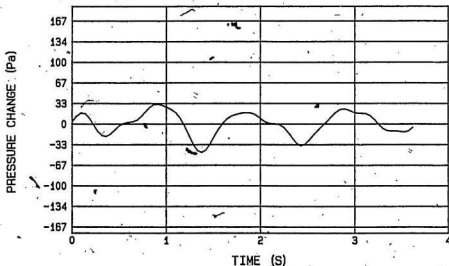


TR# 2 DEPTH= 0 mm.  
 FREQ= 1 Hz. STROKE= 34 mm

FIGURE 53

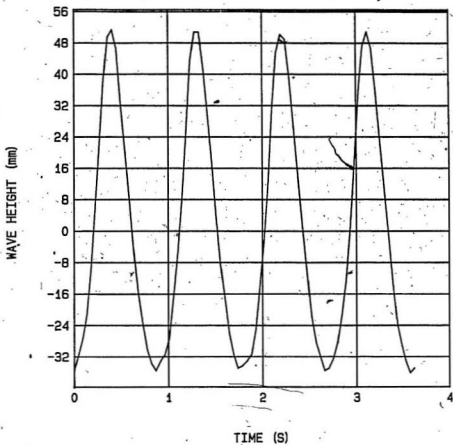


TR# 3 DEPTH= 162 mm.  
 FREQ= 1 Hz. STROKE= 34 mm



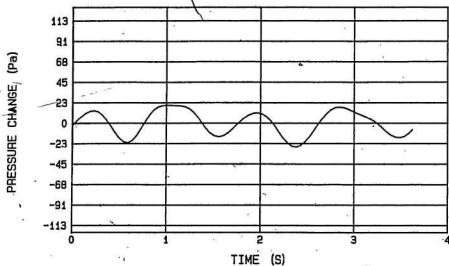
TR# 4 DEPTH= 192 mm.  
 FREQ= 1 Hz. STROKE= 34 mm

FIGURE 54

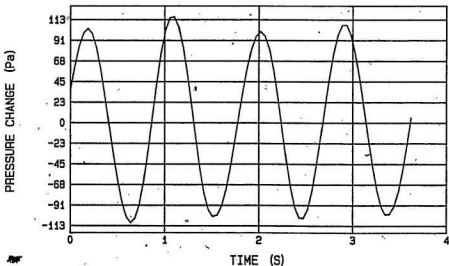


$F=1.15$  Hz.  $S=34$  mm.

FIGURE 55

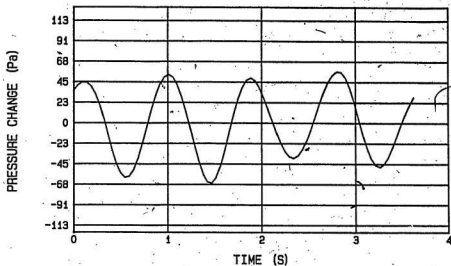


TR# 1 DEPTH= 377 mm.  
 FREQ= 1.15 Hz. STROKE= 34 mm

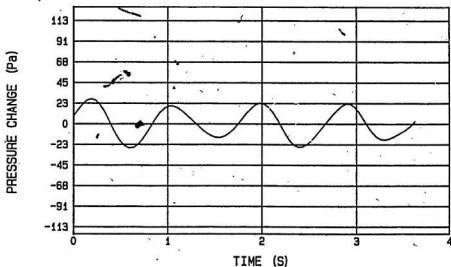


TR# 2 DEPTH= 0 mm.  
 FREQ= 1.15 Hz. STROKE= 34 mm

FIGURE 56

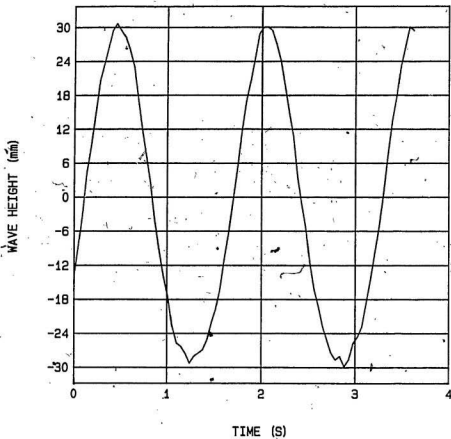


TR# 3 DEPTH= 162 mm.  
 FREQ= 1.15 Hz. STROKE= 34 mm



TR# 4 DEPTH= 192 mm.  
 FREQ= 1.15 Hz. STROKE= 34 mm

FIGURE 57



$F=0.63$  Hz.  $S=41$  mm.

FIGURE 58

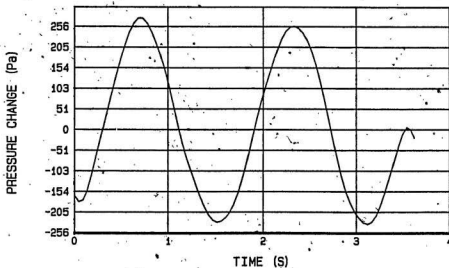
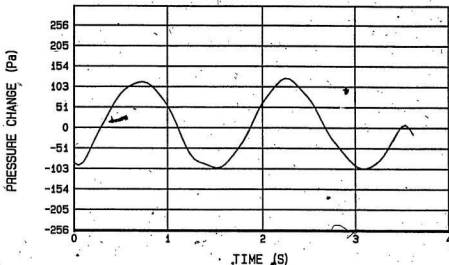
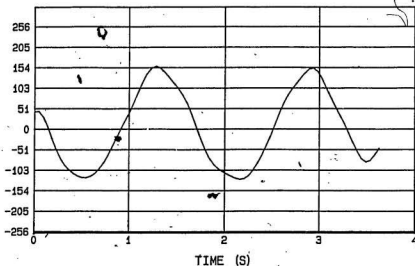


FIGURE 59

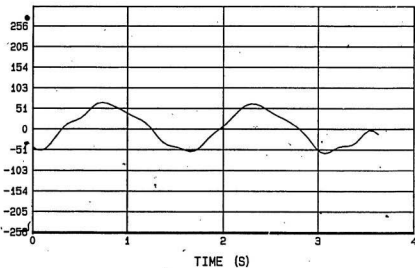
PRESSURE CHANGE (Pa)



TR# 3 DEPTH= 162 mm.

FREQ= .63 Hz. STROKE= 41 mm

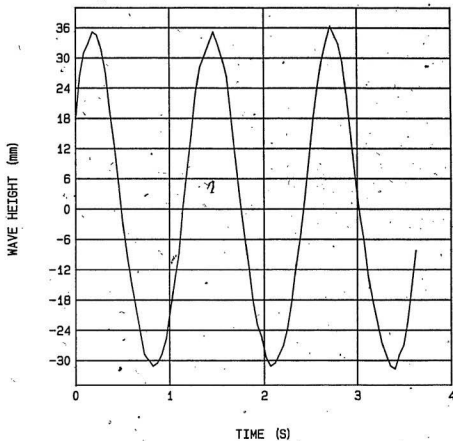
PRESSURE CHANGE (Pa)



TR# 4 DEPTH= 192 mm.

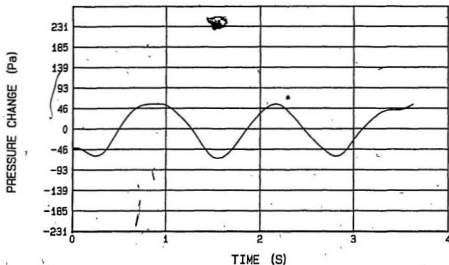
FREQ= .63 Hz. STROKE= 41 mm

FIGURE 60

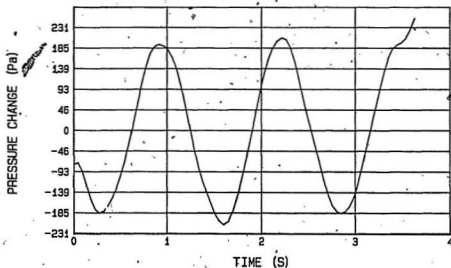


$F=0.81$  Hz.  $S=41$  mm.

FIGURE 61

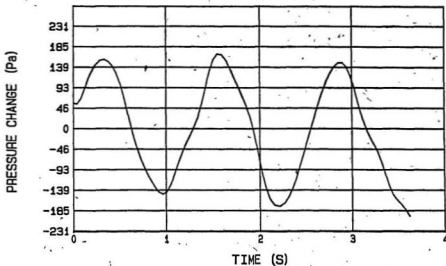


TR# 1 DEPTH= 377 mm.  
 FREQ= .81 Hz. STROKE= 41 mm

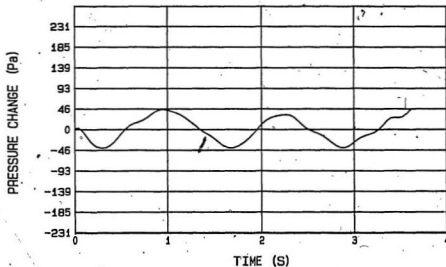


TR# 2 DEPTH= 0 mm.  
 FREQ= .81 Hz. STROKE= 41 mm

FIGURE 62

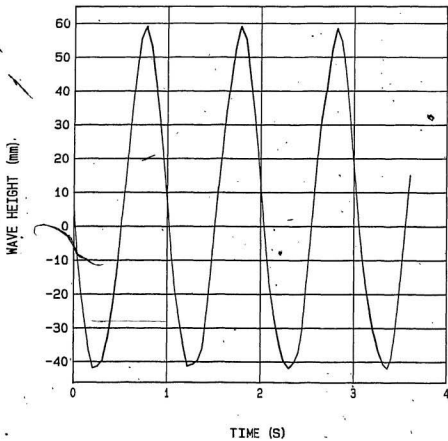


TR# 3 DEPTH= 162 mm.  
 FREQ= .81 Hz. STROKE= 41 mm



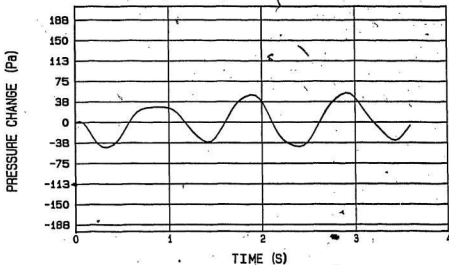
TR# 4 DEPTH= 192 mm.  
 FREQ= .81 Hz. STROKE= 41 mm

FIGURE 63

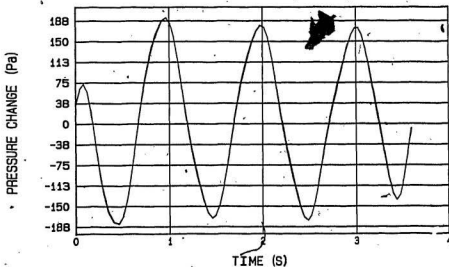


$F=1.00$  Hz.  $S=41$  mm.

FIGURE 64

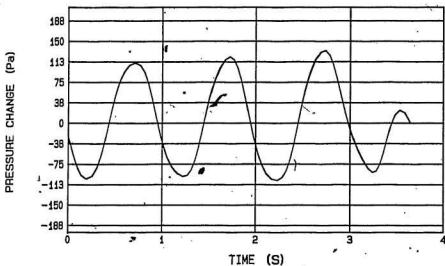


TR# 1 DEPTH= 377 mm.  
 FREQ= 1 Hz. STROKE= 41 mm

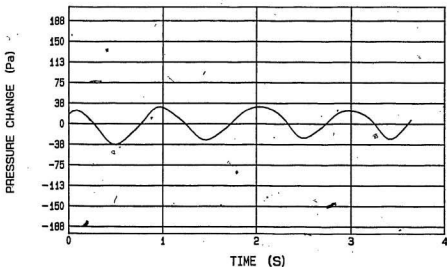


TR# 2 DEPTH= 0 mm.  
 FREQ= 1 Hz. STROKE= 41 mm

FIGURE 65

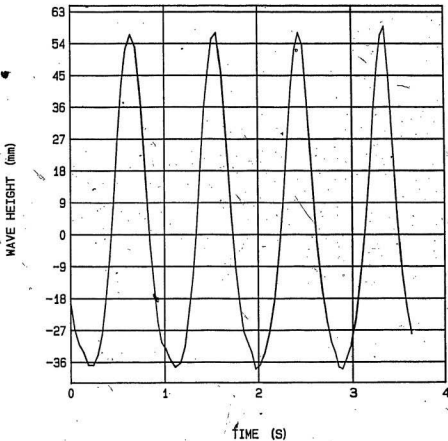


TR# 3 DEPTH= 162 mm.  
 FREQ= 1 Hz. STROKE= 41 mm



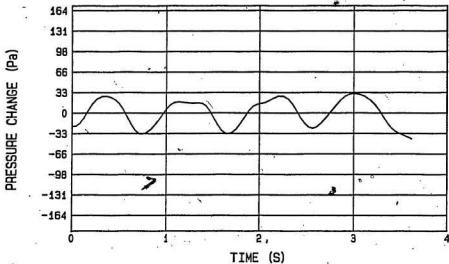
TR# 4 DEPTH= 192 mm.  
 FREQ= 1 Hz. STROKE= 41 mm

FIGURE: 66

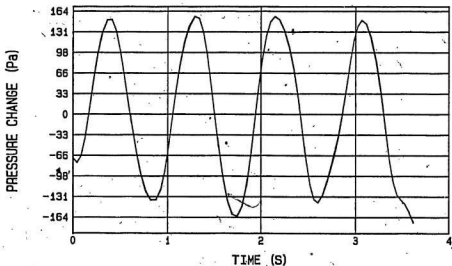


F=1.15 Hz. S=41 mm.

FIGURE 67

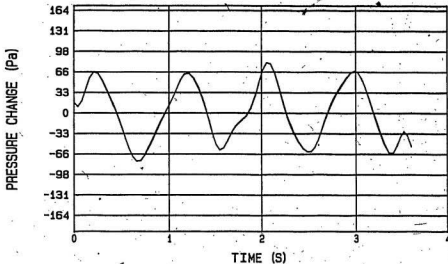


TR# 1 DEPTH= 377. mm.  
 FREQ= 1.15 Hz. STROKE= 41 mm

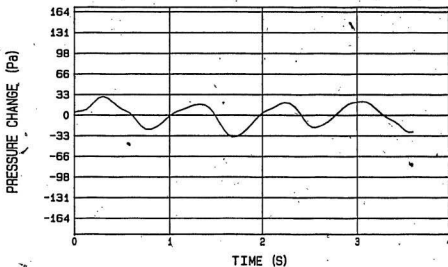


TR# 2 DEPTH= 0 mm.  
 FREQ= 1.15 Hz. STROKE= 41 mm

FIGURE 68

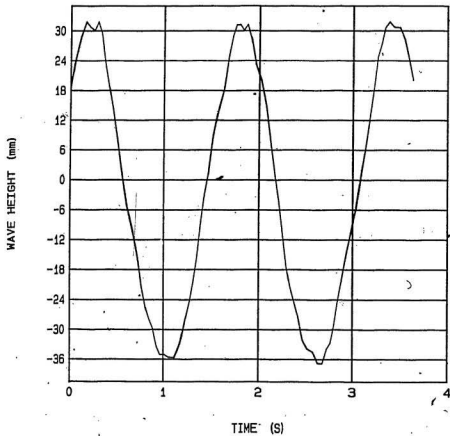


TR# 3 DEPTH= 162 mm.  
FREQ= 1.15 Hz. STROKE= 41 mm



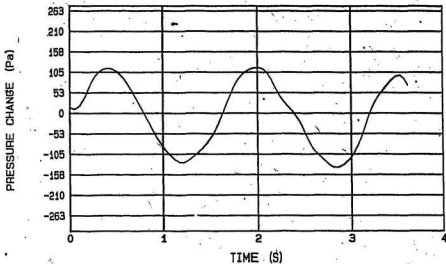
TR# 4 DEPTH= 192 mm.  
FREQ= 1.15 Hz. STROKE= 41 mm

FIGURE 69

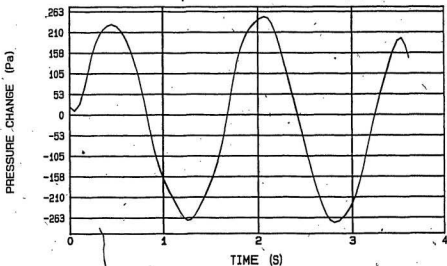


F=0.63 Hz. S=48 mm.

FIGURE 70

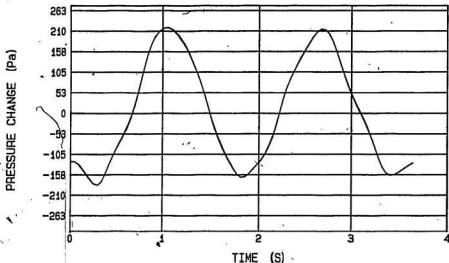


TR# 1 DEPTH= 377 mm.  
 FREQ= .63 Hz. STROKE= 48 mm

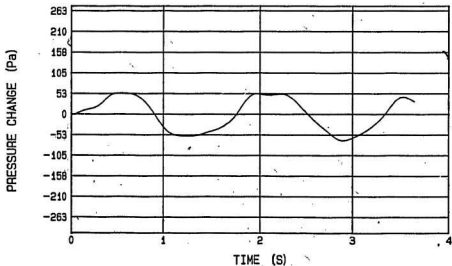


TR# 2 DEPTH= 0 mm.  
 FREQ= .63 Hz. STROKE= 48 mm

FIGURE 71

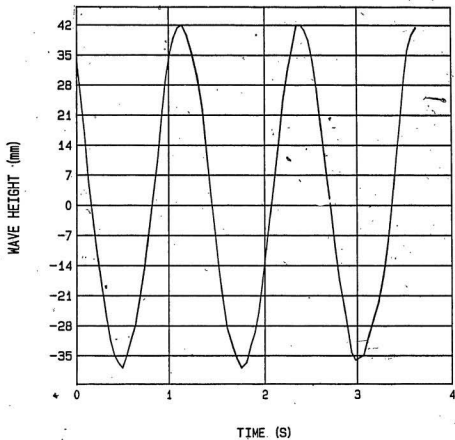


TR# 3 DEPTH= 162 mm.  
 FREQ= .63 Hz. STROKE= 48 mm



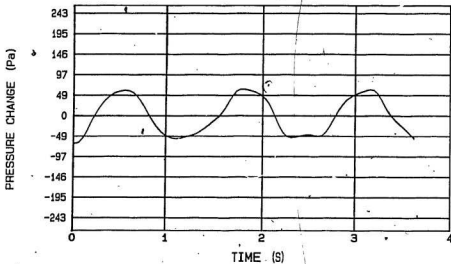
TR# 4 DEPTH= 192 mm.  
 FREQ= .63 Hz. STROKE= 48 mm

FIGURE 72

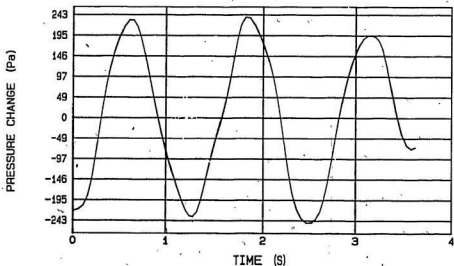


$F=0.81$  Hz.  $S=48$  mm.

FIGURE 73

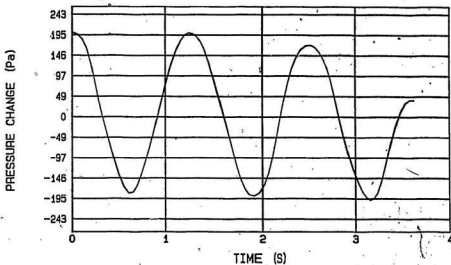


TR# 1 DEPTH= 377 mm.  
 FREQ= .81 Hz. STROKE= 48 mm

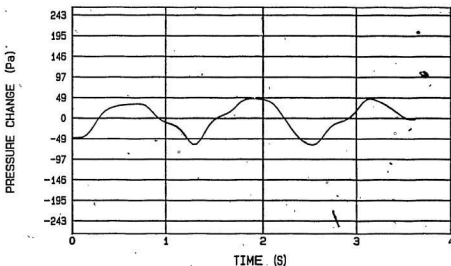


TR# 2 DEPTH= 0 mm.  
 FREQ= .81 Hz. STROKE= 48 mm

FIGURE 74

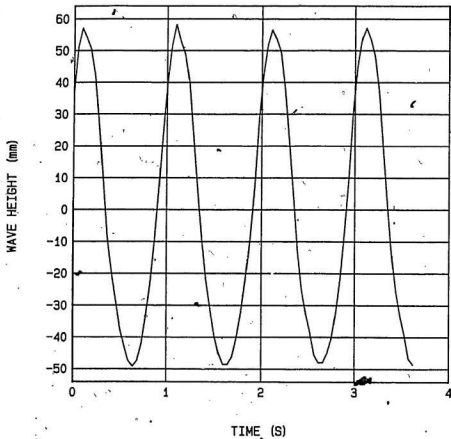


TR# 3 DEPTH= 162 mm.  
 FREQ= .81 Hz. STROKE= 48 mm



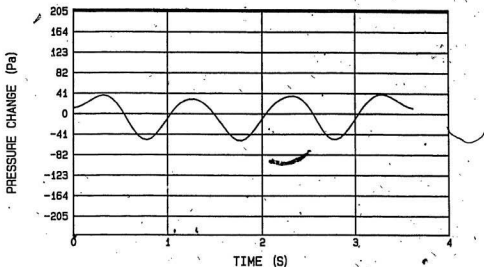
TR# 4 DEPTH= 192 mm.  
 FREQ= .81 Hz. STROKE= 48 mm

FIGURE 75

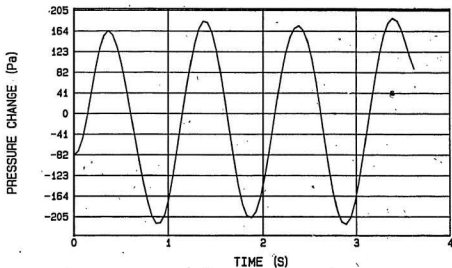


$F=1.00$  Hz.  $S=48$  mm.

FIGURE 76

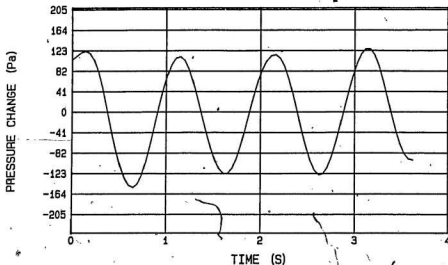


TR# 1 DEPTH= 377 mm.  
 FREQ= 1 Hz. STROKE= 48 mm

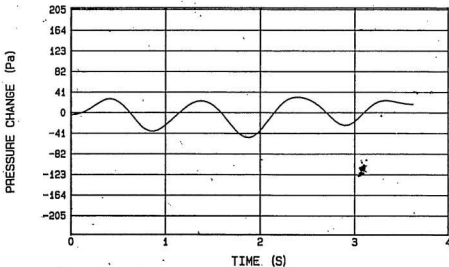


TR# 2 DEPTH= 0 mm.  
 FREQ= 1 Hz. STROKE= 48 mm

FIGURE 77

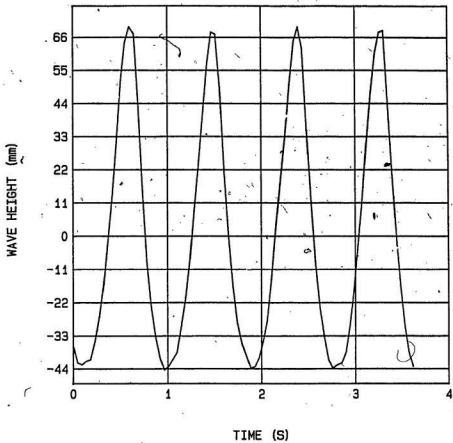


TR# 3 DEPTH= 162 mm.  
 FREQ= 1 Hz. STROKE= 48 mm



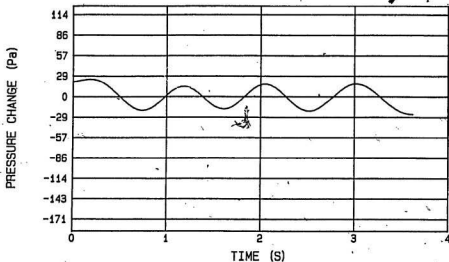
TR# 4 DEPTH= 192 mm.  
 FREQ= 1 Hz. STROKE= 48 mm

FIGURE 78

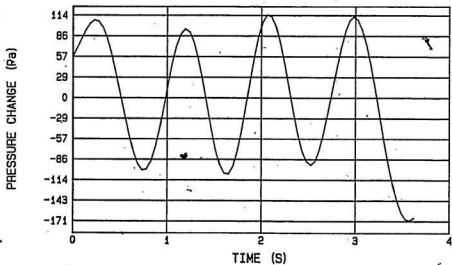


$F=1.15 \text{ Hz}$ ,  $S=48 \text{ mm}$ .

FIGURE 79

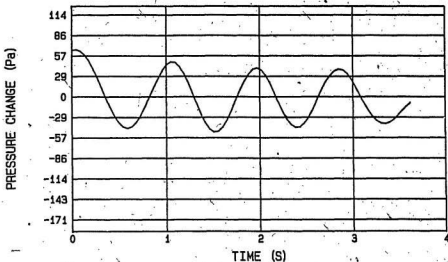


TR# 1 DEPTH= 377 mm.  
 FREQ= 1.15 Hz. STROKE= 48 mm

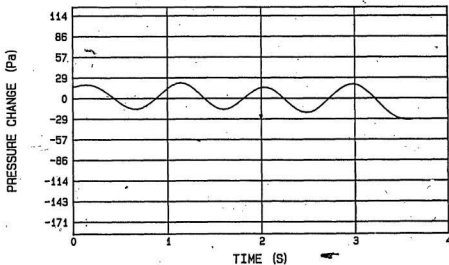


TR# 2 DEPTH= 0 mm.  
 FREQ= 1.15 Hz. STROKE= 48 mm

FIGURE 80

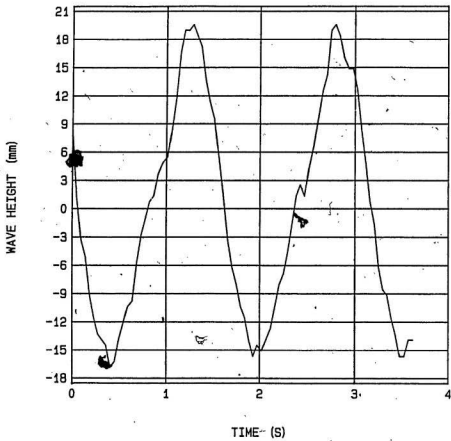


TR# 3 DEPTH= 162 mm.  
 FREQ= 1.15 Hz. STROKE= 48 mm.



TR# 4 DEPTH= 192 mm.  
 FREQ= 1.15 Hz. STROKE= 48 mm

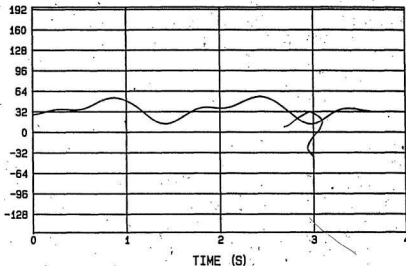
FIGURE 81



$F=0.63$  Hz.  $S=27$  mm.

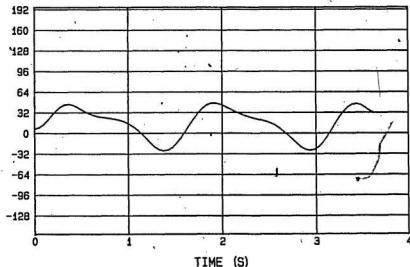
FIGURE 82

PRESSURE CHANGE (Pa)



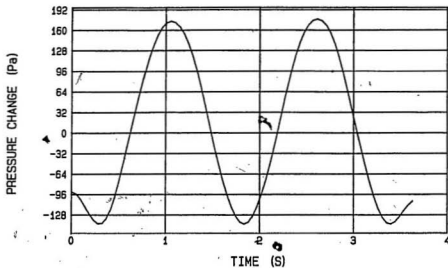
TR# 1 DEPTH= 611 mm.  
FREQ= .63 Hz. STROKE= 27 mm

PRESSURE CHANGE (Pa)

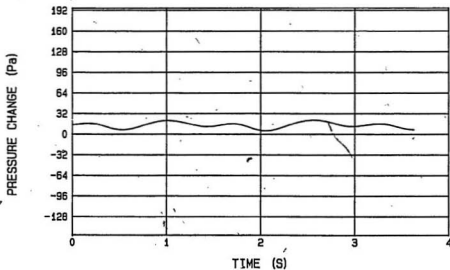


TR# 2 DEPTH= 340 mm.  
FREQ= .63 Hz. STROKE= 27 mm

FIGURE 83

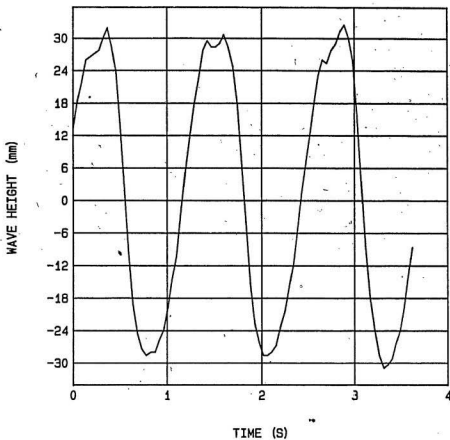


TR# 3 DEPTH= 162 mm.  
FREQ= .63 Hz. STROKE= 27 mm



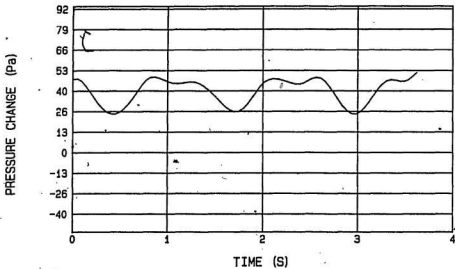
TR# 4 DEPTH= 425 mm.  
FREQ= .63 Hz. STROKE= 27 mm

FIGURE 84

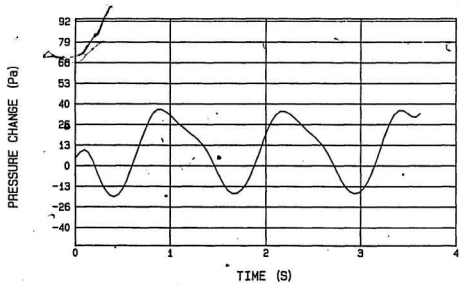


$F=0.81$  Hz.  $S=27$  mm.

FIGURE 85

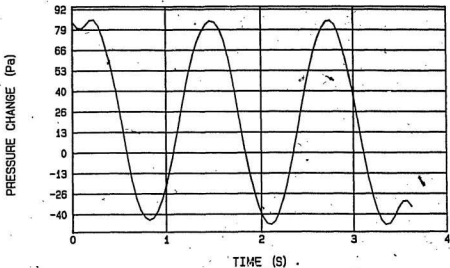


TR# 1 DEPTH= 611 mm.  
 FREQ= .81 Hz. STROKE= 27 mm



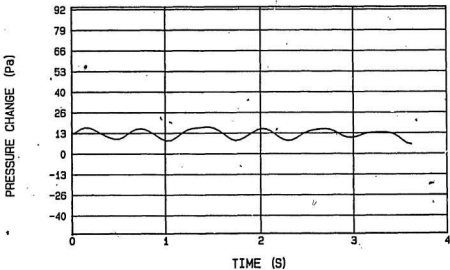
TR# 2 DEPTH= 340 mm.  
 FREQ= .81 Hz. STROKE= 27 mm

FIGURE 86



TR# 3 DEPTH= .162 mm.

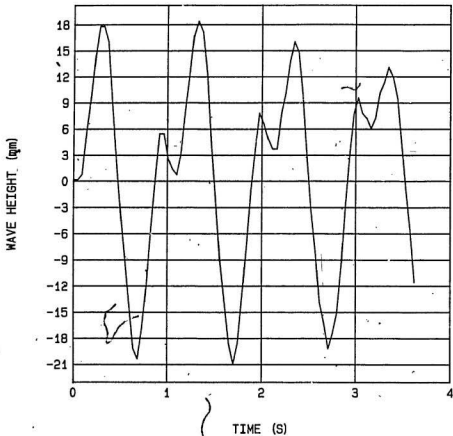
FREQ= .81 Hz. STROKE= 27 mm



TR# 4 DEPTH= 425 mm.

FREQ= .81 Hz. STROKE= 27 mm

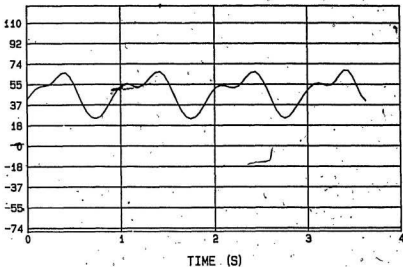
FIGURE 87



F=1.00 Hz. S=27 mm.

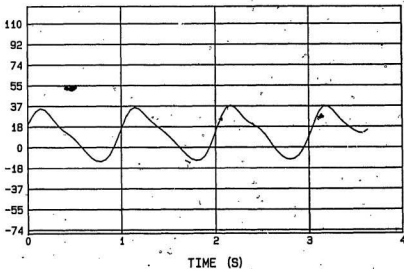
FIGURE 88

PRESSURE CHANGE (Pa)



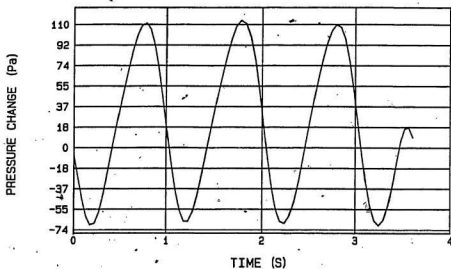
TR# 1 DEPTH= 611 mm.  
FREQ= 1 Hz. STROKE= 27 mm

PRESSURE CHANGE (Pa)

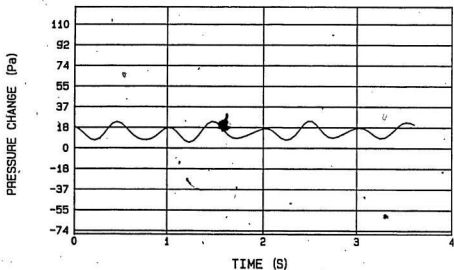


TR# 2 DEPTH= 340 mm.  
FREQ= 1 Hz. STROKE= 27 mm

FIGURE 89

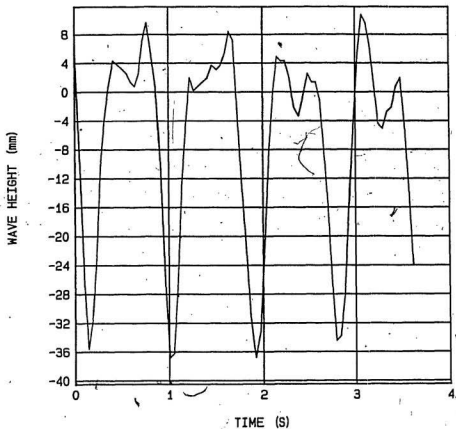


TR# 3 DEPTH= 162 mm.  
 FREQ= 1 Hz. STROKE= 27 mm



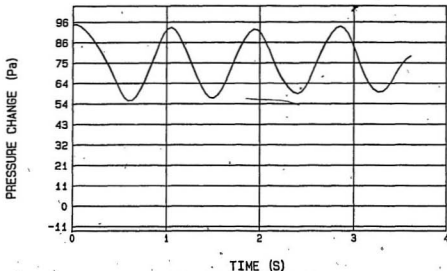
TR# 4 DEPTH= 425 mm.  
 FREQ= 1 Hz. STROKE= 27 mm

FIGURE 90

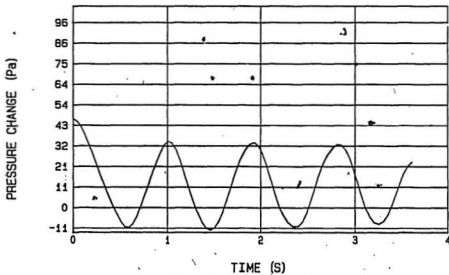


$F=1.15$  Hz.  $S=27$  mm.

FIGURE 91

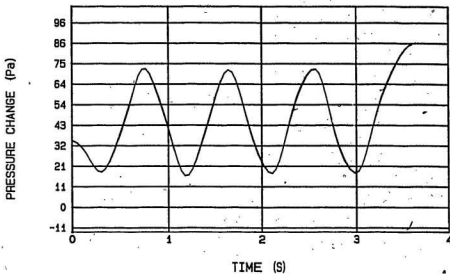


TR# 1 DEPTH= 611 mm:  
 FREQ= 1.15 Hz. STROKE= 27 mm

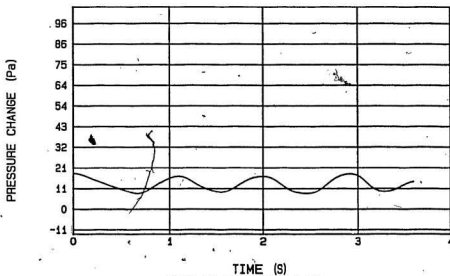


TR# 2 DEPTH= 340 mm.  
 FREQ= 1.15 Hz. STROKE= 27 mm

FIGURE 92

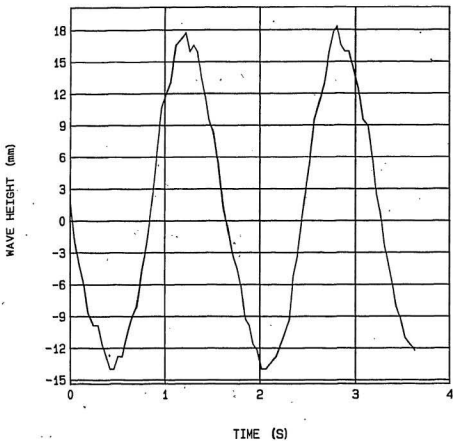


TR# 3 DEPTH= 162 mm.  
 FREQ= 1.15 Hz : STROKE= 27 mm



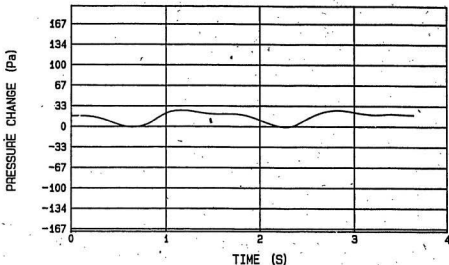
TR# 4 DEPTH= 425 mm.  
 FREQ= 1.15 Hz . STROKE= 27 mm

FIGURE 93

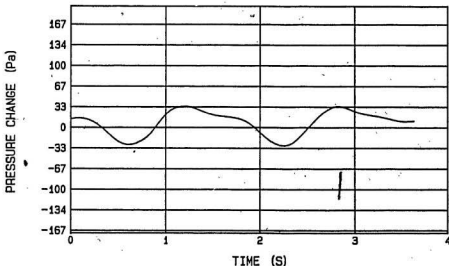


F=0.63 Hz. S=34 mm.

FIGURE 94

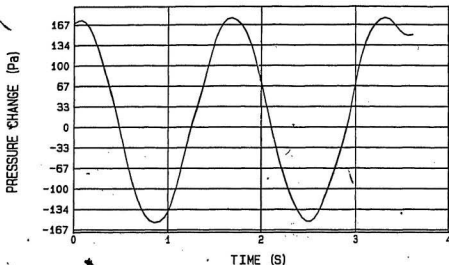


TR# 1 DEPTH= 611 mm.  
 FREQ= .63 Hz. STROKE= 34 mm

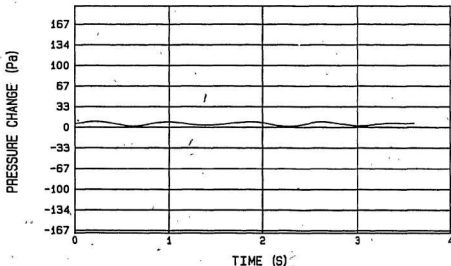


TR# 2 DEPTH= 340 mm.  
 FREQ= .63 Hz. STROKE= 34 mm

FIGURE 95

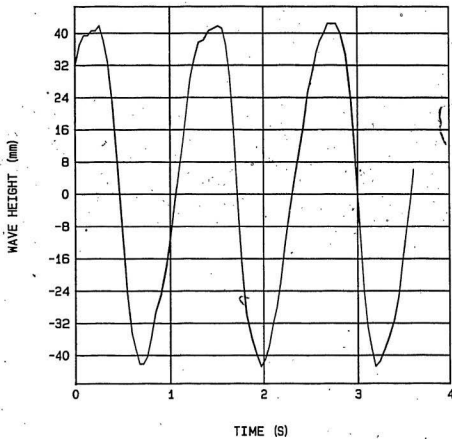


TR# 3 DEPTH= 162 mm.  
 FREQ= .63 Hz. STROKE= 34 mm



TR# 4 DEPTH= 425 mm.  
 FREQ= .63 Hz. STROKE= 34 mm

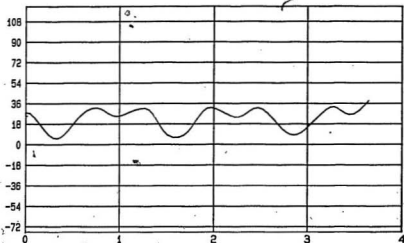
FIGURE 96



$F=0.81$  Hz.  $S=34$  mm.

FIGURE 97

PRESSURE CHANGE (Pa)

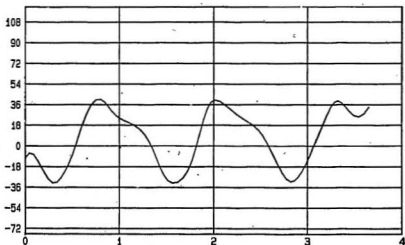


TIME (s)

TR# 1 DEPTH= 611 mm.

FREQ= .81 Hz. STROKE= 34 mm

PRESSURE CHANGE (Pa)

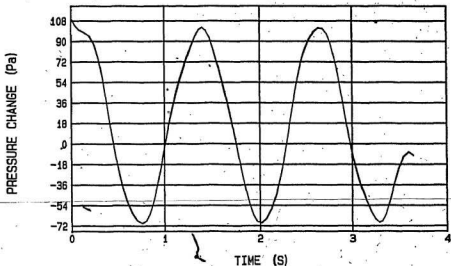


TIME (s)

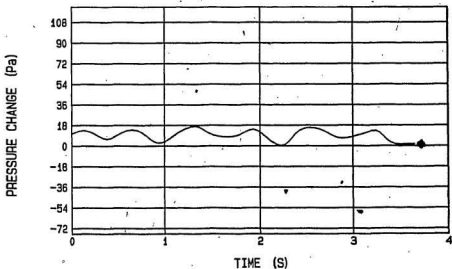
TR# 2 DEPTH= 340 mm.

FREQ= .81 Hz. STROKE= 34 mm

FIGURE 98

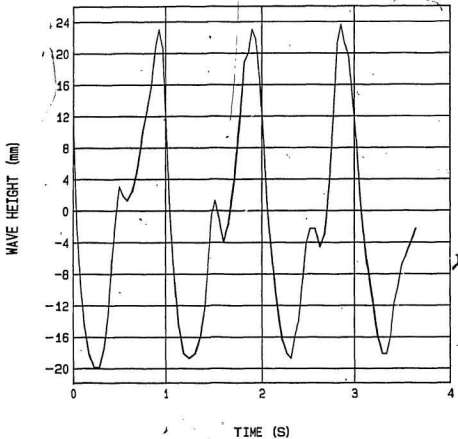


TR# 3 DEPTH= 162 mm.  
 FREQ= .81 Hz. STROKE= 34 mm



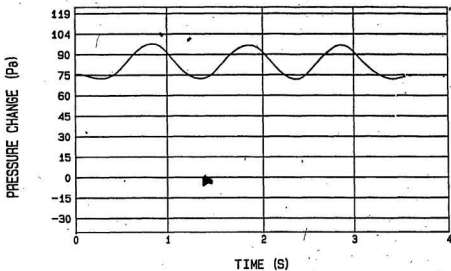
TR# 4 DEPTH= 425 mm.  
 FREQ= .81 Hz. STROKE= 34 mm

FIGURE 99

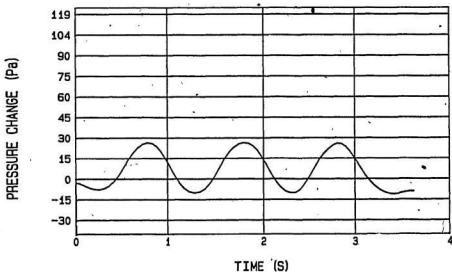


F=1.00 Hz. S=34 mm.

FIGURE 100



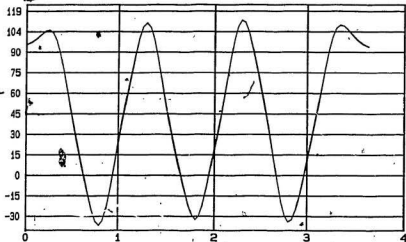
TR# 1 DEPTH= 611 mm.  
 FREQ= 1 Hz. STROKE= 34 mm



TR# 2 DEPTH= 340 mm.  
 FREQ= 1 Hz. STROKE= 34 mm

FIGURE 101

PRESSURE CHANGE (Pa)

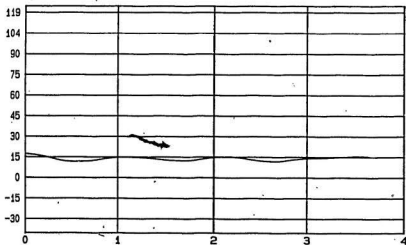


TIME (s)

TR# 3 DEPTH= 162 mm.

FREQ= 1 Hz. STROKE= 34 mm

PRESSURE CHANGE (Pa)

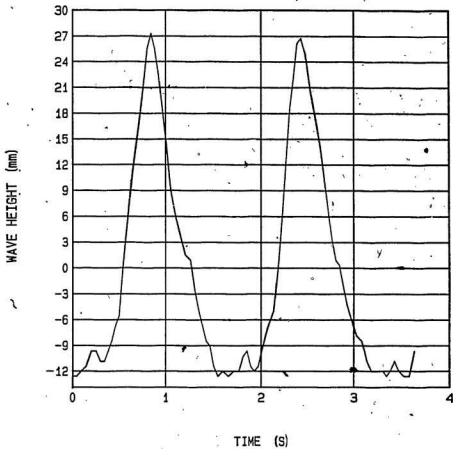


TIME (s)

TR# 4 DEPTH= 425 mm.

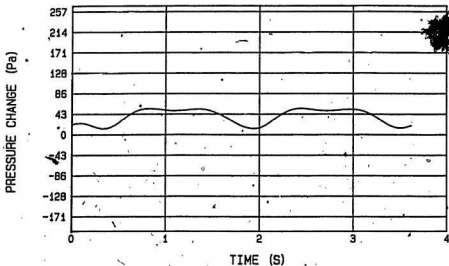
FREQ= 1 Hz. STROKE= 34 mm

FIGURE 102

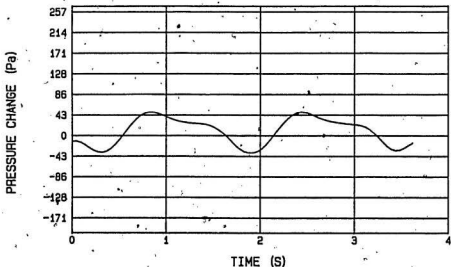


$F=0.63$  Hz.  $S=41$  mm.

FIGURE 103

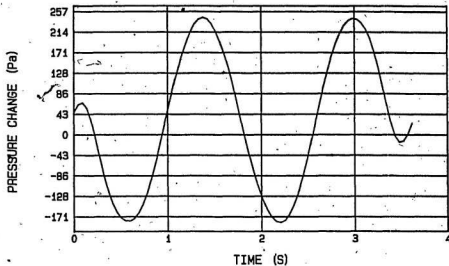


TR# 1 DEPTH= 611 mm.  
 FREQ= .63 Hz. STROKE= 41 mm

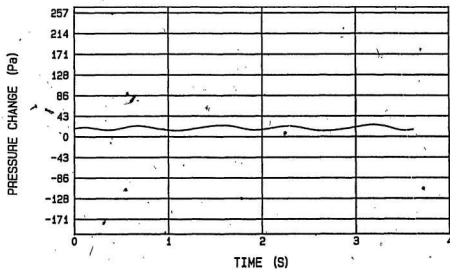


TR# 2 DEPTH= 340 mm.  
 FREQ= .63 Hz. STROKE= 41 mm

FIGURE 104

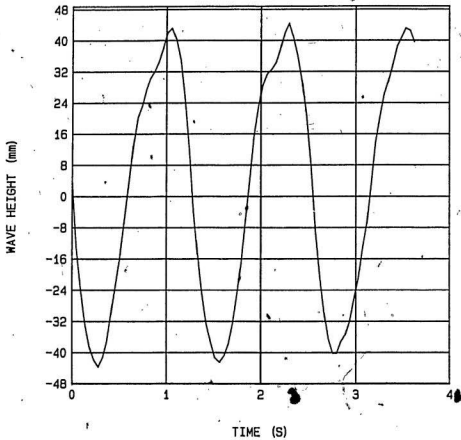


TR# 3 DEPTH= 162 mm.  
 FREQ= .63 Hz. STROKE= 41 mm



TR# 4 DEPTH= 425 mm.  
 FREQ= .63 Hz. STROKE= 41 mm

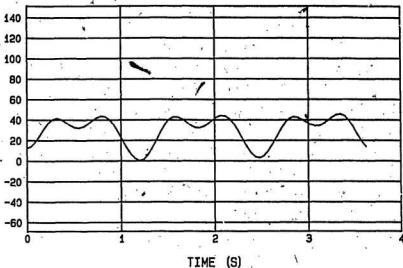
FIGURE 105



$F=0.81$  Hz.  $S_{\bar{r}}=41$  mm.

FIGURE 106

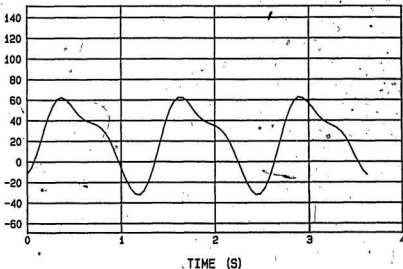
PRESSURE CHANGE (Pa)



TR# 1 DEPTH= 611 mm.

FREQ= .81 Hz. STROKE= 41 mm

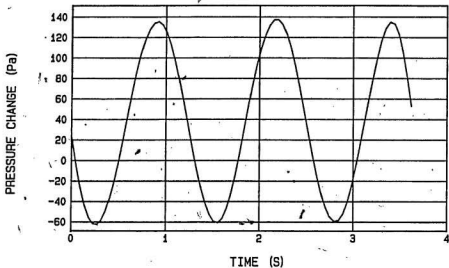
PRESSURE CHANGE (Pa)



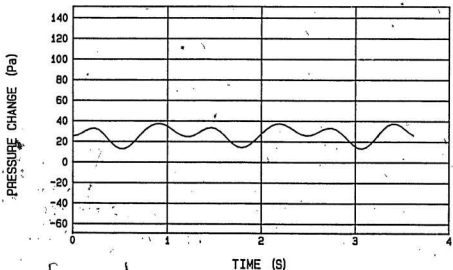
TR# 2 DEPTH= 340 mm.

FREQ= .81 Hz. STROKE= 41 mm

FIGURE 107

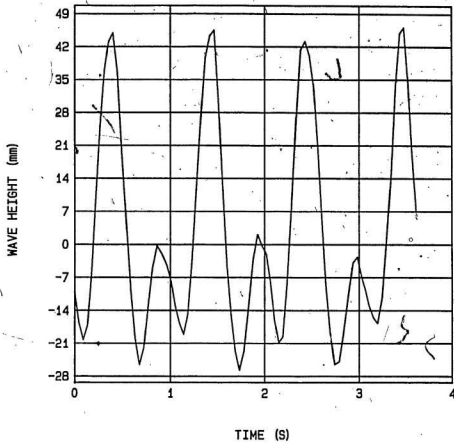


TR# 3 DEPTH= 162 mm.  
 FREQ= .81 Hz. STROKE= 441 mm



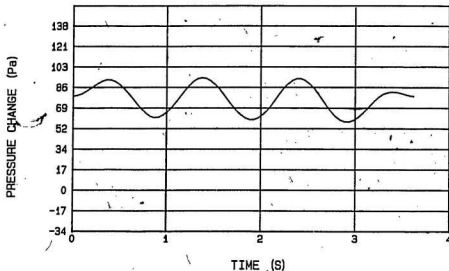
TR# 4 DEPTH= 425 mm.  
 FREQ= .81 Hz. STROKE= 441 mm

FIGURE 108.

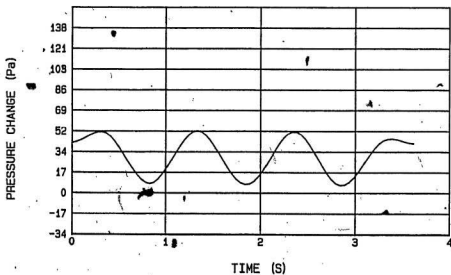


F=1.00 Hz. S=41 mm.

FIGURE 109



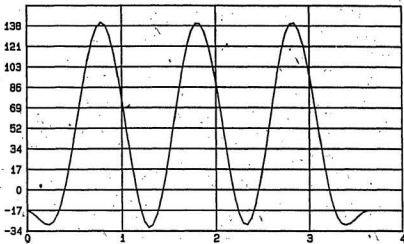
TR# 1 DEPTH= 611 mm.  
 FREQ= 1 Hz. STROKE= 41 mm



TR# 2 DEPTH= 340 mm.  
 FREQ= 1 Hz. STROKE= 41 mm

FIGURE 110

PRESSURE CHANGE (Pa)

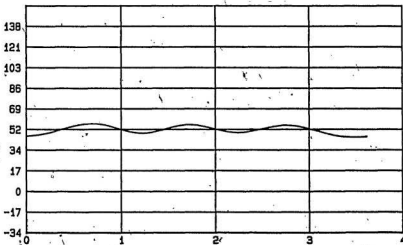


TIME (S)

TR# 3 DEPTH= 162 mm.

FREQ= 1 Hz. STROKE= 41 mm

PRESSURE CHANGE (Pa)

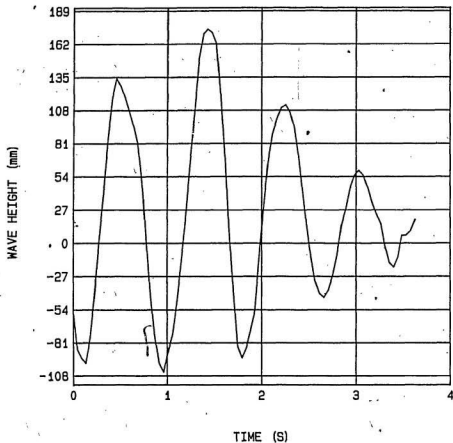


TIME (S)

TR# 4 DEPTH= 425 mm.

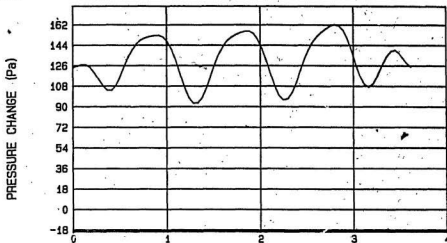
FREQ= 1 Hz. STROKE= 41 mm

FIGURE 111

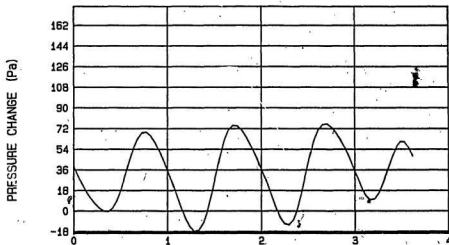


$F=1.15$  Hz.  $S=41$  mm.

FIGURE 112

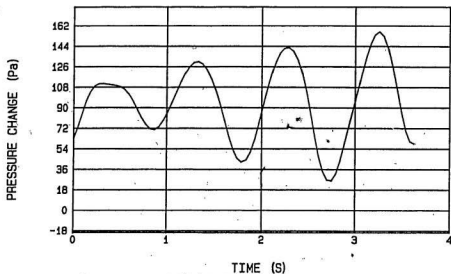


TIME (S)  
 TR# 1 DEPTH= 611 mm.  
 FREQ= 1.15 Hz. STROKE= 41 mm

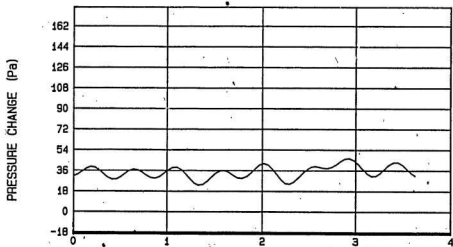


TIME (S)  
 TR# 2 DEPTH= 340 mm.  
 FREQ= 1.15 Hz. STROKE= 41 mm

FIGURE 113

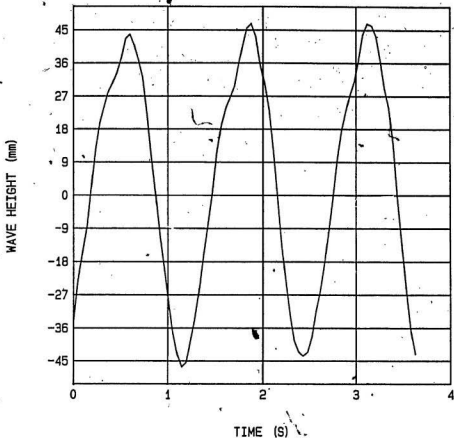


TIME (S)  
 TR# 3 DEPTH= 162 mm.  
 FREQ= 1.15 Hz. STROKE= 41 mm



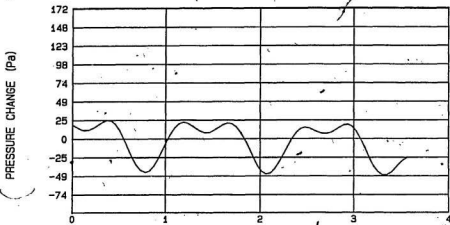
TIME (S)  
 TR# 4 DEPTH= 425 mm.  
 FREQ= 1.15 Hz. STROKE= 41 mm

FIGURE 114

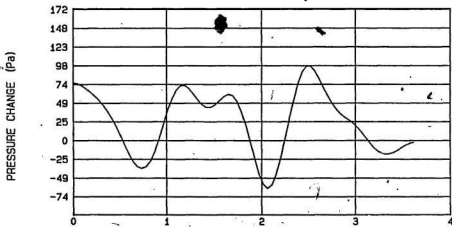


F=0.63 Hz. S=48 mm.

FIGURE 115

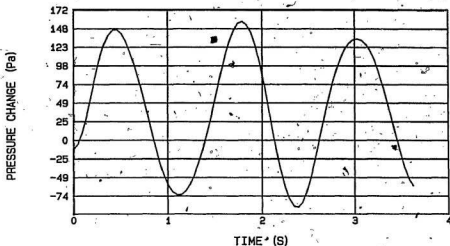


TIME (S)  
 TR# 1 DEPTH= 611 mm.  
 FREQ= .63 Hz. STROKE= 48 mm

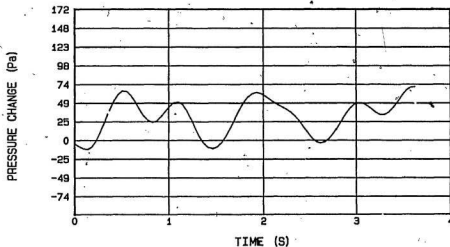


TIME (S)  
 TR# 2 DEPTH= 340 mm.  
 FREQ= .63 Hz. STROKE= 48 mm

FIGURE 116

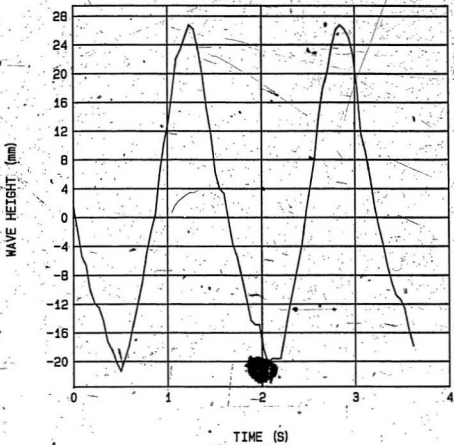


TR# 3 DEPTH= 162 mm.  
 FREQ= .63 Hz. STROKE= 48 mm



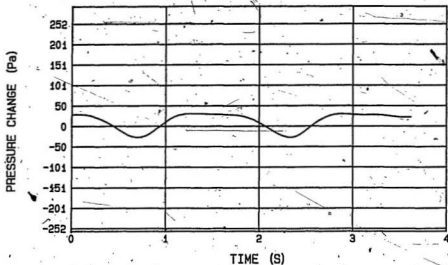
TR# 4 DEPTH= 425 mm.  
 FREQ= .63 Hz. STROKE= 48 mm

FIGURE 117

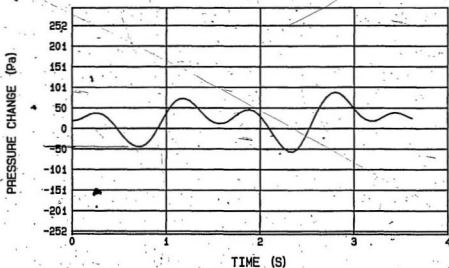


$F=0.81$  Hz.  $S=48$  mm.

FIGURE 118

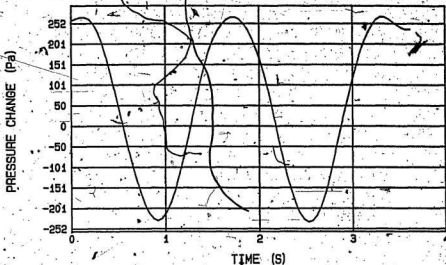


TR# 1 DEPTH= 611 mm.  
 FREQ= .81 Hz. STROKE= 48 mm



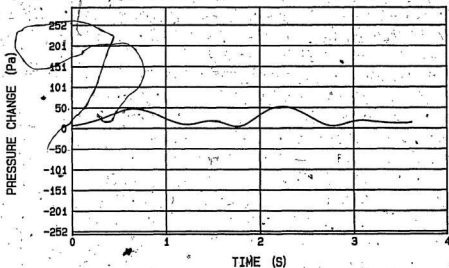
TR# 2 DEPTH= 340 mm.  
 FREQ= .81 Hz. STROKE= 48 mm

FIGURE 119



TR# 3 DEPTH= 162 mm.

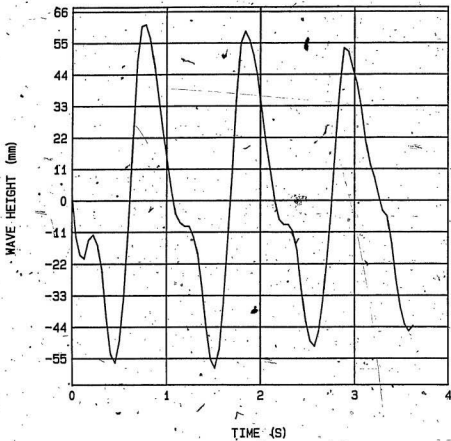
FREQ= .81 Hz. STROKE= 48 mm



TR# 4 DEPTH= 425 mm.

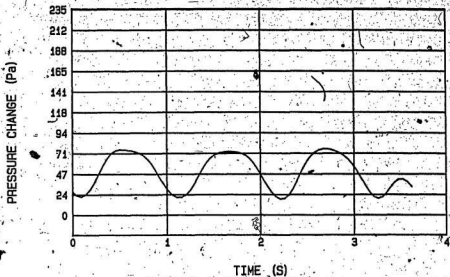
FREQ= .81 Hz. STROKE= 48 mm

FIGURE 120

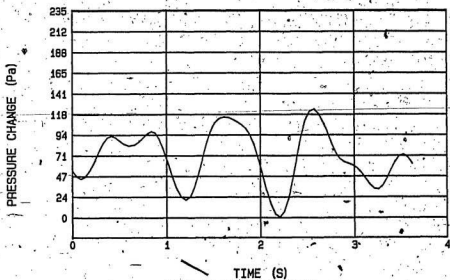


F=1.00 Hz. S=48 mm.

FIGURE 121

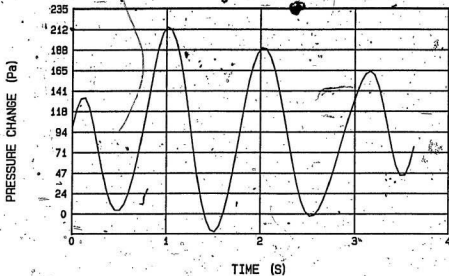


TR# 1 DEPTH= 611 mm.  
 FREQ= 1 Hz. STROKE= 48 mm

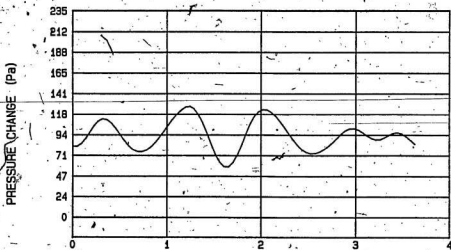


TR# 2 DEPTH= 340 mm.  
 FREQ= 1 Hz. STROKE= 48 mm

FIGURE 122

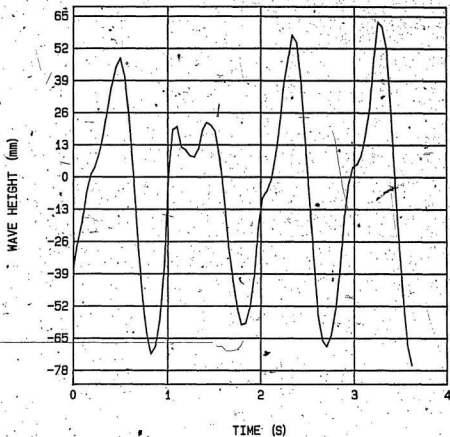


TIME (S)  
 TR# 3 DEPTH= 162 mm.  
 FREQ= 1 Hz. STROKE= 48 mm



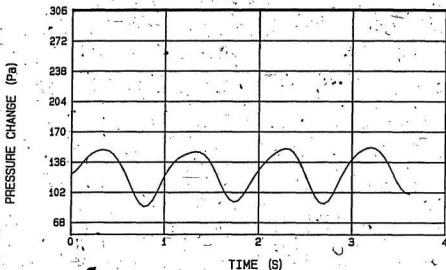
TIME (S)  
 TR# 4 DEPTH= 425 mm.  
 FREQ= 1 Hz. STROKE= 48 mm

FIGURE 123

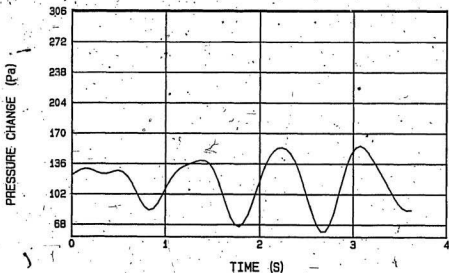


$F=1.15$  Hz.  $S=48$  mm.

FIGURE 124

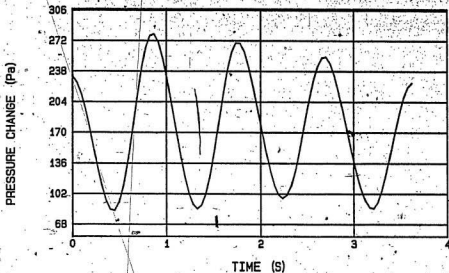


TR# 1 DEPTH= 611 mm.  
 FREQ= 1.15 Hz. STROKE= 48 mm



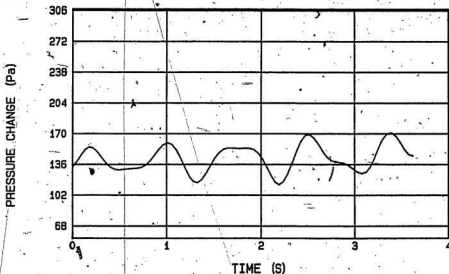
TR# 2 DEPTH= 340 mm.  
 FREQ= 1.15 Hz. STROKE= 48 mm

FIGURE 125



TR# 3. DEPTH= 162 mm.

FREQ= 1.15 Hz. STROKE= 48 mm



TR# 4 DEPTH= 425 mm.

FREQ= 1.15 Hz. STROKE= 48 mm

FIGURE 126

## REFERENCES

1. Aubanel, E.E., and Oldham, K.B., "Fourier Smoothing Without the Fast Fourier Transform". Byte Magazine Feb. 1985.
2. Becker, D.E., Jefferies, M.G., Shinde, S.B., and Crooks, J.H.A., "Pore Water Pressure in Clays Below Caisson Islands". Civil Engineering in the Arctic Offshore. Proceedings of the Conference Arctic 85. American Society of Engineers. New York. 1985.
3. Biesel, F., Etude theorique d'un certain type d'appareil à houle." Houille Blanche, 6, pp 156-165. 1951.
4. Biot, M.A., "General Theory of Three Dimensional Consolidation". Jour. of Ap. Physics. Vol. 12. Feb. 1941.
5. Cheng, A., Liu, Philip, "Seepage forces on a pipeline buried in a poroelastic seabed under wave loading." Applied Ocean Research, Vol. 8, No.1. pp 111-131. 1986.
6. Croce, P., Pane, V., Znidarcic, D., Ko H., Olsen, H., and Schiffman, R. "Evaluation of Consolidation Theories by Centrifuge Modelling." Proceedings of a Symposium on the Application of Centrifuge Modelling to Geotechnical Design, Manchester, England. April 16-18, 1984. Edited by W.H. Craig. A.A. Balkema, Rotterdam, Boston, 1985.
7. Davis, M.E., "Pore Pressure Development in Sand Beds." Paper Presented at 1985 Cdn Coastal Conf. St. John's. 1985.
8. Dawe, C.R., and Chari, T.R. "Dynamic Effects of Waves on Seabed Stability." 3rd Marine Geotechnical Conference. St. John's Newfoundland. 1986.

9. Dawson, T.H., "Correlation of Field Measurements with Elastic Theory of Seafloor Response to Surface Waves." Offshore Technology Conference. OTC 2973. 1981.
10. Demars, K.R. "Transient Stresses Induced in Sandbed by Wave Loading." Jour. of the Geotech. Eng. Div. ASCE. Vol. 109, No.4. April 1983.
11. Demars, K.R., and Vanover, E.A., "Measurement of Wave Induced Pressures and Stresses in a Sandbed." Marine Geotechnology. Vol. 6. No.1. 1985.
12. Doyle, E.H., "Soil Wave Tank Studies of Marine Soil Instability". Offshore Technology Conference. OTC 1901. 1973.
13. Finn, W.D.L., Lee, K.W., and Martin, G.R., "An Effective Stress Model for Liquefaction" Jour. of the Geotech. Eng. Div. ASCE. Vol. 103. No. GT6. June 1977.
14. Finn, W.D. Liam, Siddhathan, R., and Martin, G.R. "Response of Seafloor to Ocean Waves." Jour. of Geotech. Eng. Vol. 109. No. 4. April 1983.
15. Gilbert, G., Thompson, D.M., and Brewer, A.J., "Design Curves for Regular and Random Wave Generators." Jour. Hydraulic Research, Vol. 9, No. 2. 1971.
16. Goodings, D.J. "Relationships for Modelling Water Effects in Geotechnical Centrifuge Models." Proceedings of a Symposium on the Application of Centrifuge Modelling to Geotechnical Design, Manchester, England. April 16-18, 1984. Edited by W.H. Craig. A.A. Balkema, Rotterdam, Boston, 1985.

17. Havelock T.H., "Forced Surface Waves on Water." Phil Mag. 8, 569-576. 1929.
18. Heijnen, W.J., "The Use of Physical Models in Solving Offshore Geotechnical Problems." Joint I.Struct.E./B.R.E., Two day seminar. 1981.
19. Henkel, D.J., "The Role of Waves in Causing Submarine Landslides". Geotechnique Vol. 20. No.1.pp 75-80. 1970.
20. Hudspeth, R.T., and Chen, M., "Design Curves for Hinged Wavemakers: Theory", Jour. of the Hydraulics Division, ASCE, Vol. 10y No. HY5, May 1981.
21. Hyun, J.M., "Theory for Hinged Wavemakers of Finite Draft in Water of Constant Depth." Journal of Hydronautics, Vol. 10, No.1, Jan. 1976.
22. Janbu, N., "Soil models in offshore Engineering." Geotechnique. 35. No. 3, 241-281. 1985.
23. Jefferies, M.G., Stewart, H.R., Thompson, R.A.A., and Rogers, B.T., "Molikpaq Deployment at Tarsiut P-45". Civil Engineering in the Arctic Offshore. Proceedings of the Conference Arctic 85. American Society of Engineers. New York. 1985.
24. Keating, T., and Webber, N.B., "The generation of periodic waves in a laboratory channel: a comparison between theory and experiment." Proc. Inst. Civ. Engrs, Part 2, pp 819-832, Dec. 1977.
25. Kimura, T., Kusakabe, O., and Saitoh, K., "Geotechnical model tests of bearing capacity problems in a centrifuge."

Geotechnique. 35, No. 1, 33-45. 1985.

26. Kokkinowráchos, K., and Aserakos, S., "Hydrodynamic Analysis of Large Offshore Structures on Porous Elastic Seabed." Proc. 4th Int. Symp. on Offshore Mechanics and Arctic Engineering, Dallas Texas. 1982.

27. Liu, P.L.F., Timothy, P., and O'Donnell, "Wave Induced Forces on Buried Pipelines in Permeable Seabeds." Proceedings, 4th Conference on Civil Engineering in the Oceans, San Francisco California, 1979.

28. Liu, P.L.F., "Damping of Water Waves over Porous Bed" Jour. of the Hydraulics Div. ASCE. Vol. 99. No. HY12. Dec. 1973.

29. Liu, P.L.F., "Wave Induced Pressure Under a Gravity Structure." Journal of Waterway, Port, Coastal and Ocean Engineering, Vol. 111, No. 1, Jan. 1985.

30. Madsen, O.S., "Wave Induced Pore Pressures and Effective Stresses in a Porous Bed." Geotechnique Vol. 28. No. 4 pp 377-393. 1978

31. Mallard, W.W., and Dalrymple, R.A., "Water Waves Propagating Over a Deformable Bottom." Offshore Technology Conference. OTC 2895. 1977.

32. Massel, S.R., "Gravity Waves Propagated over Permeable Bottom." Proc. ASCE J. Waterways, Harbors and Coastal Engineering 102(WW2), 11-121. 1976.

33. Morin, P., and Cameron, D., "Laboratory Testing of the Lundrigan Silt used in the Soil-Structure Interaction Wave

Tank." Internal report. Memorial University of Newfoundland.  
1987.

34. Moshagen, H., and Torum, A., "Wave Induced Pressures in Permeable Seabeds." Jour. of the Waterways Harbors and Coastal Eng. Div. ASCE. Vol. 101. No. WW1. Feb. 1975.

35. Moshagen, H., and Monkmeyer, P.L., "Wave Induced Seepage Forces on Embedded Offshore Structures". Proceedings, 4th Conference on Civil Engineering in the Oceans, San Francisco California, 1979.

36. Mynett, A.E., and Mei, C.C., "Wave Induced Stresses in a Poroelastic Bed Beneath a Rectangular Caisson". Geotechnique 32. No.3. 235-247. 1982.

37. Nakamura, M. et al., "On the seepage in the seabed due to waves." Proc. 20th Japan Soc. Civil Engrs. Coastal Engineering Conference. 1973.

38. Natarjara, M.S., and Gill, H.S., "Ocean Wave Induced Liquefaction Analysis". Jour. of Geotech. Eng. Vol. 109. No. 4. April 1983.

39. Okusa, S., and Uchida, A., "Pore Water Change in Submarine Sediments due to Waves." Marine Geotechnology. Vol. 4, No. 2. 1980.

40. Phillips, B.A., Ghazzaly, and Kalajian, E.H., "Stability of Pipeline in Sand Under Wave Pressure." Proceedings, 4th Conference on Civil Engineering in the Oceans, San Francisco California, 1979.

41. Prindle, R.W., and Lopez, A.A., "Pore Pressures in Marine Sediments-1981 Tests of the Geotechnically Instrumented Seafloor Probe (GISP). Offshore Technology Conference. OTC 4463. 1983.
42. Putnam, J.A., "Loss of Wave Energy Due to Percolation in a Permeable Sea Bottom." American Geophysical Union, Vol. 30, No. 3, pp 349-356.
43. Prevost, J.H., and Hughes, T.J.R., "Analysis of Gravity Offshore Structure Foundations Subjected to Cyclic Wave Loading." Offshore Technology Conference. OTC 3261. 1978.
44. Reid, R.O., and Kajiura, K., "On the Damping of Gravity waves over a Permeable Seabed." Trans. Am. Geophys. Un. 30, 349-356. 1957.
45. Richards, A.F., "Modelling and the Consolidation of Marine Soils." Seabed Mechanics. Proceedings of Symposium, sponsored jointly by the International Union of Theoretical and Applied Mechanics and the International Union of Geodesy and Geophysics and held at the University of Newcastle upon Tyne, 5-9 Sept. 1983.
46. Rogers, B.T., Hardy, M.D., Neth, V.W., and Metge, M., "Performance Monitoring of the Molikpaq While Deployed at Tarsiut P-45". Proceedings of the Third Canadian Conference on Marine Geotechnical Engineering. St. John's June, 1986.
47. Rowe, P.W., "Application of Centrifugal Models to Geotechnical Structures." Proc. Symposium "Soil Mechanics, Recent Developments", Australia, 1975.

48. Seed, H.B., Martin, P.D., and Lysmer, J., "Pore Pressure Changes During Soil Liquefaction". Jour. of the Geotech. Eng. Div. ASCE. Vol. 102, No. GT4 April 1976.
49. Sharp, J.J. "Hydraulic Modelling". Butterworth and Company Ltd. Toronto, Ontario. 1981.
50. Siddhartan, R., Finn, and W.D. Liam, "STAB-MAX: Analysis of Instantaneous Instability Induced in Seafloor Sands by Large Waves," Soil Dynamics Group, Faculty of Graduate Studies, University of British Columbia, Vancouver British Columbia, 1979.
51. Silvestri, V., Soulie, M., Marche, C., and Louche, D. "Effect of Soil Anisotropy on the Wave Induced Pore Pressures in the Seabed." Jour. of Energy Resources Technology. Vol. 107. pp 441-445. Dec. 1985.
52. Sleath, J.F.A., "Wave Induced Pressures in Beds of Sands." Jour. of Hydraulics Div. ASCE. Feb. 1970.
53. Smits, F.P. "Soil Model Studies at  $\eta_g=1$ ". Proceedings of the 9th Annual Conference on Soil Mechanics and Foundation Engineering. Tokyo. 1977.
54. Spidsoe, N., and Skastad, O., "Measured Soil-Structure Interaction Properties of a Gravity Platform." Offshore Technology Conference. OTC 5222. 1986.
55. Ursell, F., Dean, R.G., and Yu, Y.S., "Forced Small Amplitude Water Waves: A Comparison of Theory and Experiment," Journal of Fluid Mechanics, Vol. 7, Part 3. pp 33-52. 1960.

56. Yamamoto, T., Koning, H.L., Sellmeijer, H., and van Himm, E.P., "On the Response of a Poro-Elastic Bed to Water Waves." Jour. of Fluid Mech(1978), Vol. 87. Part 1. 1978.

57. Yamamoto, T., "Seabed Instability from Waves." Offshore Technology Conference." OTC 3262. 1978.

## Appendix 1-Calibration of Wavemaker

### Introduction

For a flap type wavemaker, the wavemaker gain factor,  $a/s$ , is given by:

$$a/s = \frac{2 * \sinh(\lambda d) * (1 - \cosh(\lambda d) + \lambda d * \sinh(\lambda d))}{(\lambda d) * (\lambda d + \sinh(\lambda d) * \cosh(\lambda d))}$$

where:

$a$  = wave amplitude,  $s$  = wavemaker stroke,  $\lambda$  = wave number,  
 $d$  = water depth.

To determine the performance of the wavemaker, a series of waves of different frequencies and wavemaker strokes was generated and measured using a capacitance wave probe and a meter stick with millimetre divisions. Theoretical wave heights were computed using the wavemaker gain factor for water depth 0.8 m adjacent to the wavemaker. Table 3 shows the wavemaker stroke, wave heights measured by the ruler and the wave probe, the theoretical wave heights and the ratio of theoretical to actual wave heights measured by the wave probe.

### Observations

1. The wave heights measured by the meter stick and wave probe agree closely for small waves and low frequencies but vary

2. Using Equation 1 with water depth of 0.8 m, the wave heights were considerably overestimated; that is the theoretical wave height is higher than the measured wave height. The average over-estimates were: 0.63 Hz.-39%, 0.81 Hz.-33%, 1.0 Hz.-55%, 1.15 Hz.-28%.

3. All waves were theoretically below the breaking limit of  $H_p/L = 0.142$  which is predicted by linear wave theory.

4. Waves of 1 Hz. and 1.15 Hz. are deep water waves ( $d/L > 0.5$ ). The lower frequency waves were transitional waves. If the water depth over the soil bed is used to calculate the ratio  $d/L$ , then all waves are transitional.

#### Discussion

Since waves were measured by the wave probe, it was not necessary to define the operating characteristics of the wavemaker. However, the limited testing and calibration does indicate that the theory of Hyun (1981) is not adequate to predict wave heights in a tank configured with two depth regimes. Wave heights were consistently overestimated by an average of 39%. The loss in wave energy is likely due to absorption in the soil bed and on the initial sloping beach in front of the wavemaker.

Appendix 2Pore Pressures-Actual and TheoreticalSoil Bed Alone-0.63 Hz.

		AC.	TH.	AC.	TH.
<u>Str(mm)</u>	<u>Hp(mm)</u>	<u>T1(Pa)</u>	<u>T1(Pa)</u>	<u>T2(Pa)</u>	<u>T2(Pa)</u>
27	39	-61	-73	-130	-152
		60	73	127	152
34	44	-64	-90	-164	-188
		60	90	170	188
41	60	-98	-112	-230	-235
		114	112	275	235
48	65	-128	-122	-270	-254
		115	122	230	254

0.63 Hz.

		AC.	TH.	AC.	TH.
<u>Str(mm)</u>	<u>Hp(mm)</u>	<u>T3(Pa)</u>	<u>T3(Pa)</u>	<u>T4(Pa)</u>	<u>T4(Pa)</u>
27	39	-90	-105	-26	-99
		100	105	30	99
34	44	-130	-129	-60	-122
		131	129	51	122
41	60	-121	-162	-56	-153
		157	162	66	153
48	65	-185	-175	-56	-166
		220	175	53	166

0.81 Hz.		AC.	TH.	AC.	TH.
<u>Str(mm)</u>	<u>Hp(mm)</u>	<u>T1(Pa)</u>	<u>T1(Pa)</u>	<u>T2(Pa)</u>	<u>T2(Pa)</u>
27	44	-35	-47	-130	-146
		44	47	138	146
34	55	-39	-58	-175	-182
		30	58	161	182
41	68	-58	-72	-186	-225
		56	72	194	225
48	79	-55	-84	-234	-262
		60	84	234	262

0.81 Hz.		AC.	TH.	AC.	TH.
<u>Str(mm)</u>	<u>Hp(mm)</u>	<u>T3(Pa)</u>	<u>T3(Pa)</u>	<u>T4(Pa)</u>	<u>T4(P)</u>
27	44	-100	-75	-25	-77
		86	75	25	77
34	55	-136	-94	-25	-96
		130	94	30	96
41	68	-148	-116	-42	-119
		156	116	45	119
48	79	-180	-134	-62	-138
		200	134	33	138

1.00 Hz.

AC.

TH.

AC.

TH.

<u>Str(mm)</u>	<u>Hp(mm)</u>	<u>T1(Pa)</u>	<u>T1(Pa)</u>	<u>T2(Pa)</u>	<u>T2(Pa)</u>
27	62	-22	-31	-108	-160
		38	31	123	160
34	82	-32	-41	-160	-213
		50	41	160	213
41	100	-46	-50	-182	-259
		28	50	194	259
48	110	-52	-55	-200	-285
		37	55	165	285

1.00 Hz.

AC.

TH.

AC.

TH.

<u>Str(mm)</u>	<u>Hp(mm)</u>	<u>T3(Pa)</u>	<u>T3(Pa)</u>	<u>T4(Pa)</u>	<u>T4(Pa)</u>
27	62	-70	-53	-15	-66
		70	53	15	66
34	82	-110	-70	-21	-88
		100	70	20	88
41	100	-102	-85	-38	-107
		121	85	30	107
48	110	-151	-94	-38	-117
		120	94	28	117

1.15 Hz.		AC.	TH.	AC.	TH.
<u>Str(mm)</u>	<u>Hp(mm)</u>	<u>T1(Pa)</u>	<u>T1(Pa)</u>	<u>T2(Pa)</u>	<u>T2(Pa)</u>
27	65	-30	-16	-90	-131
		35	16	80	131
34	87	-23	-21	-115	-175
		23	21	115	175
41	94	-33	-23	-135	-189
		26	23	151	189
48	110	-33	-27	-169	-220
		28	27	175	220

1.15 Hz.		AC.	TH.	AC.	TH.
<u>Str(mm)</u>	<u>Hp(mm)</u>	<u>T3(Pa)</u>	<u>T3(Pa)</u>	<u>T4(Pa)</u>	<u>T4(Pa)</u>
27	65	-50	-27	-20	-43
		45	27	20	43
34	87	-45	-36	-25	-58
		45	36	25	58
41	94	-70	-39	-22	-62
		65	39	30	62
48	110	-78	-46	-30	-73
		78	46	30	73

With Model-O.63 Hz. (All values are actual)

<u>Str(mm)</u>	<u>Hp(mm)</u>	<u>T1(Pa)</u>	<u>T2(Pa)</u>	<u>T3(Pa)</u>	<u>T4(Pa)</u>
27	36	10	-30	-150	5
		55	45	170	20
34	33	0	-28	-150	1
		25	34	177	8
41	39	12	-30	280	12
		53	50	250	22
48	89	-44	-36	-72	-10
		25	72	145	60

0.81 Hz.

<u>Str(mm)</u>	<u>Hp(mm)</u>	<u>T1(Pa)</u>	<u>T2(Pa)</u>	<u>T3(Pa)</u>	<u>T4(Pa)</u>
27	60	20	-20	-40	7
		48	34	80	14
34	82	6	-30	-63	3
		30	36	100	15
41	80	0	-28	-60	14
		43	62	135	38
48	50	-30	-44	-45	0
		30	73	53	44

## 1.00 Hz.

<u>Str(mm)</u>	<u>Hp(mm)</u>	<u>T1(Pa)</u>	<u>T2(Pa)</u>	<u>T3(Pa)</u>	<u>T4(Pa)</u>
27	39	30	-10	-52	8
		60	30	102	20
34	44	72	-7	-36	11
		100	26	105	16
41	63	50	-4	-64	40
		100	60	167	64
48	110	20	43	0	74
		74	92	214	112

## 1.15 Hz.

<u>Str(mm)</u>	<u>Hp(mm)</u>	<u>T1(Pa)</u>	<u>T2(Pa)</u>	<u>T3(Pa)</u>	<u>T4(Pa)</u>
27	46	50	-17	13	5
		92	36	75	16
34	74	112	-5	5	20
		160	40	100	50
41	108	93	-17	42	26
		156	75	130	43
48	120	89	-26	85	130
		150	140	280	160

### Appendix 3

#### Beach Reflection Coefficient

The absorption of wave energy by a beach is not perfect; as a result part of the incident wave is reflected and a standing wave is set up in the wave tank. As a result, wave height is not the same at all points, but varies with distance from the wavemaker. Ursell(1960) found that if the maximum and minimum values of the variation are denoted by  $H_{max}$  and  $H_{min}$ , the reflection coefficient,  $E_r$ , may be computed as

$$E_r = (H_{max} - H_{min}) / (H_{max} + H_{min})$$

#### Procedure

To determine  $E_r$ , the variation in wave heights was measured by attaching two wave probes to the travelling carriage in the wave tank and moving the carriage down the tank while waves were being generated. The output from the probes was directed to a strip chart recorder and the variation in wave height measured directly from the chart.

#### Results

The calculated reflection coefficient ranged from 7 to 10 percent.

#### Appendix 4

##### Calibration of Instrumentation

###### Wave Probe

The wave probe was calibrated by lowering it and raising in the water 10 mm intervals and recording the output voltage. Two probes were used and a number of trials run. Linear regressions were calculated for the data generated and the following relationships established for the wave probes.

Probe 1:  $H(\text{mm}) = 0.59 * \text{voltage (mV)}$

Probe 2:  $H(\text{mm}) = 0.60 * \text{voltage (mV)}$

###### Pore Pressure Measuring System

The pressure transducers, tubing, porous stones and electronics were calibrated by varying the head on them at fixed increments and recording the output voltages. Transducer response varied depending on whether the tank was being filled or emptied and whether the piezometric stones were buried or on the surface. For the work with the model in place and the stones buried, the tank was emptied and filled a number of times and an average value used to determine the proper calibration factors. Amplifier gain was increased to 200 before the model was installed to attempt to reduce the noise. This appeared to be successful, as the data collected was less noisy than data collected at a gain of 20. The calibration factors used were:

Transducer 1: Pore Pressure(Pa) = 53400 \* voltage (mV)  
Transducer 2: Pore Pressure(Pa) = 53400 \* voltage (mV)  
Transducer 3: Pore Pressure(Pa) = 56600 \* voltage (mV)  
Transducer 4: Pore Pressure(Pa) = 53600 \* voltage (mV)







